

Dense Cores in
Galactic Cirrus Clouds

Dissertation

zur

Erlangung des Doktorgrades (Dr. rer. nat.)

der

Mathematisch-Naturwissenschaftlichen Fakultät

der

Rheinischen Friedrich-Wilhelms-Universität
zu Bonn

vorgelegt von

Christoph Böttner

aus Lobenstein

Bonn, März 2005

Angefertigt mit Genehmigung
der Mathematisch-Naturwissenschaftlichen Fakultät
der Rheinischen Friedrich-Wilhelms-Universität Bonn

1. Referent: Priv. Doz. Dr. Andreas Heithausen
2. Referent: Professor Dr. Ulrich Klein

Tag der Promotion: 01. Juli 2005

Diese Dissertation ist auf dem Hochschulschriftenserver der ULB Bonn
http://hss.ulb.uni-bonn.de/diss_online elektronisch publiziert

Für Astrid

Contents

1	Introduction: The Interstellar Medium	3
1.1	Cirrus Clouds	4
1.2	Dense Cores	6
1.3	Star Formation	8
1.4	Aim and Outline of this Thesis	11
2	The Core Sample	13
2.1	MCLD 123.5+24.9	14
2.2	MCLD 126.6+24.5	21
2.3	L 1457	23
2.4	MBM 32	25
2.5	Draco	27
3	Dust Continuum Observations	29
3.1	Dust Continuum Emission	29
3.2	Observations	30
3.3	Data Reduction	31
3.4	Results	32
4	Molecular Line Observations	39
4.1	CS as a Dense Core Tracer	39
4.2	CS (2 \rightarrow 1) Mapping Observations	40
4.2.1	Observations	40
4.2.2	Data Reduction	41
4.2.3	Results	41
4.3	Additional Observations with the IRAM 30-m Telescope	47
4.3.1	Observations and Data Reduction	47
4.3.2	Results	48
4.4	Interferometric Observations of MCLD 123.5+24.9	55
4.4.1	Observations and Data Reduction	55
4.4.2	Results	56

5	Physical Core Properties and Scaling Relations	59
5.1	Column Densities and Core Masses	60
5.1.1	Two Dimensional Gaussian Fits	60
5.1.2	Determination of the Column Density	63
5.1.3	Determination of the Mass	64
5.2	Core Structure within the CS-maps	65
5.3	Scaling Relations	69
5.3.1	The Size – Line Width Relation	69
5.3.2	The Size – Density Relation	72
5.3.3	The Mass – Line Width Relation	75
5.3.4	Virial Masses of the Cores	77
6	Chemical Core Properties and Star Formation Capability	81
6.1	Abundance Variations	82
6.2	Gas Chemistry in Cirrus Cloud Cores	86
6.3	Core Stability and Star Formation Capability	88
7	Conclusions and Future Prospects	91
7.1	The Results of this Study	91
7.2	Future Prospects	92
8	Summary	95
	References	99
	Acknowledgments	105
	Lebenslauf	107

Abstract

In this thesis I study the formation and evolution of dense cores in cirrus clouds. Cirrus clouds are diffuse and translucent molecular clouds widely spread within the galaxy. Dense cores in molecular clouds are the locations of the origin of star formation. The knowledge of how cores form and how they evolve is the key to understand the initial conditions of the star formation process. Especially the starting conditions are still poorly known, despite recent progress. Studies of cores in various regions with different physical conditions will help to assess the important processes within the formation and evolution of these cores. A fair number of investigations have already been made towards regions with known star formation. However, there the processes are often more complicated by the feedback actions of new-born or young stars. Translucent cirrus clouds, on the other hand, are relatively simple and quiescent objects, dominated mostly by turbulent gas motions. Due to the lack of active star formation they are thought to show a more simple behaviour than many of the dark molecular clouds. The investigation of cirrus cloud cores could therefore help to reveal the importance of particular conditions and events.

Using the IRAM 30-m radio telescope and the bolometer arrays I observed a small sample of 5 dense cores in cirrus clouds in the thermal dust continuum. The dust continuum emission appears to be one of the best tracers of the H_2 column density and is particularly suited to locate and map the core regions. However, it does not provide any kinematic information and hence no access to the kinetic energy in the cores. Additionally, I observed the cores with the FCRAO 14-m radio telescope in the CS ($2 \rightarrow 1$) transition, and several other molecular lines with the IRAM 30-m telescope. Molecular line observations provide kinematic properties, but because of abundance variations they are often difficult to interpret. Hence, the gas chemistry in the core becomes important and has to be considered.

Together, these data provide the possibility to obtain a more realistic view of the core properties. I calculate core parameters and analyse the physical conditions. A comparison of cores in cirrus clouds with cores in star-forming regions and dark clouds shows the similarities but also some important differences. One particular core is observed in even more detail using the Plateau de Bure and the OVRO interferometer in CS and HC_3N . These data reveal most interesting insights into the core sub-structure and demonstrate the need for observations with high spatial resolution. The star-forming ability of the studied cores is discussed, together with the question if cirrus clouds are able to form stars at all.

1

Introduction: The Interstellar Medium

One of the most fundamental hurdles to understanding the structure and evolution of the Milky Way is our knowledge of the evolutionary cycle of matter in the *Interstellar Medium* (ISM). Though a lot of progress has been achieved in recent years, we still know little about how the ISM cycles through its various phases to arrive at star formation. The principal starting point is the atomic phase. The gas then cools and forms molecules, leading to the molecular phase. Through the interplay of turbulence and gravity molecular clouds form, fragment and form cores, which may condense further and eventually form stars.

The formation of a star is probably one of the most exciting astrophysical processes one can study. Certainly, it is a very important process in our universe, enabling the formation of metals and complex molecules we are all made up of. In recent years we learned a lot about how and where star formation occurs. Nevertheless, there are still many questions to be asked and especially, the very first steps and starting conditions of the processes are still poorly understood.

Single low-mass stars like our sun are thought to form mostly in relatively quiescent clouds like, for instance, Taurus. The Taurus-Auriga molecular cloud complex has a relatively low spatial density of *Young Stellar Objects* (YSOs) and is believed to be representative of the isolated or distributed mode of low-mass star formation (e.g., Motte & André 2001). By contrast, more massive and denser clouds like Orion, Perseus, or ρ Ophiuchi seem to produce a number of high-mass stars and clusters of stars (e.g., Johnstone et al. 2001). The processes of massive and clustered star formation are thought to be different from low-mass star formation and dominated by feedback effects and interactions.

A significant fraction of the interstellar medium in our galaxy is, however, distributed in diffuse and translucent molecular clouds, often called *Cirrus Clouds* because of their appearance as thin filaments. The question arises what kind of stars, if any, are formed in such diffuse clouds. Certainly they will be low-mass objects. But does the mass of a core in such a cloud allow for a star or is it merely able to produce a brown dwarf? A object with a mass less than about 0.08 times the mass of the sun never develops enough pressure

and a high enough temperature for hydrogen fusion, so it slowly radiates its trapped gravitational energy away and disappears. These low mass objects are brown dwarfs. However, the formation of brown dwarfs is still being discussed. It could be similar to the low-mass star formation mode (e.g., Luhman 2004) or could need the influences of clustered star formation (e.g., Whitworth & Zinnecker 2004).

It has been found that the star-forming efficiency in cirrus clouds must be very low (e.g., Hearty et al. 1999). So far, no low-mass T-Tauri stars associated with cirrus clouds have been detected, with the possible exception of L1457 (Hearty et al. 2000). In this special case, however, it is not clear, whether the detected T-Tauri stars belong to the cloud complex or not. Nevertheless, evidence for signatures of ongoing core formation has recently been reported (Heithausen 1999), and some T-Tauri stars were discovered far from any actively star-forming region (e.g., Neuhäuser 1999). Their origin remains completely unknown. Are they runaway stars that were ejected from the parent molecular cloud, or were they born in a diffuse cloud which then dispersed? An answer may come from the star-forming ability of cirrus clouds, investigated in this study for the first time to this extent.

1.1 Cirrus Clouds

Galactic cirrus clouds are diffuse and translucent molecular clouds widely spread within our galaxy and often arranged in huge complexes. They are distributed all over the galactic disc and are often thought to build a connection between the disc and the halo, too. The most easily seen, and therefore the best studied ones, are those at high galactic latitudes. Of these, the most prominent are the nearest ones, located only about 100 pc to 300 pc away from our sun and hence, still well within the galactic disc.

Sometimes they are called *Low Velocity Clouds* (LVCs) as their systemic velocities are in the range of $\pm 10 \text{ km s}^{-1}$. In contrast, molecular clouds located further away, like for instance the Draco cloud, do mostly have higher absolute systemic velocities in the range of 10 and 50 km s^{-1} . Therefore, they are called *Intermediate Velocity Clouds* (IVCs).

A third class may be represented by the so called *High Velocity Clouds* (HVCs), located within the Halo of the Galaxy (e.g., Westmeier 2003) or between the galaxies of the Local Group (e.g., Wakker 2004). They can be observed in HI and may contain a significant fraction of molecular H_2 . However, the densities of these clouds are low and no signs of CO or other tracer molecules could be detected. It is not even clear up to now if they are not completely different in nature (e.g., Wakker 2004). In the latter study HVCs are thought to be an intergalactic type of clouds that are not a part of the galactic ISM cycle. The most difficult problem in this connexion is the distance, which is very hard to determine.

The nearby cirrus clouds or LVCs gained the attention of the scientific community in the mid of the eighties. Some of them were already catalogued by Lynds (1962, 1965) as dark

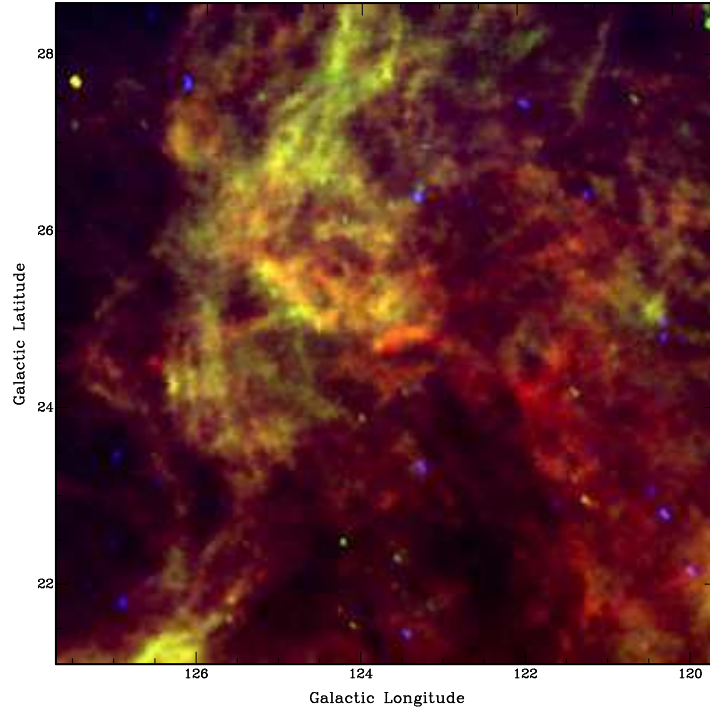


Figure 1.1: IRAS 3 color composite of the Polaris Flare region around MCLD 123.5+24.9. The thermal dust emission at $100\ \mu\text{m}$ is displayed in red, $60\ \mu\text{m}$ in green, and $25\ \mu\text{m}$ in blue.

or bright nebulae. But they became particularly interesting and important as large-scale, extended, filamentary emission observed by the *Infrared Astronomical Satellite* (IRAS) mission. This satellite was sensitive to the thermal continuum emission of dust particles between 12 and $100\ \mu\text{m}$, and made an all-sky survey at four wavelength bands. Low et al. (1984) described the filaments as "infrared cirrus" ubiquitous in the ISM. They identified several cirrus features with prominent HI clouds but also noted the presence of cirrus emission at some places without prominent HI, and vice-versa.

At the same time, Blitz, Magnani, & Mundy (1984) reported the detection of a large number of high galactic latitude molecular clouds (often referred to as HLCs - *High Latitude Clouds*) not previously cataloged, and mapped them in CO (Magnani, Blitz, & Mundy 1985, herein after referred to as MBM). These maps showed a wide range of morphologies of clouds with angular sizes sometimes exceeding 10° . However, most of these clouds display a very amorphous structure and only a few seem to look centrally condensed.

Weiland et al. (1986) established a close correlation between the infrared cirrus emission

observed with IRAS and the CO emission from these high latitude molecular clouds. Especially, the dust emission at $100\ \mu\text{m}$ represents similar features and shows intensity peaks at the same positions as the integrated CO emission line. Generally speaking, the MBM molecular clouds seem to be the denser parts of the extended cirrus clouds. It was also noted, that this association demonstrates that at least some of the cirrus emission originates from the local ISM with distances of about 100 to 300 pc. It was the first reliable estimate of the distance of the IRAS cirrus emission.

Because their typical optical extinction is near unity (e.g., Magnani & de Vries 1986) they are sometimes classified as *Translucent Clouds* (TLCs) (van Dishoeck & Black 1988) in which the *Interstellar Radiation Field* (ISRF) plays the major role for the chemical reactions throughout the molecular cloud. None of the cirrus clouds did show clear evidence of star-forming activity (e.g., Magnani et al. 1996 or Hearty et al. 1999). However, the principal capability of cirrus clouds to form stars is still being discussed. Most of the investigations mentioned before were made with strongly limited angular resolution or sensitivity. This work is intended to contribute to the discussion with new, high spatial resolution and high sensitivity observations. For this, we had to concentrate on very few and relatively small objects within the tremendous galactic cirrus.

Cirrus clouds are interesting from an astrophysical point of view, because their proximity allows us to observe the basic physical processes of molecular clouds on small spatial scales, and their low optical depth and lack of active star formation eliminates effects that often complicate the study of larger molecular clouds. Detailed studies also reveal that cirrus clouds contain density structures on a wide variety of scales. At the latest with the detection of more complicated molecules, like for instance NH_3 (Mebold et al. 1987), it became clear that these objects are not at all as simple as it has been thought for a long time. The interplay between gravity, turbulent motions, irradiation, and chemistry leads to the formation of small dense cores, that are the very first steps in the star formation process.

1.2 Dense Cores

Dense cores are the basic units of the star formation process. The study of the physical structure and kinematics of these cores is crucial for our understanding of the initial conditions of star formation. It is still somewhat unclear how cores form out of clouds. Gravitational fragmentation and turbulent motions certainly play the main role in this. However, the influences of each and especially the interactions between gravitation, turbulence, irradiation and chemistry are only little understood. Furthermore, the earliest evolution of a cloud core is very poorly constrained, and its evolutionary track is unclear. In particular, the initial conditions are highly important in defining the collapse dynamics, the likely mass of the later emanating star (and globally, the Initial Mass Function), the

timescales for their evolution, and the likelihood of the detection of sources in different evolutionary periods.

The motivation to study the physical conditions in dense cores comes from the theoretical consideration of a simple situation. If a cloud, with only thermal support, exceeds the Jeans (1928) mass limit it should collapse and form a star in basically the free-fall time (Spitzer 1978). Regarding the "typical" conditions in the ISM with a kinetic temperature of $T = 10$ K and particle densities $n \approx 50 \text{ cm}^{-3}$ (e.g., Evans 1999) the numbers of both these values are approximately $M_{\text{Jeans}} \leq 80 M_{\odot}$ and $t_{\text{ff}} \leq 5 \times 10^6$ years. Our Galaxy contains about $3 \times 10^9 M_{\odot}$ of molecular gas (Clemens et al. 1988) and the majority of this gas is distributed in clouds that are more massive than the typical Jeans-mass. It should be highly unstable and a free-fall collapse should lead to star formation at an extremely high rate. Admittedly, the recent average star formation rate of our galaxy is only about $1 M_{\odot}/\text{year}$ (Noh & Scalo 1990) and therefore, most of the clouds cannot collapse at free fall. There have to be support mechanisms and two possibilities have been considered: magnetic fields and turbulence. Both are not entirely satisfactory and compatible with the observations, but very recently magnetohydrodynamic (MHD) supersonic turbulence is thought to solve some of the problems, at least in theory (e.g., Mac Low & Klessen 2004 for a recent review on simulations). By the interplay of turbulence and gravity molecular clouds fragment into dense cores embedded in a less dense surrounding gas. But then the same questions arise again: Under what conditions does the collapse of the cores start? How does a core evolve? At what time does the star form and how does it affect the conditions? These are the very basic questions of the earliest phases of low-mass star formation.

Most of the studies on dense cores are conducted in regions of known star-forming activity (e.g., Motte et al. 1998). However, the interpretation of the data is often difficult and feedback processes of young stars, such as jets and outflows, or intensive radiation and shocks, do complicate the situation even more. In cirrus clouds the ISRF plays the leading part for the energetic input. For this reason, dense cores in the relatively quiescent environment of cirrus clouds are the ideal targets to investigate the physical conditions of the core formation process.

Although, with observations at just one wavelength we are not able to determine the exact structures of the cores. Dust continuum observations do provide only line-of-sight integrated properties. Therefore, we are limited to the projected geometry of the objects. Of course, it is clear that cores are intrinsically three-dimensional. From the observations, and cirrus clouds do play a leading part in this, we know that molecular clouds often appear in filamentary structures. It seems obvious that the cores will also often have such shapes. One possibility to reveal the exact three-dimensional structure of the cores may be dust continuum observations at various wavelengths together with absorption studies. The simultaneous theoretical fitting of all observational information within a three-dimensional model may uncloak the object structure in detail (Steinacker et al. 2003). This would improve our knowledge significantly. Unfortunately, it is highly complicated to obtain all the observations at an adequate quality.

A further interesting information is the overall number of dense cores in the galactic halo

and whether these objects do contribute to the baryonic dark matter content (e.g., Pfen- niger & Combes 1994, or Heithausen 2004 for a recent discovery). In order to understand this, one has to keep in mind that the vast majority of the core content, the H_2 , is all but invisible. Small, dense, and cold cores in the halo are virtually not detectable with previous or current instruments. The detailed exploration of such cores in our neighbour- hood can help to understand the formation criteria. It would enable us to estimate an occurrence frequency. This then leads to new insights of the state and the evolution of our galaxy.

1.3 Star Formation

The process of star formation is one of the most exciting and most important events in our universe. In the last years many discoveries have been made and many new insights into the process were achieved. However, we still know little about the precise details. The results of various investigations indicate that star formation in low density environ- ments, representative of the isolated mode of star formation, differs from that in high density environments, representative of cluster-forming star formation. The latter is the dominant mode of star formation (e.g., Myers 1998), heavily influenced by feedback pro- cesses and interactions. The evolution is much more dynamic, with frequent clump-clump interactions, than it is the case for isolated star formation. Nevertheless, the isolated low- mass star formation mode is of great importance. However, the initial conditions and the very beginnings of the formation processes in the low density environment are only poorly determined as already quoted above.

The current picture or qualitative model of low-mass star formation is as follows (e.g., Nordlund & Padoan 2002): Supersonic turbulence in the ISM, produced by large amounts of kinetic energy at large scales, dissipates in fragmenting molecular clouds (preventing a global collapse of the clouds) into highly anisotropic filaments as a result of the random convergence of the velocity field. These filaments form dense cores of typical dimensions 0.01 pc to 0.1 pc. Cooling becomes more efficient as density increases in these cores, which then may become self-gravitating and begin to collapse. Possibly, such a collapsing core forms a class 0 object. This may then further evolve via accretion into a star.

Although well understood qualitatively, many important details about the formation of low-mass stars remain ill determined. The collapse of a proto-stellar core depends almost entirely on the initial conditions. But what are the temperatures, densities, or kinetic energy distributions needed to start the collapse? When does collapse begin and how does collapse proceed? Shu (1977) formulated the inside-out collapse model that is still valid but also has its limitations. In this model the pre-collapse configuration is an isothermal sphere with a density profile $n(r) \sim r^{-2}$. However, many cores are neither spherical nor do they have such a density profile. There are many other theoretical solutions to the collapse problem, ranging from the inside-out collapse to overall collapse (see Evans 1999 for a review). Most of them have still to be tested by observations but inevitably, irregularities

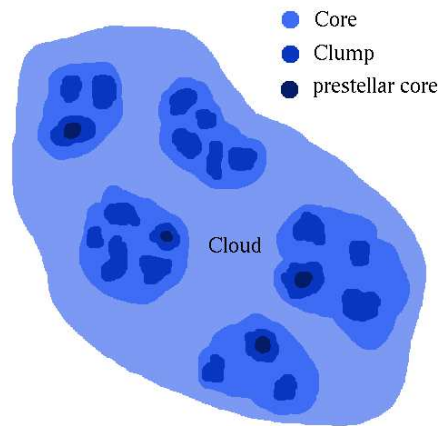


Figure 1.2: A sketch of a molecular cloud harbouring several cores, which contain several (sub-)clumps each. Only a few of the clumps may be dense and large enough to become pre-stellar cores, which collapse and form a stellar object. A darker colour means higher density.

in the density and velocity fields will confuse matters in real sources.

What fraction of the total mass of a core goes into the central object? The accretion phase is still a mystery. When the star is born, the remaining material forms a disc from which the star further accretes. At the same time a proto-stellar jet along the rotation axis of the proto-star develops, normally driving an outflow. The mechanisms during this phase are still somewhat unclear, but essentially hydromagnetic in nature. Therefore, we also cannot definitely answer the question as to how massive the new-born star will become in the end.

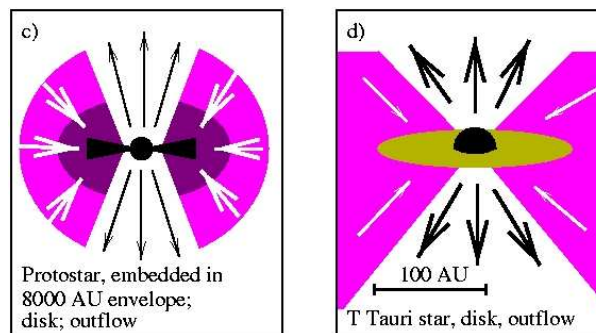


Figure 1.3: A sketch of the outflow phase of a typical new-born star in the standard scenario of low-mass star formation (adapted from Hogerheijde 1998).

We know that new-born stars follow the stellar *Initial Mass Function* (IMF). The mass function of stars in the range of 1 and 10 solar masses is a power law with a relatively constant slope of -2.35 (Salpeter 1955, but see Kroupa 2001 for a study on the variation

of the IMF). Below about 1 solar mass the IMF seems to deviate to a lognormal form (Chabrier 2003), but it cannot be ruled out that this is just an effect of an incomplete sampling, because such stars are difficult to observe. It is also possible to describe the observed IMF by a half-Gaussian distribution in $\log M$ (Miller & Scalo 1979) and comparisons with theoretical star formation models agree roughly for $M \geq 2 M_{\odot}$. However, most star formation models are unable to account for the flattening at the low-mass end. Therefore, the discrepancy can either be due to insufficient observations or to imperfect models.

The processes of fragmentation, accretion, and outflow control what fraction of the mass of an interstellar cloud eventually goes into each star that forms within the cloud. However, there cannot be a simple relation between the core mass function and the IMF of stars. Nevertheless, Motte et al. (1998) claimed the detection of the direct progenitors of individual stars in their dust map of the rho-Ophiuchi main cloud. They identified about 60 cores and the found core mass function mimics the stellar IMF. Similar results have been obtained in the Serpens cloud (Testi & Sargent 1998), Orion (Motte et al. 2001), and the Taurus region (Onishi et al. 2002). This would suggest that the IMF is solely determined by the fragmentation of the cloud into cores and accretion and outflow mechanisms do not contribute at all. Furthermore, it is unclear whether the identified cores do form stars at all, a single star, or possibly several stars. Therefore, these results are difficult to interpret and are still being discussed (e.g., Chabrier 2003). For the low-mass end of core masses well below $1 M_{\odot}$, most of the core observations are insufficient and do not allow for a strong statement up to now.

1.4 Aim and Outline of this Thesis

In this thesis a study of the physical conditions of five dense cirrus cloud cores is presented. Their capability of star formation is investigated and we try to answer the question if cirrus clouds are able to form stars or brown dwarfs at all. Even if the efficiency of cirrus clouds to form stars is low, it would contribute to the evolution of the whole galaxy in a non-negligible way. It is the first study of this kind. Nevertheless, the study shows that important processes in our immediate solar neighbourhood are sometimes hard to observe and not as easy to interpret.

The analysis is based on dust continuum observations at 1.2 mm made with the MAMBO arrays at the IRAM 30-m radio telescope and various molecular line observations conducted with several radio telescopes. The dust continuum emission is used to determine the basic properties of the cores, such as size, column density, and mass. The molecular lines, on the other hand, provide the kinematic information, excitation conditions, and, due to abundance variations, give us hints towards the age and evolutionary state of the cores. With this basic data set the possibility of single low-mass star formation in these cores is discussed.

Chapter 2 introduces our core sample and gives an overview on their properties known so far and some details of previous observations. The cores itself or at least their parental clouds are already fairly well studied. Chapters 3 and 4 present the observations we have conducted and give some technical details. The data reduction is described as well. Chapter 5 focuses on the analysis and we derive the properties of the cores or sub-clumps and study the scaling relations. The goal is to find similarities or differences to cores in dark clouds and star-forming regions. Chapter 6 first concentrates on the chemistry in the cores and abundances of several molecules are calculated and also compared with cores in star-forming regions. The values obtained are discussed and we speculate on the star-forming capability of cirrus clouds in general. Chapter 7 resumes the conclusions and gives some suggestions for future projects. Finally, in Chapter 8 a summary of the work is presented.

2

The Core Sample

Our core sample, listed in Table 2.1, was selected by inspecting the available database. All cores chosen were previously observed in CO and various other molecules, though with different intenseness. The best and in most detail studied core is the one in MCLD 123.5+24.9. Of this we do have already an extraordinary database and several detailed investigations were carried out and are available in the literature. In this chapter I will briefly introduce each core and the data available so far. Our goal was to select cores that are typical for cirrus clouds, and to search for evidence of ongoing star-formation or core-formation processes. We chose cores that were already known to harbour a multitude of molecules and hence, being dense enough to look for the dust continuum and other molecular species like NH_3 or HC_3N .

Table 2.1: The cores of our sample

Core	Galactic Longitude	Galactic Latitude	α_{2000} [h m s]	δ_{2000} [° ' "]
MCLD 123.5+24.9	123.69	+24.89	01 59 24.1	87 39 42.1
MCLD 126.6+24.5	126.61	+24.55	04 23 02.5	85 48 16.3
L 1457	159.25	-34.48	02 56 10.1	19 26 59.5
MBM 32	146.85	+40.66	09 33 52.4	66 06 05.0
Draco	89.53	+38.40	16 49 17.9	59 56 26.9

A short notice considering the terminology. Throughout this thesis, I will use the core name equal to the cloud name where this core is located in. Cirrus clouds harbour only a very few dense cores each, which then often separate into a number of sub-clumps if observed with higher angular resolution. The nomenclature is chosen to simplify matters and it should always become clear within the context of each paragraph what is meant.

In the literature there is no clear standard for the denotation of cores and often clumps and cores are simply named according to their parental cloud and labeled by characters or numbers, if necessary. Furthermore, I will use the term core for the dense part of the cloud appointed by molecular line or dust continuum observations. If it separates further, I will use the term clump or sub-clump.

2.1 MCLD 123.5+24.9

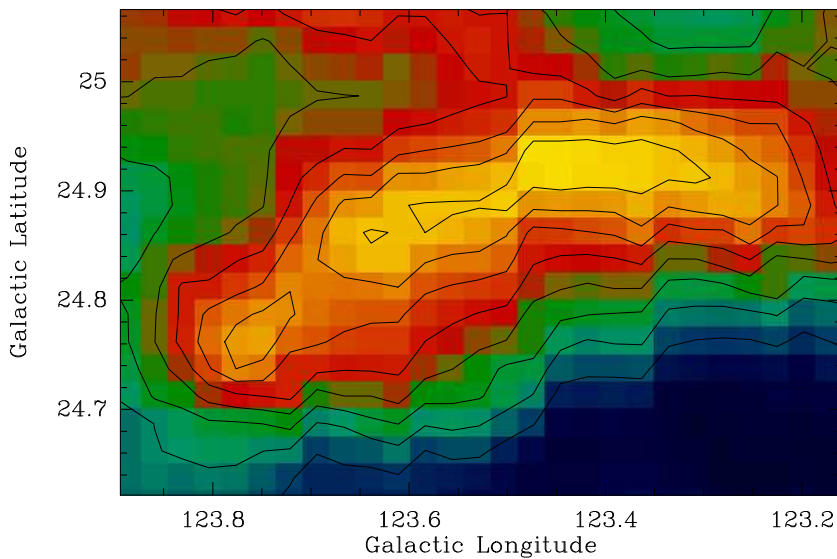


Figure 2.1: Map of the IRAS $100\ \mu\text{m}$ emission of MCLD 123.5+24.9. The contours start at $6\ \text{MJy/sr}$ with an increment of $1\ \text{MJy/sr}$. The resolution is about $5'$. It shows the outline of the cloud well, but hardly any core can be seen.

MCLD 123.5+24.9 is located in the Polaris Flare (see Figure 1.1), a large cirrus cloud complex in the direction of the north celestial pole (Heithausen & Thaddeus 1990). It is our prime example of a cirrus cloud core and has already seen a fair number of various studies.

The cloud itself (see Figure 2.1 for the outline) was first described in detail by Großmann et al. (1990) in a study of OH, CO, and ^{13}CO emission, and H_2CO absorption based on the IRAS $100\ \mu\text{m}$ emission map (Figure 2.1). At $100\ \mu\text{m}$ the warm dust component accounts for the major fraction of the emission. The investigators found a good overall correlation of the molecules (the OH much better than the CO) with the dust emission, and an enhanced hydroxyl abundance.

The ^{13}CO emission line and the H_2CO absorption already show the existence of several small cores along the filamentary cloud. But there was one especially prominent one at the

north-east part of the cloud, which is also visible in extinction in deep B band images (see Bernard et al. 1999). For an outline of the core see Figure 2.2. Großmann & Heithausen (1992) later concentrated on this core and conducted observations in several rare isotopes and high dipole moment molecules ($C^{18}O$, HCO^+ , HCN , HNC , and NH_3). The findings of this investigation were:

- Substructure in all molecules down to the highest angular resolution of $40''$.
Large differences in the intensity distribution of the various molecules.
- Lower abundances for most of the molecules than in typical dark clouds.
- The core itself is much closer to virial equilibrium than the whole cloud
- Kinetic temperatures of the molecules ranging from 6 K to 15 K
- The HNC/HCN ratio of about unity excludes shock interactions and indicates low temperature gas chemistry.

Further molecules detected in the core were SO (Heithausen et al. 1995), CS , DCO^+ , CCH , C_3H_2 , and HCS^+ (Gerin et al. 1997). Surprisingly, the SO emission found is strong and fairly extended, resulting in a high abundance, which is typical for cores in dark clouds. Standard chemical models for cool, dense cores cannot explain this high SO abundance in accord with the lower abundance of other molecules. A further surprise was the very low deuterium fractionation observed by Gerin et al. (1997) which is equally hard to interpret. We should also note here the differences of the integrated intensity distributions of the various molecules (see Figure 2.3).

Bernard et al. (1999) presented dust continuum observations made with IRAS, ISO and PRONAOS ("PROjet NAtional d'Observation Submilletrique", a balloon-borne instrument). They found indications for cold dust at 13 K with a steep dust emissivity index of $\beta = 2.2$ for the cloud and even lower values for the core ($T_d = 11.5$ K, $\beta = 2$). They concluded that the dust temperature is too low for such a low visual extinction and that the dust particles are different to the solar neighbourhood, possibly indicating a lack of very small grains. This could be caused by the adsorption of small particles onto the surface of larger size grains.

The distance of the cloud is, nevertheless, only inaccurately determined to between 100 pc and 240 pc (cf. Heithausen et al. 1993). There are some reasons for this. The first argument is the low v_{LSR} (Local System of Rest) velocity of -4.3 km s $^{-1}$, which is one indication that the cloud is nearby. Zagury et al. (1999) conducted an optical study and tried to explain the illumination of the cloud by the star Polaris, the North star, 1° north of the cloud position. Within this interpretation, the cloud would be located between 105 pc and 125 pc from the Sun and 6 pc to 25 pc in front of Polaris.

The upper limit of 240 pc follows from extinction measurements. Absorption line studies towards nearby stars indicate a lower limit of about 100 pc. It then would be located

directly at the borders of the local cavity filled with a very hot, low-density gas, often referred to as the Local Hot Bubble (Snowden et al. 1998) and extending about 90 pc in this direction. Most of the above described papers assume a distance of 200 pc or even 240 pc, however, in the most recent papers of Heithausen (1999) and Heithausen et al. (2002) a value of 150 pc is assumed, which we shall adopt here as well, for comparableness. In Table 2.2 we have compiled the basic properties of the core, known so far.

Table 2.2: The basic properties of the core in MCLD 123.5+24.9.

Parameter	Value	Reference
Cloud name	MCLD 123.5+24.9	Großmann et al. (1990)
Galactic coordinates	l=123.69, b=+24.89	Großmann et al. (1990)
Right ascension α	01:59:24.09	
Declination δ	+87:39:42.05	
Distance	100 pc - 240 pc	Heithausen et al. (1993)
Adopted distance	150 pc	Heithausen (1999)
Systemic velocity	-4.3 km s ⁻¹	Großmann & Heithausen (1992)
Mass	1.2 M _⊙	Heithausen (1999)
Kinetic temperature	6 K - 15 K	Heithausen (1999)
Dust temperature	11.5 - 13 K	Bernard et al. (1999)

Heithausen (1999) reported evidence for inward motion in the core based on new CS mapping observations in three transitions ((J=2 → 1), (3 → 2), and (5 → 4)) made with the IRAM 30-m telescope with the high angular resolution of 24'' at 98 GHz, 16'' at 147 GHz, and 10'' at 245 GHz. The core appears as a filamentary structure harbouring three dense condensations or sub-clumps, denoted as CS-A, CS-B, and CS-C (see Figure 2.3). The southernmost one shows asymmetric self-absorbed CS (2 → 1) and (3 → 2) lines with the blue shifted part brighter than the red shifted, and the (5 → 4) line exactly at the absorption dip. This feature represents the classical signature of inward motion as it is predicted by the Shu-model (Shu 1977) of a inside-out collapse (e.g., Evans 1999 for a review).

This discovery raised the question of the star-forming ability of cirrus clouds anew. Heithausen et al. (2002) observed the core in the dust continuum emission at 250 GHz with MAMBO at the IRAM 30-m telescope with an angular resolution of 11''. In Figure 2.3 the result is shown together with a C¹⁸O map from Falgarone et al. (1998). The core is clearly detected as an elongated filament, similar to the CS structure, but with significant differences. For instance, there is no indication of three sub-clumps. The best correlation between dust and molecular line emission can be found for the C¹⁸O (1 → 0) line.

In this paper, Heithausen et al. (2002) also presented new observations of the HC₃N (3 → 2), (4 → 3), and (10 → 9) transitions carried out with the MPIfR 100 m telescope in

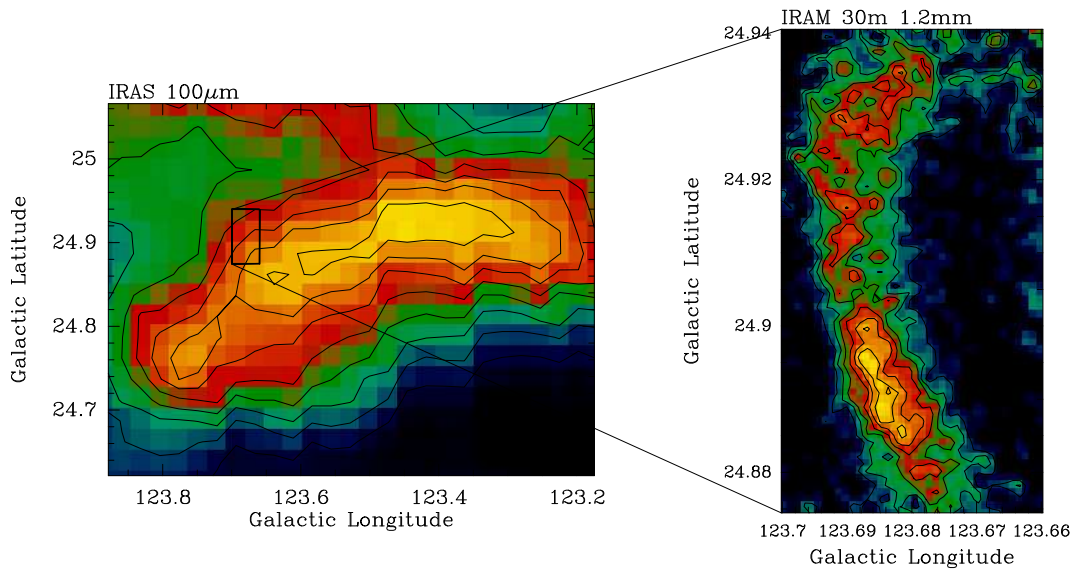


Figure 2.2: Map of the $100\ \mu\text{m}$ emission of the cloud obtained by the IRAS satellite and the $1.2\ \text{mm}$ dust continuum emission map of the core observed with MAMBO at the IRAM 30-m telescope by Heithausen et al. (2002). Contours are every $1\ \text{MJy/sr}$ starting at $6\ \text{MJy/sr}$ for the IRAS map and every $2\ \text{mJy}$ starting at $0\ \text{mJy}$ for the MAMBO map. The resolution of the IRAS map is about $5'$, whereas the resolution of the MAMBO map is about $11''$.

Effelsberg and the IRAM 30-m telescope in Granada/Spain. The angular resolution of the maps is about $30''$. The distribution of this molecule is very different from the dust continuum and also from the CS emission. The filamentary core is only rudimentary visible, instead it peaks at two distinct clumps, located at the ends of the filament and denoted as $\text{HC}_3\text{N-A}$ and B (see Figure 2.3). A similar behaviour was only found for the ammonia molecule (Großmann & Heithausen 1992), made with a lower angular resolution of about $40''$. The HC_3N clumps do somewhat overlap with the condensations seen in CS, labeled CS-A and CS-C, however, the intensity peaks are clearly shifted toward the ends of the filament. The CS sub-clump in the mid, denoted as CS-B, has no corresponding HC_3N feature, only some very weak emission, but at the detection limit, can be seen there.

The reason for this behaviour of the HC_3N emission could be either a strong variation in the excitation conditions, or, alternatively, strong variations of the abundance of the molecule on smallest scales. It is very unlikely, that the excitation conditions vary strongly along the filament. The environment is very quiescent and the core is embedded within the larger cloud complex. Furthermore, other tracers of the gas like, C^{18}O and the dust emission, correlate very well. Could it therefore be, that this is an effect of strong variations in the abundance of the HC_3N molecule along the filament? In their paper, Heithausen et al. (2002) speculate that the molecular abundance gradient is an age effect, caused by the different timescales the molecules need to build up after the formation of the core. CS,

for example, is formed very fast, whereas HC_3N and NH_3 need at least a few 10^5 years to reach measurable high abundances.

The shifting of the peak emission of HC_3N relative to $\text{CS}(2 \rightarrow 1)$, on the other hand, could also be an effect of the self-absorption seen in this CS transition. On this account, the integrated intensity of the $\text{CS}(2 \rightarrow 1)$ line is not a reliable tracer. Another effect that may play a role is depletion, due to freezing out of molecules on dust grains, what would appear also as a change in the abundance.

We now have a so far unequalled set of observations of this cirrus cloud core in the dust continuum and all kinds of molecules and their different transitions. In Figure 2.3 we show a selection of the integrated intensity maps to give a visual overview about what we explained in this section. Based on the data, collected up to this point, a complicated, sometimes even chaotic picture of the core emerged. Clearly more observations were needed, especially with a higher angular resolution, because the CS and HC_3N data did not resolve the individual clumps. In this study we concentrate on the most interesting clump, the southernmost, because it shows the infall motion signature. But, if possible, we also collected data for the other parts of the core, that are definitely worth to be published.

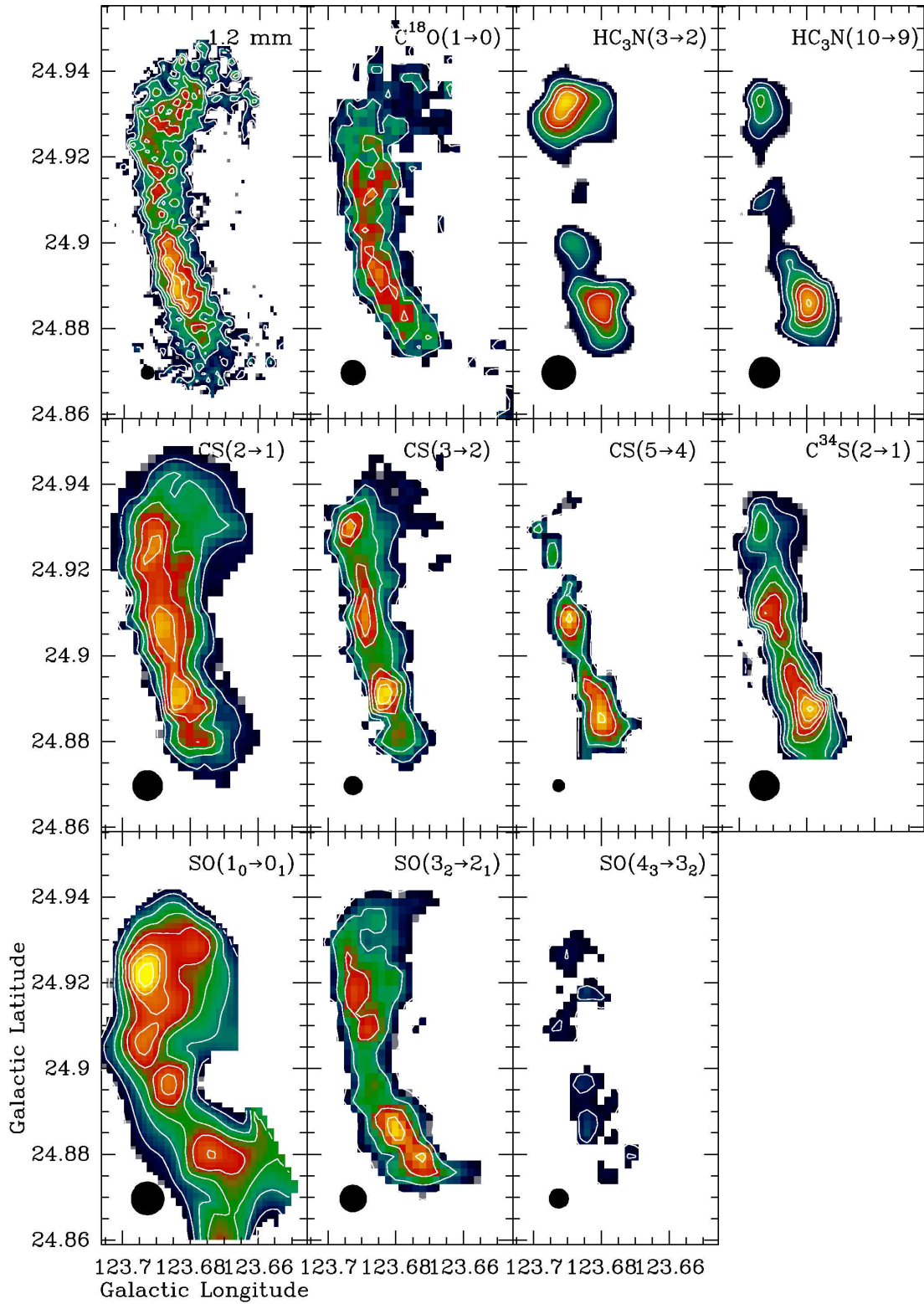


Figure 2.3: A compilation of integrated intensity distributions of the core in MCLD 123.5+24.9. Beam sizes are indicated in the lower left corners. References are given in the text.

2.2 MCLD 126.6+24.5

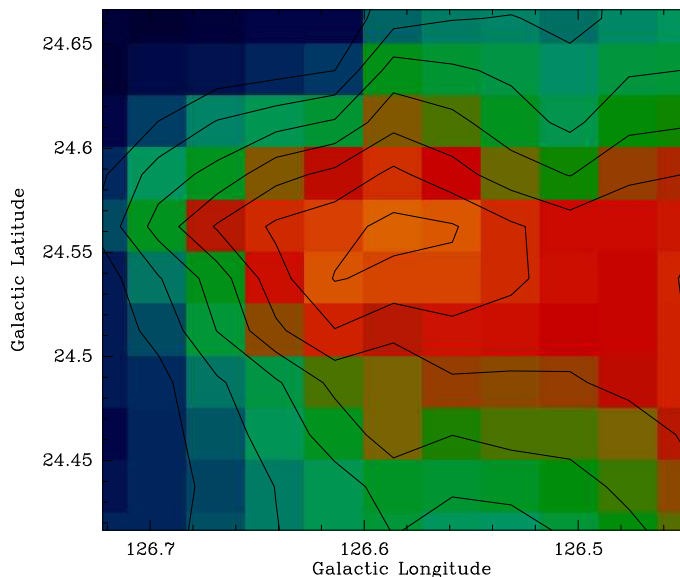


Figure 2.4: Map of the IRAS $100\ \mu\text{m}$ emission of MCLD 126.6+24.5. The contours start at $4.4\ \text{MJy/sr}$ with an increment of $0.6\ \text{MJy/sr}$. The resolution is about $5'$.

MCLD 126.6+24.5 is located in the Polaris Flare, too. It has also seen a fair number of molecular line studies and a variety of molecules were detected. The cloud was first noted by Lynds (1965) as the small reflection nebula LBN 628 (Lynds Catalogue of Bright Nebulae) on the POSS (Palomar Observatory Sky Survey). It reemerged in 1987 as one of the first high latitude clouds detected in NH_3 (Mebold et al. 1987). Boden & Heithausen (1993) presented a multi-molecular study of this cloud in CO , ^{13}CO , H_2CO , and NH_3 . They found abundances of the molecules normal for dark clouds and substructures down to the scale of the smallest beam-size. They mapped the ammonia core with the Effelsberg 100 m telescope with an angular resolution of $40''$ and the following studies all concentrated on this core. We shall mention here the discovery of sulphur monoxide (SO) by Heithausen et al. (1995) and the investigation of Heithausen et al. (1998) where they presented an detailed analysis of an extensive SO mapping of the core and a SO -to- CS comparison. The SO map (Figure 2.5) shows 17 small, individual sub-clumps and does not correlate with other dense gas tracers, especially not with the CS molecule.

The distance of this cloud is even less well determined than that of MCLD 123.5+24.9, despite the fact, that it is located just a few degrees away and belongs to the same cloud complex. Although, some of the papers cited above just assume a distance of 100 pc, we will here in this study adopt an equal distance as for MCLD 123.5+24.9, which is 150 pc. This assumption seem also justified by the low systemic velocity of $-3.8\ \text{km s}^{-1}$, which is even a bit lower than that of MCLD 123.5+24.9.

In Figure 2.4 we show the IRAS 100 μm emission map of the cloud and in Table 2.3 we summarize the basic properties of the core in MCLD 126.6+24.5, known so far.

Table 2.3: The basic properties of the core in MCLD 126.6+24.5.

Parameter	Value	Reference
Cloud name	MCLD 126.6+24.5	Boden & Heithausen (1993)
	LBN 628	Lynds (1965)
Galactic coordinates	$l=126.61, b=+24.55$	Boden & Heithausen (1993)
Right ascension α	04:23:02.46	
Declination δ	+85:48:16.3	
Distance	100 pc - 240 pc	Heithausen et al. (1995)
Adopted distance	150 pc	
Systemic velocity	-3.8 km s^{-1}	Heithausen et al. (1995)

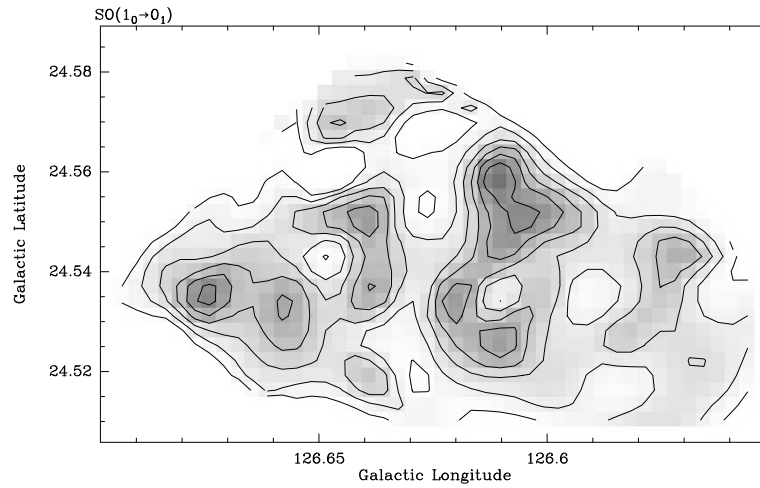


Figure 2.5: Map of the integrated $\text{SO}(1_0 \rightarrow 0_1)$ transition at 30 GHz obtained with the Effelsberg 100 m telescope. Contours are every 0.12 K km s^{-1} starting at 0.2 K km s^{-1} . The beam-size is about $30''$. From Heithausen et al. (1998)

2.3 L 1457

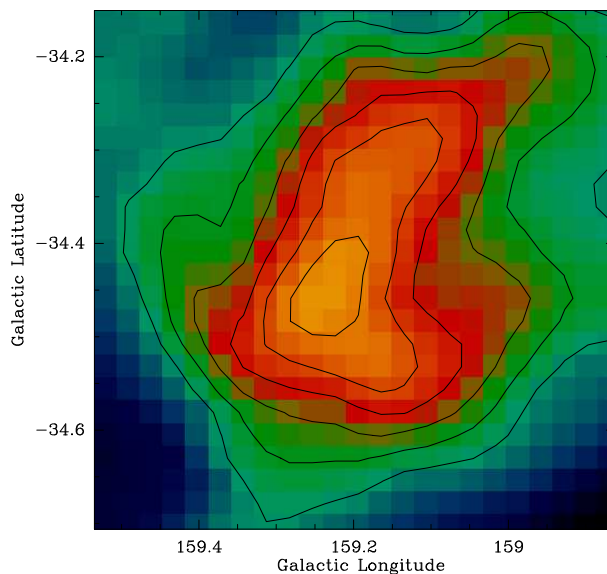


Figure 2.6: Map of the IRAS $100\ \mu\text{m}$ emission of the core in L 1457. The contours start at $20\ \text{MJy/sr}$ with an increment of $3\ \text{MJy/sr}$. The resolution is about $5'$.

The cirrus cloud L 1457 (originally LDN 1457, from Lynds Catalogue of Dark Nebulae (LDN), Lynds 1962) is part of the well known cirrus cloud complex MBM 12 (MBM 1985) located in the constellation Aries directly at the southwestern corner of the huge Perseus-Taurus-Auriga cloud complex. It was first noted by Lynds (1962) on the POSS as a low-absorption dust cloud. Ungerechts & Thaddeus (1987) mapped the Perseus-Taurus-Auriga-Aries complex in $^{12}\text{CO}(1 \rightarrow 0)$ at an angular resolution of $0''.5$. L 1457 lies within their cloud # 1 which covers $4''.7$. They noted an extremely large line width of $7\ \text{km s}^{-1}$, probably caused by the blending of several clumps. Referring to the close neighbourhood of the Pleiades they placed it at a distance of roughly 125 pc.

MBM (1985) already cataloged it together with LDN 1458 as cloud # 12 and later determined the distance of the cloud to 65 pc by measuring absorption lines of nearby stars (Hobbs, Blitz, & Magnani 1986). This made L 1457 the nearest molecular cloud known, lying within the local, very hot, low-density gas known as the *Local Hot Bubble* (Snowden et al. 1998), which extends to about 90 pc in this direction. However, this distance estimate may not be valid for the whole cloud, but only for one or some components. Andersson et al. (2002) claim that there are two components toward the MBM 12 cloud, with a dense part at 360 pc and a thin layer at 80 pc, whereas Luhman (2001) suggests the distance of the whole cloud to be 275 pc estimated from photometric measurements of nearby foreground and background stars.

Altogether, a distance between 65 pc and 200 pc seems consistent with the published data. We want refer also to Hearty et al. 2000 and Straizys et al. 2002 for additional, different

distance estimates. We will adopt the distance of 65 pc throughout this work, but may keep in mind a possible larger distance of about 200 pc, alternatively.

Pound et al. (1990) presented an extensive map of the cloud in various CO lines with an angular resolution of $100''$. They found a large number of substructures down to the scale of the beam. None of the clumps appeared gravitationally bound and they saw no evidence for recent star-forming activity. Further fragmentation into smaller pieces within the clumps seemed very likely. However, they claimed that a relatively large amount of energy is needed to explain the kinematics and spacial distribution of the CO clumps and a possible explanation could be an evaporating molecular cloud that is eaten away by the hot interstellar medium. This scenario would rule out ongoing star-formation as the lifetime of the cores is much too short in such a case.

On the other hand, Zimmermann & Ungerechts (1990) presented a similar CO mapping with the KOSMA telescope and an angular resolution of $2''$. Their conclusions differ in some aspects from the findings of Pound et al. (1990). Their maps show also a lot of substructures and the high velocity dispersion. But they argue, that it could not be ruled out that some cores within the clumps are gravitationally bound, as one finds more and more substructures with higher and higher angular resolution. They also claimed that the distance of 65 pc may not be valid for a significant part of the cloud. A further distance would make the clumps more massive and therefore the cores within could well be bound.

Table 2.4: The basic properties of the core in L 1457.

Parameter	Value	Reference
Cloud name	L 1457 or LDN 1457 part of MBM 12	Lynds (1962) MBM (1985)
Galactic coordinates	l=159.25, b=-34.48	Pound et al. (1990)
Right ascension α	02:56:10.11	
Declination δ	+19:26:59.53	
Distance	65 pc - 160 pc	Zimmermann & Ungerechts (1990)
Adopted distance	65 pc	
Systemic velocity	-5.06 km s ⁻¹	Pound et al. (1990)

Another detail makes the cloud a special case and different from most other cirrus clouds. A small number of low-mass T-Tauri stars have been detected in the direction of the cloud. They are located north of the core investigated by us and the nearest ones are more than $30'$ away. The first ones were already detected by Herbig & Bell (1988). A good overview can be found in the paper by Hearty et al. (2000), where they presented ROSAT observations. Jayawardhana et al. (2001) detected proto-planetary discs around some of them, and Hogerheijde et al. (2003) even found indications for grain growth in some of the cold dust discs surrounding the stars. However, it is still not clear, whether these T-Tauri stars are associated with the cloud or if they belong to an older, already

dispersed cloud. Exact distance estimates of both the cloud and the T-Tauri stars could reveal a possible relationship.

For these reasons, L 1457 is the core were we would expect soonest to find indications of ongoing star-formation activities.

In Figure 2.6 we show the IRAS $100\ \mu\text{m}$ emission map of the core region and in Table 2.4 we summarize the basic properties of the core in L 1457 known so far.

2.4 MBM 32

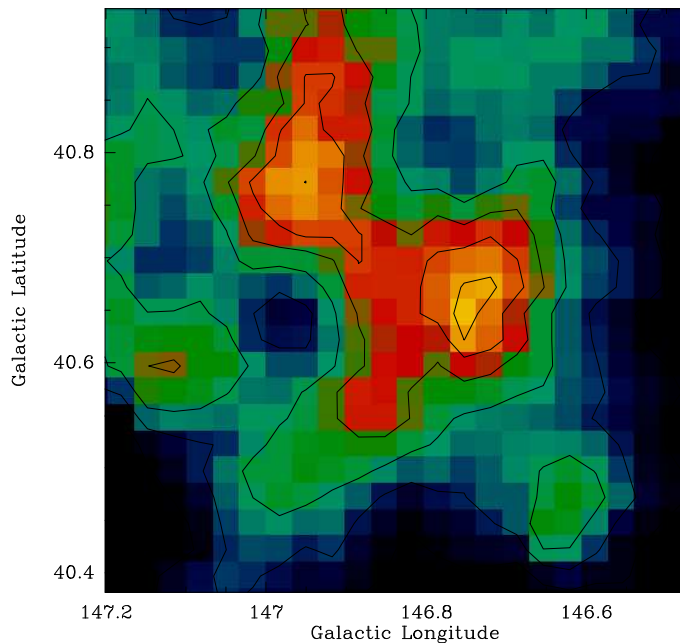


Figure 2.7: Map of the IRAS $100\ \mu\text{m}$ emission of the core in MBM 32. The contours start at $4\ \text{MJy/sr}$ with an increment of $1\ \text{MJy/sr}$. The resolution is about $5'$.

The cirrus cloud MBM 32 was first catalogued as LBN 691 by Lynds (1965) and later as MBM 32 by MBM (1985). It is located in the complex known as the Ursa Major cirrus cloud (de Vries et al. (1987)). This cloud is one of the first cirrus clouds where H_2CO (Heithausen et al. 1987) and NH_3 (Mebold et al. 1987) were detected. Based on a multi-transition CO and NH_3 study at one position, Schreiber et al. (1993) derived a kinetic temperature of $24_{-5}^{+10}\ \text{K}$ and were able to model 7 different CO transitions with a beam averaged ($4'$) H_2 column density of about $2 \times 10^{20}\ \text{cm}^{-2}$ and a power law density distribution.

Wouterloot et al. (2000) presented a new multi-line CO study of the cloud and showed that it consists of three components - a main cloud component at $v_{\text{LSR}} \approx 2$, a smaller component at $v_{\text{LSR}} \approx 0$, and in addition some emission in between those two velocities. They also

derived a dust temperature from the ratio of the IRAS $60\ \mu\text{m}$ and $100\ \mu\text{m}$ emission of 20 K.

The core we will concentrate on, was first defined through the NH_3 detection and shows only the main-cloud component at v_{LSR} about $+3.5\ \text{km s}^{-1}$. It is located north-west of the cloud centre. Heithausen et al. (1998) also detected $\text{SO}(1_0 \rightarrow 0_1)$ and relatively weak $\text{CS}(2 \rightarrow 1)$ emission towards this position. A comparison of the CS emission with a non-detection by Reach et al. (1995) was interpreted as a low beam filling factor caused by clumping.

A distance towards MBM 32 has not yet been determined. Most papers just assume a distance of 100 pc and we will follow this example throughout this work by lack of other possibilities.

Table 2.5: The basic properties of the core in MBM 32.

Parameter	Value	Reference
Cloud name	MBM 32	MBM (1985)
	LBN 691	Lynds (1965)
Galactic coordinates	$l=146.85, b=+40.66$	Heithausen et al. (1998)
Right ascension α	09:33:52.38	
Declination δ	+66:06:05.04	
Distance	100 pc	Wouterloot et al. (2000)
Adopted distance	100 pc	
Systemic velocity	$3.5\ \text{km s}^{-1}$	Heithausen et al. (1998)

2.5 Draco

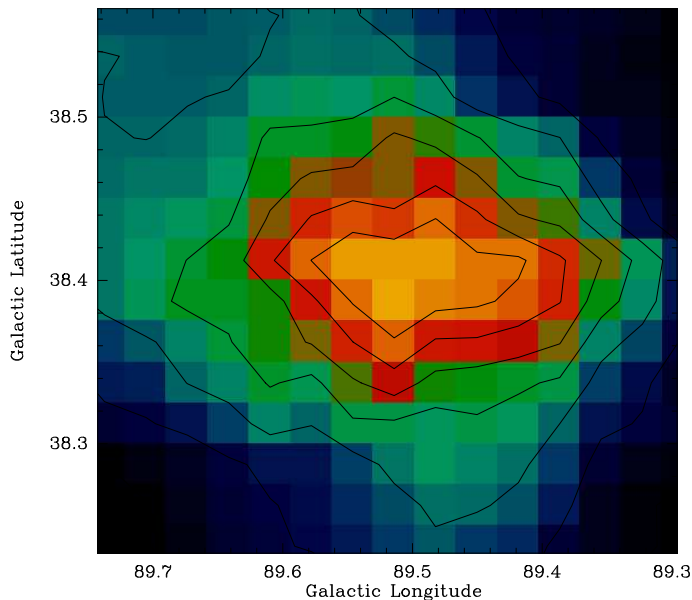


Figure 2.8: Map of the IRAS $100\ \mu\text{m}$ emission of the core in Draco. The contours start at $1\ \text{MJy/sr}$ with an increment of $1\ \text{MJy/sr}$. The resolution is about $5'$.

The Draco molecular cloud is not a nearby cirrus cloud, but a more distant *Intermediate Velocity Cloud* (IVC). Nevertheless, it was classified by MBM (1985) as MBM 41, belonging to a larger cloud complex and investigated in more detail by Mebold et al. (1985). They observed CO and H₂CO and addressed the question if the cloud is a halo object merging with the galaxy. The findings were a large total mass for the whole cloud complex of about $10^4\ M_{\odot}$ for a assumed distance of 800 pc and probably gravitationally bound clumps. One of their clumps is the core shown in Figure 2.8 as seen with IRAS in the $100\ \mu\text{m}$ dust emission.

Draco is probably the best studied IVC and can also be seen very good in X-ray absorption (e.g., Kerp 1994), providing a direct hint for the hot ISM in the halo of our Galaxy. It is strongly suggested that the cloud is interacting with this hot plasma and therefore somewhat different from the nearby cirrus clouds.

In a very detailed investigation Gladders et al. (1998) derived a distance bracket to the cloud of 463_{-136}^{+192} to 618_{-174}^{+243} pc, by estimating the distances of foreground and background stars from spectroscopic parallaxes. The errorbars are, however, still quite large of about between 25% and 40%.

On the other hand, Penprase et al. (2000) conducted a photometric study and derived a distance bracket to the cloud of $800 < d < 1300$ pc. This would correspond to a height $|z| = 640$ pc above the galactic plane and linear dimensions as large as 40 pc for the cloud. They noted that with this distance the Draco cloud would be quite an exceptional object.

Hence, additional observations and theoretical work are clearly needed to provide more accurate constraints on the properties of the Draco nebula.

Throughout this work we will assume a distance of 500 pc to simplify matters. This introduces a additional error in our derived values, but it is very small compared to other uncertainties.

Table 2.6: The basic properties of the core in Draco.

Parameter	Value	Reference
Cloud name	Draco	Mebold et al. (1985)
	MBM 41	MBM (1985)
Galactic coordinates	l=89.53, b=38.40	Heithausen et al. (1998)
Right ascension α	16:49:17.88	
Declination δ	+59:56:26.89	
Distance	327 pc - 861 pc	Gladders et al. (1998)
Adopted distance	500 pc	
Systemic velocity	-24.1 km s ⁻¹	Heithausen et al. (1998)

3

Dust Continuum Observations

"The most fundamental fact about molecular clouds is that most of their contents are invisible" (Evans 1999). This phrase describes the problems one experiences by studying the ISM very well. Neither the H_2 nor the He in the majority of the clouds can directly be observed. There are some observations of fluorescent emission of H_2 over the face of clouds (Luhman & Jaffe 1996) and in shocked regions H_2 emits rovibrational lines that are useful (e.g., Draine & McKee 1993). But these are very special cases and they do not trace the bulk of molecular clouds. Absorption lines of H_2 in far-UV spectra of background sources can also be used but are restricted to a few cases (e.g., Richter 1999).

To probe the physical conditions of the molecular clouds we need the help of trace constituents such as dust particles and molecules other than H_2 . This is possible because the ISM is generally well mixed. The inference to the H_2 , however, is difficult since abundance and properties of the tracer may differ strongly from region to region, even at smallest scales. One very good tracer, becoming more and more important, is the dust, or more accurately, the thermal continuum emission of dust particles heated by the ISRF. It is also the one least understood up to now. We do not even know yet, how dust particles look like.

3.1 Dust Continuum Emission

Dust particles attenuate light at short wavelengths (UV to near infrared) and re-emit at longer wavelengths (far infrared to millimeter). The critical points in this business are the assumption of a (constant) gas-to-dust ratio and the dust grain properties. The gas-to-dust ratio can be adopted to be nearly constant in a manageable volume because of the very efficient mixing of the ISM. If the same value, however, can also be applied to very different regions, e.g., the galactic halo or other galaxies, is questionable. The dust grain properties are even more difficult, in fact, up to now we know very little about it

and have to rely on quite simplistic models. The models suffer from the fact that the geometrical structure as well as the exact chemical composition of interstellar dust grains is only vaguely known. Nevertheless, these models are able to reproduce the observations successfully in a variety of cases.

In general the models consist of large grains with sizes of a few tens of Å to about one μm and of transiently heated particles (see, e.g., Draine (2003) for a review). Because of their high heat capacity the large grains are in thermodynamical equilibrium with the interstellar radiation field and reach temperatures typically of 10 to 30 K. The emission can be described by a "grey body", which means a black body Planck curve modified by the optical depth. This follows from the equation of radiative transfer in the case of optically thin emission. And as the optical depth is related to the column density of the H_2 , this relates the observed dust emission intensity directly to the H_2 column density (see section 5.1 for the formulas).

The dust continuum emission provides one of the best estimates of the H_2 column density, much more reliable than the commonly used H_2 -tracer CO. This is because CO reacts very sensitive to metallicity and radiation distinctions. The dust, on the other hand, should react much less to variations, as it consists of various components. The observation of dust continuum emission itself is difficult as well. Only recently the technics became available to map larger areas with adequate large telescopes from the ground. The development of bolometer arrays (e.g., Kreysa 1990), one can almost call them cameras, and, last but not least, the fast evolution in computational power are the crucial points in this.

3.2 Observations

The observations of the dust continuum emission at 1.2 mm wavelength are the starting point of our study and were carried out in 2000 and 2001 with the Max-Planck-Millimeter-Bolometer (MAMBO) arrays at the IRAM 30-m telescope on Pico Veleta in Granada/Spain (see Figure 3.1).

The MAMBO arrays are developed and build by the *Max-Planck-Institut für Radioastronomie* (MPIfR) in Bonn. One bolometer consists of a Neutron-Transmutation-Doped Germanium element cooled by a ^3He cryostat to about 300 mK. Bolometers are broadband receivers, actually heat detectors, and sensitive to all incoming radiation (photons). By means of filters one defines the sensitivity range and the effective frequency. MAMBO is sensitive between about 210 and 290 GHz with an effective frequency of 250 GHz. The arrays are arranged in a hexagonal structure (see Figure 3.2) with a spacing of $23''$ between the individual beams. The FWHM of one beam is $11''$ at the effective wavelength of 1.2 mm. A detailed description of the design and the characteristics of the 37-channel array can be found in Kreysa (1990) and Thum et al.(1992), the 117-channel array exhibits in principle similar properties.



Figure 3.1: The IRAM 30-m telescope on Pico Veleta near Granada/Spain.

In a first attempt we mapped the 5 cores introduced in the prior chapter with the MAMBO 37-channel array and detected all of them. However, due to the wide extent of the emission and unstable weather conditions these maps were not sufficient enough to properly restore the emission structure. Hence, we re-observed them in the next period with the then new MAMBO 117-channel array.

All observations were done in double-beam on-the-fly mode, with scanning the source along lines of constant azimuth and chopping the secondary mirror in the same direction at a speed of 4 or $5''\text{s}^{-1}$. The spacing between the lines is $4''$. This method produces heavily oversampled maps with an on-off signature inside - so called "double beam" maps. These have to be restored.

Pointing and focus were checked at regular intervals on planets and strong continuum sources. The pointing accuracy was found to be mostly better than $4''$. To obtain the atmospheric opacity the sky emission was measured regularly at a number of elevation angles (so called "skydip" measurements). On availability primary (planets) or secondary (HII-regions or YSOs) calibrators were observed to derive the flux conversion factor.

3.3 Data Reduction

The data reduction was conducted using the program MOPSI written by Robert Zylka and the basic script for map reduction written by Frank Bertoldi. The first step was to identify and delete "bad channels", showing no signal or having an extremely increased

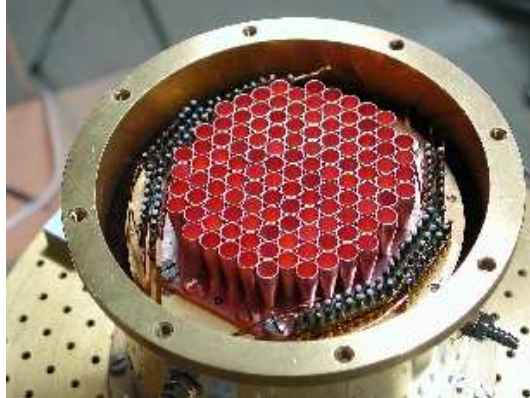


Figure 3.2: The MAMBO 117 array build by the MPIfR. The horns are arranged in a hexagonal structure and the whole detector is then placed in a cryostat and cooled down to about 300 mK.

noise level. Some of them are present all the time and some appear from time to time due to problems in the electronics. Next was to remove spikes, which frequently appear within the electronics by interferences or due to cosmic rays. Further steps were to correct for the individual gains of the single channel-bolometers and for the sky opacity. Afterwards each scan was calibrated, i.e. the signal was converted from counts to Jy/beam, using the conversion factor calculated with a linear interpolation between the adjacent calibrator flux measurements.

After this the maps had to be restored using the Emerson-Klein-Haslam (EKH) algorithm (Emerson, Klein, & Haslam 1979). This was done with the task "dbf" of the MOPSI program package. At last, all the individual maps that were considered to be sufficiently good had to be coadded together. Since we tried to map in different directions and with different map sizes to avoid systematical observing errors, the resulting map is relatively large, however, at the edges the noise increases highly. Hence, the boundaries were cut away by applying a mask. This is mainly done to improve the representation. Unfortunately, two of the cores are located or widespread near to one boundary and some of the features seen there may partly be caused by the higher noise level.

3.4 Results

Figures 3.3, 3.7, 3.5, and 3.9 show the results of our 1.2 mm dust continuum observations. The cores could all be detected, however, mostly at a low signal-to-noise ratio (1σ contour lines). The morphology of the core sample is neither simple spherical nor pure filamentary but rather complicated. However, the maps are way too small to speculate about the filamentary structure. Much larger maps would be needed for this purpose. We here only

concentrated on surveying and mapping the cores that are already known from previous line observations.

In order to enhance the sensitivity of the maps and the visibility of the core structures we convolved each map with a $20''$ Gaussian, similar to the analysis of Tafalla et al. (2002). The results are shown in Figures 3.4, 3.8, 3.6, and 3.10. However, this is done only for the purposes of presentation, all the analysis were carried out on the original maps. Admittedly, in these maps the signal-to-noise ratio is not very high. In fact, most of the very small structures one can see, are possibly due to the map noise in conjunction with the high resolution. Hence, we do not trust the exact small scale structures of the cores and only derive the basic overall properties.

The cores in MCLD 126.6+24.5 and Draco do not show a plain central condensation. In fact, they do appear more like a loose accumulation of small sub-clumps. However, some of the small clumps visible are most likely caused by the noise of the map and an additional effect of the high resolution, as stated above. Nevertheless, the core region clearly raises in flux intensity from the background and is detected with a signal-to-noise of about 3 to 4σ .

In L 1457 two small roundish clumps and a larger condensation, possibly also consisting of smaller clumps, are visible. Each one has a rather high flux density and they are detected with a signal-to-noise of more than 4σ . Nevertheless, there are also strong indications for a more diffuse component between these clumps. We will denote the clumps from down right to up left with A, B, and C. At this, C is the larger condensation, which is without much doubt caused by a superposition of several smaller clumps.

In MBM 32 one eventually sees a central condensed core, nevertheless, containing a lot of substructure and an elliptical shape. However, the flux density is quite low and the core is scarcely detected with a signal-to noise of about 3σ . There are also some indications of a more diffuse component we missed with the observing technique.

Table 3.1: The results of the dust continuum observations. Listed are the map centres and the achieved rms.

Core	l [deg]	b [deg]	α_{2000} [h m s]	δ_{2000} [$^{\circ}$ ' '']	rms [mJy]
MCLD 126.6	126.61	24.55	04 23 02.5	85 48 16.3	3.1
L 1457	159.26	-34.48	02 56 11.8	19 26 42.9	2.7
MBM 32	146.84	40.66	09 33 54.4	66 06 29.4	1.9
Draco	89.52	38.41	16 49 14.0	59 55 51.8	2.9

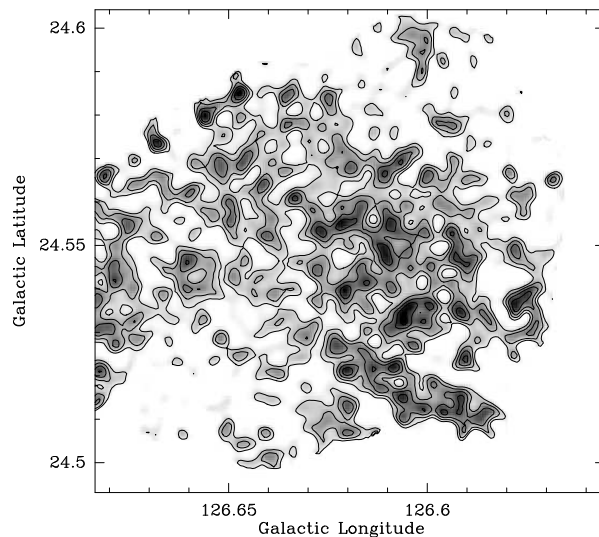


Figure 3.3: Dust continuum emission map of the core in MCLD 126.6+24.5 at 1.2 mm made with MAMBO at the IRAM 30-m on Pico Veleta. Contours are in steps of 3 mJy/beam (1σ) starting at 3 mJy/beam. The angular resolution of the map is $11''$. The edges are masked out.

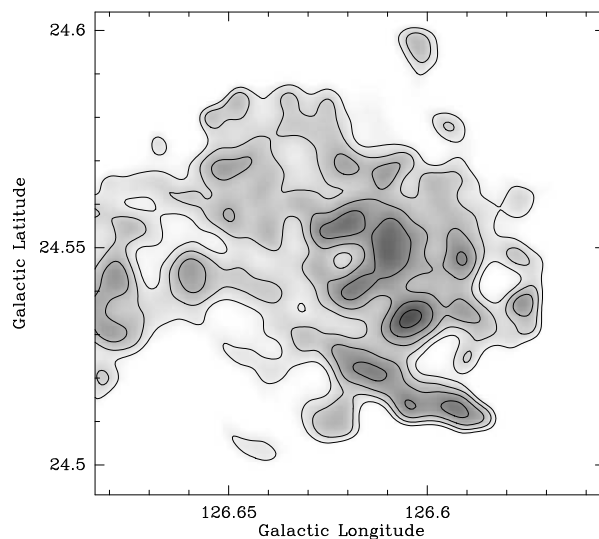


Figure 3.4: Dust continuum emission map of the core in MCLD 126.6+24.5 at 1.2 mm, same as in Figure 3.3. In order to enhance the sensitivity the map has been convolved with a $20''$ Gaussian. Contours are in steps of 2 mJy/beam starting at 2 mJy/beam. Edges are masked out.

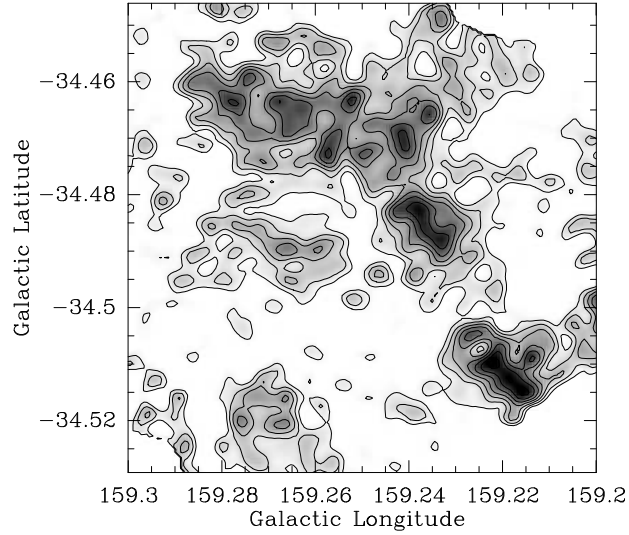


Figure 3.5: Dust continuum emission map of the core in L1457 at 1.2 mm made with MAMBO at the IRAM 30-m on Pico Veleta. Contours are in steps of 3 mJy/beam (1σ) starting at 2 mJy/beam. The angular resolution of the map is $11''$. The edges are masked out.

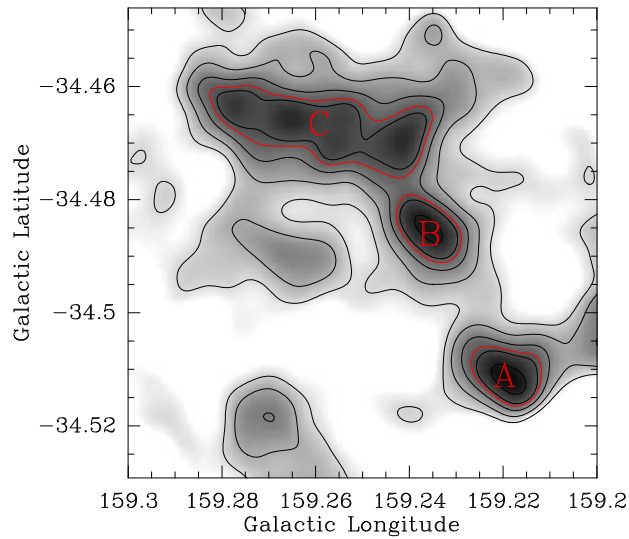


Figure 3.6: Dust continuum emission map of the core in L1457 at 1.2 mm, same as in Figure 3.5. In order to enhance the sensitivity the map has been convolved with a $20''$ Gaussian. Contours are in steps of 3 mJy/beam starting at 2 mJy/beam. Edges are masked out. The red characters and contour lines denote the identified individual sub-clumps.

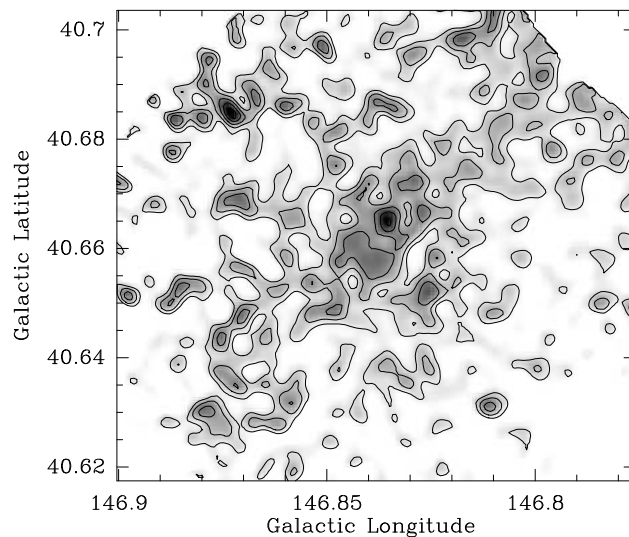


Figure 3.7: Dust continuum emission map of the core in MBM 32 at 1.2 mm made with MAMBO at the IRAM 30-m on Pico Veleta. Contours are in steps of 2 mJy/beam (1σ) starting at 2 mJy/beam. The angular resolution of the map is $11''$. The edges are masked out.

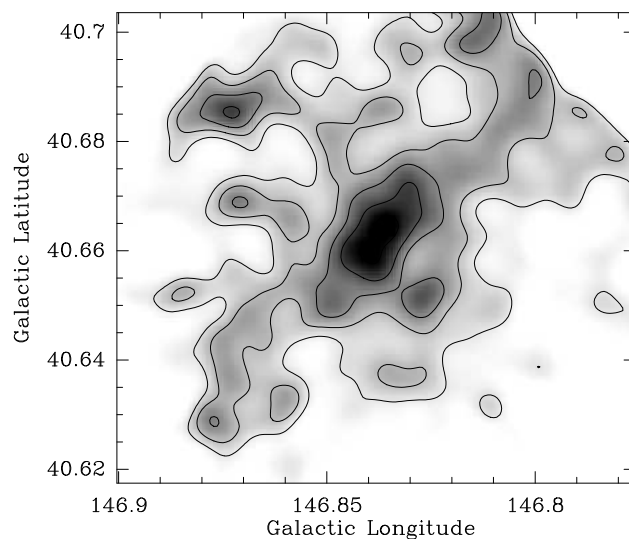


Figure 3.8: Dust continuum emission map of the core in MBM 32 at 1.2 mm, same as in Figure 3.7. In order to enhance the sensitivity the map has been convolved with a $20''$ Gaussian. Contours are in steps of 1.2 mJy/beam starting at 1.2 mJy/beam. Edges are masked out.

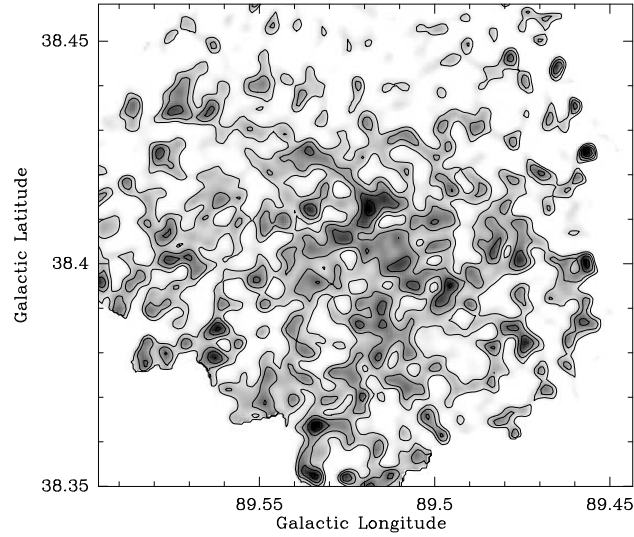


Figure 3.9: Dust continuum emission map of the core in Draco at 1.2 mm made with MAMBO at the IRAM 30-m on Pico Veleta. Contours are in steps of 3 mJy/beam (1σ) starting at 3 mJy/beam. The angular resolution of the map is $11''$. The edges are masked out.

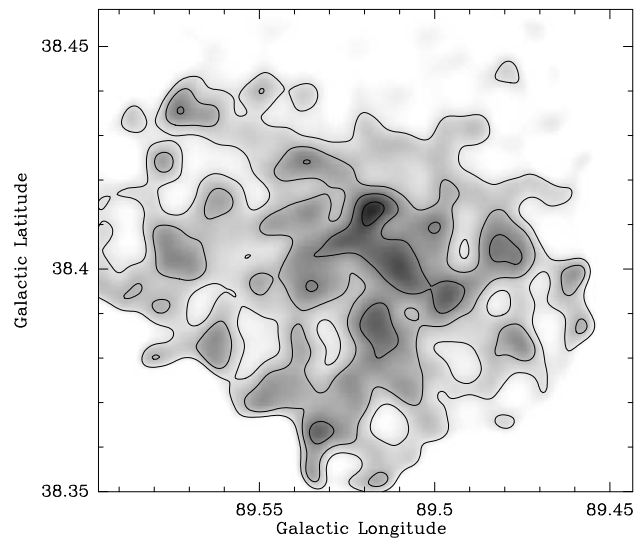


Figure 3.10: Dust continuum emission map of the core in Draco at 1.2 mm, same as in Figure 3.9. In order to enhance the sensitivity the map has been convolved with a $20''$ Gaussian. Contours are in steps of 2 mJy/beam starting at 2 mJy/beam. Edges are masked out.

4

Molecular Line Observations

Observations of the dust continuum provide a good basis to derive the core attributes, however, they only show integrated properties and do not allow any insights into the kinematics or the chemistry. Therefore molecular line observations are crucial. They also probe density and temperature through their excitation, but also turbulent and systematic motions through their line width and Doppler shifts. Admittedly, these observations are often harder to interpret, because the abundance of one molecular species can vary significantly within a fraction of a parsec. It is also sometimes unclear from which part of the core the line emission is actually emanating. However, molecular lines constitute the unique possibility to obtain informations about the kinematic and chemical properties of cores.

4.1 CS as a Dense Core Tracer

The most abundant molecule after H_2 is carbon monoxide (CO). On large scales it correlates well with other density tracers even when the line is quite opaque, however, on small scales it fails to trace the column density and rarer isotopomers or other molecules have to be used. Besides CO the CS is one of the most abundant molecules and commonly used as a tracer of dense cores. It is formed fast after the core formation and the lower transitions mostly are opaque. For this reason CS is also often used to trace a core collapse where the lower transition shows the typical self-absorbed profile and the higher, optically thin, transition peaks between the two peaks of the opaque line (e.g., Evans 1999 for a review).

However, recently it became clear that also the CS is not the best tracer for the densest part of the cores because of the depletion by freezing on dust grains (e.g., Tafalla et al. 2002). If this effect also plays an important role in cirrus cloud cores we will investigate partly in this study together with a following observational program. To get a first overview

about the cores, their extent and shape in CS we conducted mapping observations with the FCRAO 14-m telescope. Additionally we made multi-transition CS observations with the IRAM 30-m telescope at the central positions of the cores or clumps identified in the dust continuum maps. Together with the already introduced previous observations of the cores we exhibit a unique dataset for cirrus cloud cores.

4.2 CS ($2 \rightarrow 1$) Mapping Observations

4.2.1 Observations

Observations with the Five College Radio Astronomy Observatory (FCRAO) 14-m telescope (Figure 4.1) were carried out in April 2003. The telescope is located near Amherst (MA) and operated by the University of Massachusetts, together with Amherst College, Hampshire College, Mount Holyoke College and Smith College. It is build in a radome structure and equipped with a 3 mm single sideband 32 element focal plane receiver array called SEQUOIA (SEcond QUabbin Optical Imaging Array). The primary frequency to



Figure 4.1: The FCRAO 14-m telescope dome near Amherst. The telescope is enclosed in a radome structure.

which we tuned the receiver was 97.98 GHz for the CS ($2 \rightarrow 1$) line. We also tuned to 96.41 GHz for the $C^{34}S$ ($2-1$) line, simultaneously. The 14-m telescope has a beam-width at 98 GHz of about $54''$. We took maps of $10'$ by $10'$ in On-The-Fly (OTF) mapping mode. Pointing and Focus were made regularly on Orion, RCAS, and RLEO. They were

also used to check the calibration. Unfortunately, the weather was not ideal and we were only able to fully map three of the cores, MCLD 126.6+24.5, L 1457, and MBM 32. The achieved rms in the spectra amounts to approximately 0.02 K to 0.03 K and the lines are detected at a more than 3σ level. For Draco we only got a short coverage where the noise of the spectra is still much too high (≈ 0.12 K) to detect the line. We could not detect any $C^{34}S$ (2-1) line in our maps, partly since the noise in these maps is still relatively high and the expected line strength is low.

4.2.2 Data Reduction

The data reduction was done with the FCRAO "otftool" (Heyer et al. 2001) and later with the CLASS software of the GILDAS packet developed by IRAM. A zero order baseline was applied to each spectrum and then all spectra of one single position were added weighted by one over sigma squared. Then the data were regridded on a regular, Nyquist sampled grid, because the raw data are sampled on an irregular grid. After this a third order baseline was removed if required. As the centre of the map was covered more often than the outer parts of the map the noise level is much lower there. We therefore cut off the outskirts and edges of the maps.

4.2.3 Results

Figures 4.2, 4.4 and 4.6 show the resulting total integrated line intensity maps of the three cores we observed and detected with the FCRAO. In Table 4.1 the map centre positions and the achieved rms of the observations are listed.

Table 4.1: The results of the CS mapping observations carried out with the FCRAO telescope. Listed are the map centre positions and the achieved rms of the maps.

Core	l [deg]	b [deg]	α_{2000} [h m s]	δ_{2000} [$^{\circ}$ ' "]	rms [Kkm s $^{-1}$]
MCLD 126.6	126.675	24.535	04 24 24.3	85 44 56.2	0.020
L 1457	159.266	-34.484	02 56 12.3	19 26 21.0	0.025
MBM 32	146.835	40.665	09 33 58.1	66 06 33.3	0.012

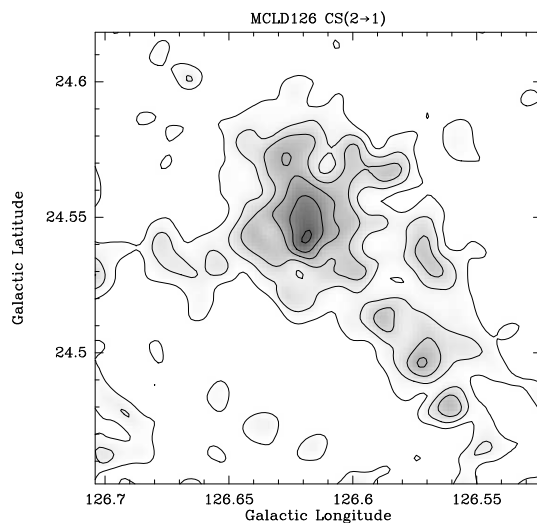


Figure 4.2: The integrated line intensity distribution of the CS ($2 \rightarrow 1$) transition of the core in MCLD 126.6+24.5. The Contour lines are in steps of 0.02 Kkm s^{-1} (1σ) starting at 0.06 Kkm s^{-1} . The beam size is $54''$.

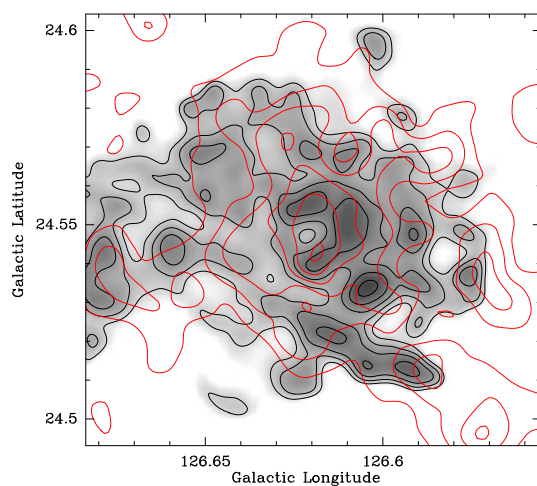


Figure 4.3: Contours of the integrated line intensity of the CS ($2 \rightarrow 1$) emission (Figure 4.2) superposed on the grey scale image of the dust continuum emission map of the core in MCLD 126.6+24.5 (Figure 3.4). The black contours denote the dust emission in steps of 2 mJy/beam starting at 2 mJy/beam , while the red contours trace the CS emission in steps of 0.02 Kkm s^{-1} starting at 0.06 Kkm s^{-1} .

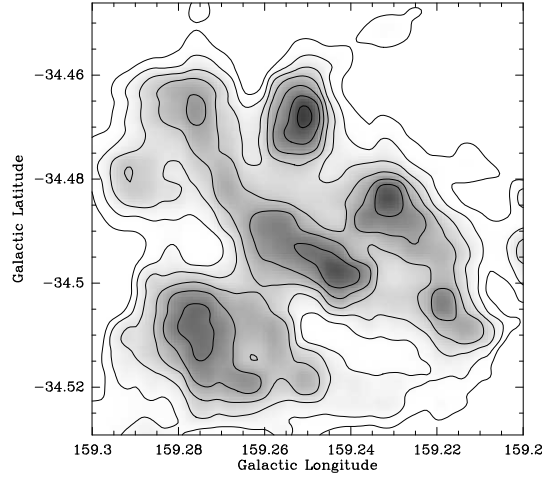


Figure 4.4: The integrated intensity distribution of the CS ($2 \rightarrow 1$) emission line of the core in L1457. Contour lines are in steps of 0.025 Kkm s^{-1} (1σ) starting at 0.3 Kkm s^{-1} . The beam size is $54''$.

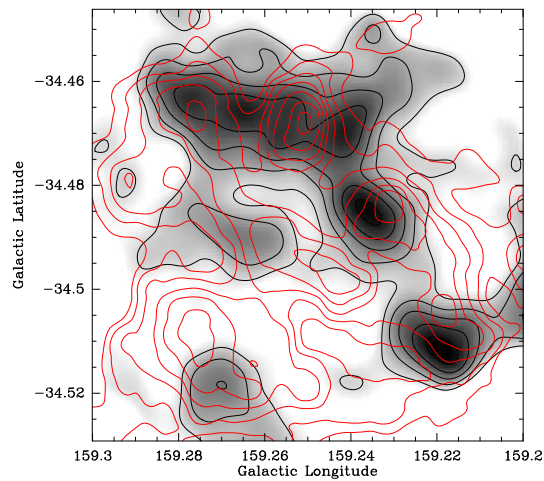


Figure 4.5: Contours of the integrated line intensity of the CS ($2 \rightarrow 1$) emission (Figure 4.4) superposed on the grey scale image of the dust continuum emission map of the core in L1457 (Figure 3.6). The black contours denote the dust emission in steps of 3 mJy/beam starting at 2 mJy/beam , while the red contours trace the CS emission in steps of 0.025 Kkm s^{-1} starting at 0.3 Kkm s^{-1} .

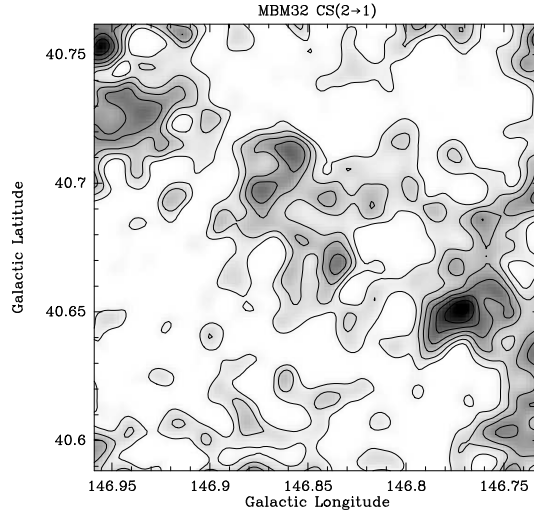


Figure 4.6: Integrated intensity distribution of the CS ($2 \rightarrow 1$) emission line of the core in MBM 32. Contours are every 0.012 Kkm s^{-1} (1σ) starting at 0.06 Kkm s^{-1} . The beam size is $54''$.

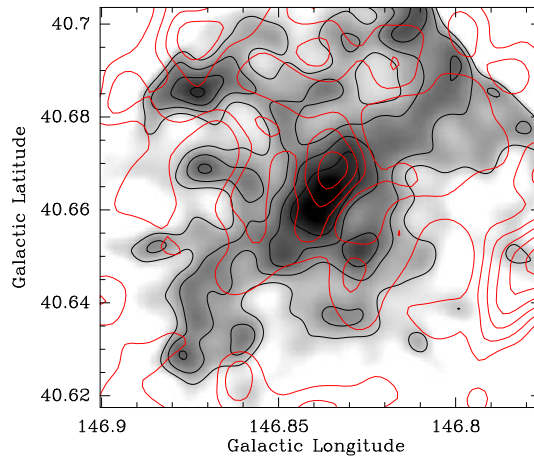


Figure 4.7: Contours of the integrated line intensity of the CS ($2 \rightarrow 1$) emission (Figure 4.6) superposed on the grey scale image of the dust continuum emission map of the core in MBM 32 (Figure 3.8). The black contours denote the dust emission in steps of 1.2 mJy/beam starting at 1.2 mJy/beam , while the red contours trace the CS emission in steps of 0.012 Kkm s^{-1} starting at 0.06 Kkm s^{-1} . Note that the dust emission map is much smaller than the CS-map.

The core in MCLD 126.6+24.5 is clearly detected at a level of more than 3σ . The overall appearance of the CS emission is nearly roundish and centrally condensed, however, it also shows some filamentary extensions and indications of a clumpy substructure. The integrated intensity maximum is located at exactly the same position as the dust continuum emission peak. Even the size of the core is similar in both tracers, however, the dust continuum map is not large enough to fully cover the filamentary extensions visible in the CS-map (Figure 4.3). The CS-map does not show a lot of diffuse emission and the line profile looks relatively simple (Figure 4.8).

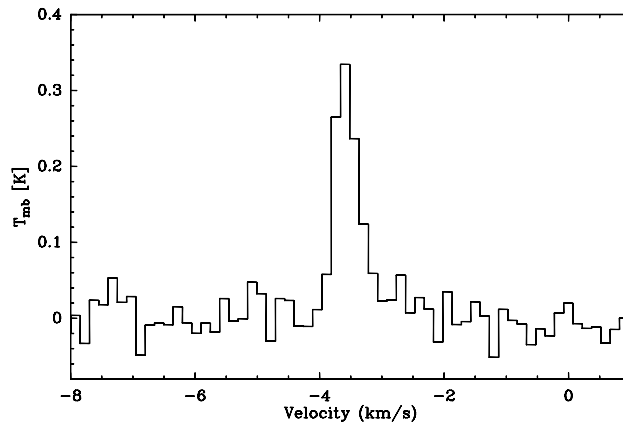


Figure 4.8: The averaged CS ($2 \rightarrow 1$) emission line spectrum towards the core in MCLD 126.6, obtained with the FCRAO 14-m telescope. The spectra inside $1'$ to the centre position are combined.

The core in L 1457 is detected at a level of more than 10σ . Surprisingly, the overall structure of the core region in L 1457 is fairly similar to the structure visible in the dust continuum emission, indicating, that the clumpy structure is real and not solely caused by projection effects. We see multiple lines (3 components) and blending in the CS-spectra. The kinematic information of the line-emission observations is in this case essential to interpret the dust emission map correctly.

However, there are also significant differences. First of all, the clump labeled A, and the strongest in the dust continuum map, is only faintly visible. In contrast, there is a strong intensity maximum within though not at the centre of dust clump C. Furthermore, a quite strong diffuse intensity is measured (note that the contours start at 0.3 K km s^{-1}) and yet another maximum, strong and fairly extended, can be seen in the south-west corner of the map. For this there exists an indication in the dust continuum map, but relatively faint and at the edge of the map. Hence, we have to refer again to the observing method, used to carry out the dust continuum emission observation, and the therefore presumably missing diffuse, large scale component.

Furthermore, the intensity peaks of the CS map are always displaced, compared to the dust continuum maxima. This is shown more clearly in Figure 4.5, where we superposed the integrated CS map on the smoothed dust continuum map. The integrated CS ($2 \rightarrow 1$) line

emission is displayed by the red contour lines similar to the contours in Figure 4.4, while the dust continuum map is shown as grey scale image with black contour lines.

Nevertheless, the tracers show a remarkably similar appearance, considering the different resolution of the observations and the problematical structure with sub-clumps and various velocity components. Figure 4.9 shows a combined spectrum of the inner $1'$ of the map. Due to the large beam ($54''$), the 3 velocity components are not totally resolved, but 2 of them are blended. In the next section we show a comparison with roughly the same spectrum, obtained with the IRAM 30-m telescope at a resolution of $24''$.

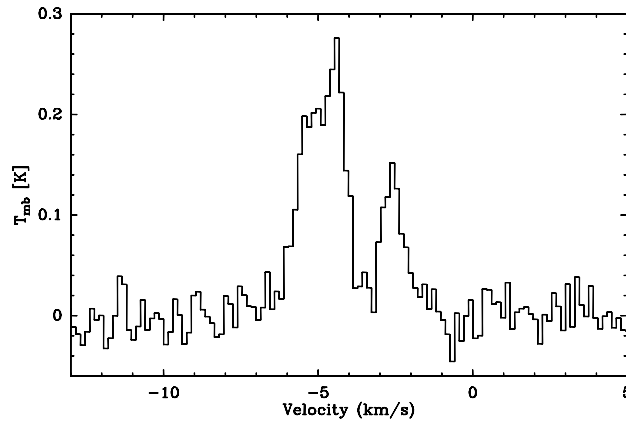


Figure 4.9: The averaged CS ($2 \rightarrow 1$) emission line spectrum towards the core in L 1457, obtained with the FCRAO 14-m telescope. The spectra inside $1'$ to the centre position are combined.

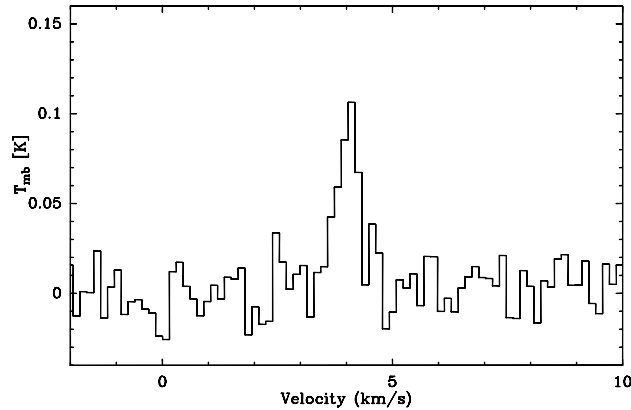


Figure 4.10: The averaged CS ($2 \rightarrow 1$) emission line spectrum towards the core in MBM 32, obtained with the FCRAO 14-m telescope. The spectra inside $1'$ to the centre position are combined.

The core in MBM 32 is clearly detected at a 3σ level, but a centrally condensed structure cannot be seen at all. At the position of the dust continuum core, a faint local intensity

maximum is visible (Figure 4.7), however, the overall appearance of the CS emission is rather diffuse. Additional maxima show up next to the central position, nearly forming a ring-like structure. Specifically noticeable is the diagonal trend opposite to the elliptical form of the dust core. The dust continuum emission map seems to be way too small as the CS maximum is located outside this map. Hence, a significant fraction of the dust emission may be absent. The line profile appears to be relatively simple (Figure 4.10).

4.3 Additional Observations with the IRAM 30-m Telescope

4.3.1 Observations and Data Reduction

Observations of CS ($2 \rightarrow 1$), CS ($5 \rightarrow 4$), and HC₃N ($10 \rightarrow 9$) with the IRAM 30-m radio telescope on Pico Veleta were conducted in autumn 2002 as backup project for pooled observations. We used the A and B SIS line receivers and the VESPA digital correlator with a velocity resolution better than 0.06 km s^{-1} . The observations were done in position switching mode with an off position of about $10'$ away, assigned by looking at the IRAS maps. Small raster maps were obtained with 25 positions around the core or clump centres for Draco and L 1457. The spacing between the individual positions is $12''$ and the beam-sizes are $27''$ at 90 GHz, $24''$ at 98 GHz, and $10''$ at 245 GHz. For MBM 32 only the central position was observed due to the not ideal weather conditions. Pointing and Focus were checked regularly and a pointing accuracy better than $3''$ was found. To check for the calibration we observed W3OH regularly.

The Data were reduced using the CLASS software by applying a baseline of order three or less and sum up all spectra of the individual positions weighted by their noise. The line parameters then were derived from simple Gaussian fits to the spectra. For the cores in MCLD 123.5+24.9 and MCLD 126.6+24.5 we already have good CS data at our disposal (based on the data published by Heithausen 1999 and Heithausen et al. 1998, respectively), which were introduced in chapter 2.

In August 2004 we conducted an additional observing run at the 30-m telescope. Our main focus was on the N₂H⁺ ($1 \rightarrow 0$) transition, a project that is still ongoing and will not be discussed further in this thesis. For the second receiver we chose the C¹⁸O ($2 \rightarrow 1$) line, as it turned out for MCDL 123.5+24.9 that this molecule can be used as a possible density tracer for these cores. We used again the A and B receivers and the VESPA backend. The observations were done similarly to the CS observations. This project is, however, not yet finished and the data are preliminary. We will use them to get an estimate of the molecular abundances, and to investigate the chemistry within the cores in more detail.

4.3.2 Results

CS ($2 \rightarrow 1$)

We detected all cores in the CS ($2 \rightarrow 1$) transition. The signal to noise is not as good as we would have liked, nevertheless, the data are sufficient for our basic analysis. The parameters of the obtained spectra are compiled in Table 4.2.

In Figure 4.11 we display the spectra obtained towards the positions of the cores in MCLD 126.6+24.5, L 1457, MBM 32, and Draco. For L 1457 the spectrum towards the position of clump A is shown. Note that the positions of the CS spectra do not always perfectly match the central positions of the dust continuum cores derived from the Gaussian fits, since this analysis was applied later on and the CS observing positions were defined by inspecting the (preliminary) dust maps by eye.

Table 4.2: The parameters of the CS spectra obtained with the IRAM 30-m telescope towards the positions of the dust cores or clumps. The last column indicates whether a small map of 5×5 points around this position could be obtained.

Core	l [deg]	b [deg]	α_{2000} [h m s]	δ_{2000} [$^{\circ}$ ' "]	rms [K]	map
L 1457 A	159.220	-34.511	02 56 00.5	19 26 15.0	0.073	no
L 1457 B	159.254	-34.471	02 56 12.0	19 27 20.0	0.035	yes
L 1457 C	159.279	-34.468	02 56 17.0	19 26 48.0	0.033	yes
MBM 32	146.835	40.665	09 33 58.0	66 06 35.0	0.043	no
Draco	89.520	38.414	16 49 12.0	59 55 50.0	0.031	yes

Towards the sub-clumps B and C of the core in L 1457 a relatively complicated line structure consisting of three different velocity components is detected. The assignment to the dust continuum clumps is not well-defined and very difficult. In Figures 4.12 and 4.13 the obtained spectra maps towards clump B and C are shown. The offsets are in arcsec relative to the centre positions. The 3-component structure is visible in nearly all spectra, although, towards clump B the third velocity component at -2.64 km s^{-1} is weaker. It is possible that this structure is also caused by self-absorption. However, we are not able to definitely distinguish between these two possibilities. For this purpose interferometric observations with very high resolution are needed to resolve the structures.

As already visible in the FCRAO CS-map the line emanates from a larger volume than merely from the individual clumps. This is an additional hint that we may have missed the diffuse component in our dust map, and that the individual clumps do strongly overlap and maybe even interact with each other. Nevertheless, we think it is possible to spot a

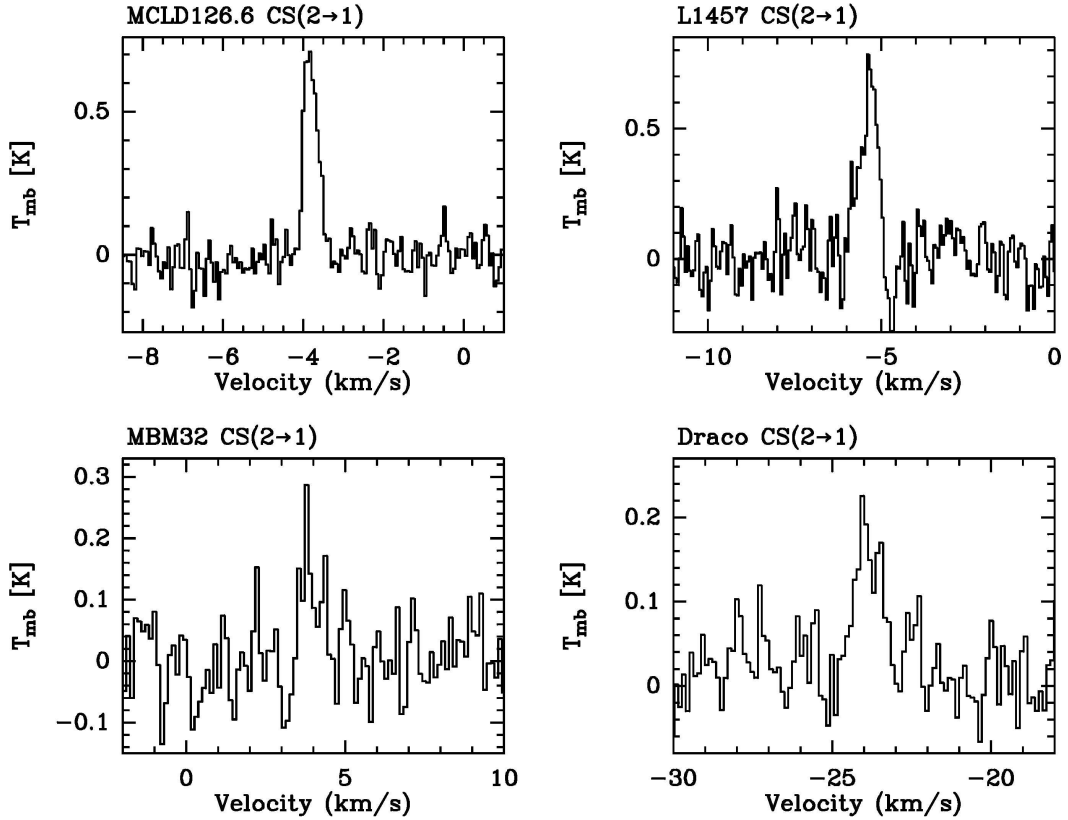


Figure 4.11: CS ($2 \rightarrow 1$) emission line spectra towards the core or clump centre positions in MCLD 126.6+24.5, L 1457-A, MBM 32, and Draco, obtained with the IRAM 30-m telescope. The parameters of the spectra are listed in Table 4.2.

trend within the maps (Figure 4.15). Therefore, we decided to allocate each one of the CS lines to one of the identified dust continuum clumps, for lack of any other information.

Starting from a detailed analysis of the single spectra, as well as of the combined spectrum, we extracted the properties of the 3 components towards each clump by Gaussian fits. Figure 4.14 shows the combined spectrum, similar to the one shown in Figure 4.9 for the FCRAO observation. Table 4.3 lists the values for each of the sub-clumps. In Figure 4.15 integrated intensity maps (FCRAO observation) for each of the 3 components are shown. We only integrated over the line widths determined from the 30-m spectra and listed in Table 4.3 to point up the trend we spotted.

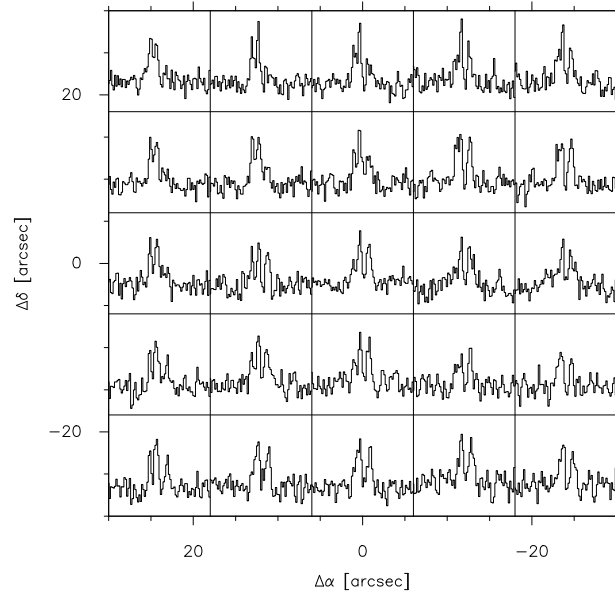


Figure 4.12: Maps of the CS($2 \rightarrow 1$) emission line spectra towards the clump B in L1457 obtained with the IRAM 30-m telescope. Positions are offsets in arcsec relative to (RA,DEC)(2000) = (02:56:12, +19:27:20). The temperature scale is $-0.25 \leq T_{\text{mb}} \leq 0.65$ K and the velocity scale is $-13 \leq v_{\text{LSR}} \leq 5$ km s $^{-1}$.

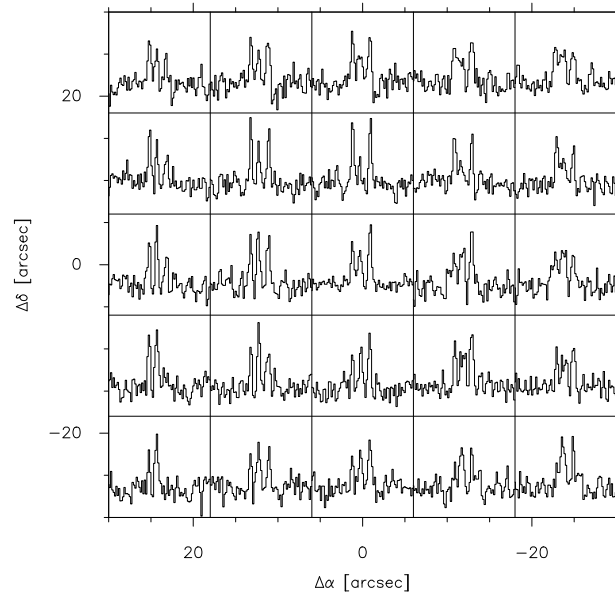


Figure 4.13: Maps of the CS($2 \rightarrow 1$) emission line spectra towards the clump C in L1457 obtained with the IRAM 30-m telescope. Positions are offsets in arcsec relative to (RA,DEC)(2000) = (02:56:17, +19:26:48). The temperature scale is $-0.25 \leq T_{\text{mb}} \leq 0.65$ K and the velocity scale is $-13 \leq v_{\text{LSR}} \leq 5$ km s $^{-1}$.

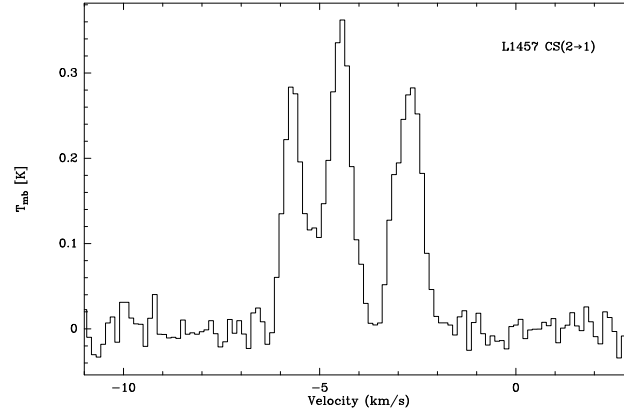


Figure 4.14: CS ($2 \rightarrow 1$) emission line spectrum towards the core in L 1457 obtained with the IRAM 30-m telescope. All observed spectra are combined. Please note the difference to the spectrum shown in Figure 4.9, which is mostly caused by the higher angular resolution.

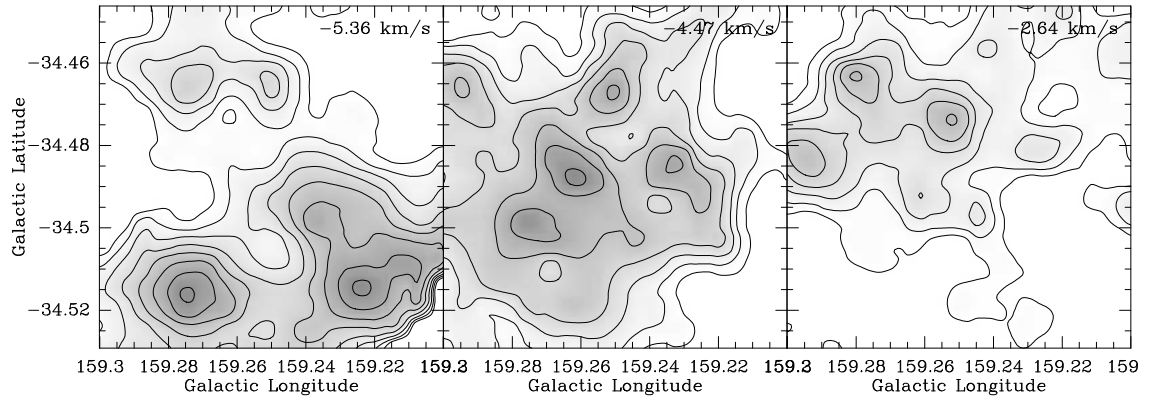


Figure 4.15: Integrated line intensity maps for each of the identified line components. The maps were integrated over the line widths given in Table 4.3, and the central velocity is quoted in the upper right corner. The contour lines are in steps of $0.012 \text{ K km s}^{-1}$ (1σ) starting at 0.05 K km s^{-1} . A trend is clearly visible, however, a significant fraction of the emission obviously arises from the diffuse gas between the individual clumps.

For the most negative component, at -5.36 km s^{-1} , it can clearly be seen that a significant fraction of the intensity arises from the position of clump A. However, there is also emission at the positions of clump C and the south-west peak, as well as a fairly diffuse fraction. The second component at -4.47 km s^{-1} is best visible towards clump B, however, most of the intensity seems to arise from the diffuse gas. The third component, at -2.64 km s^{-1} , is eventually restricted to clump C, however, all 3 components are clearly detected within this clump. Hence, the real structure of L 1457 is possibly much more complicated than assumed here.

We therefore have to note that this analysis is not very accurate, since the assignment of one line to one clump is only a wild guess. The quoted errors in Table 4.3 represent only the formal errors derived from the Gaussian fits and do not include any of the discussed uncertainties.

Table 4.3: Allocation of the CS ($2 \rightarrow 1$) velocity components and the dust continuum sub-clumps. The quoted errors represent only the formal errors derived from the Gaussian fits.

Sub-clump	l [deg]	b [deg]	v_{LSR} [km s $^{-1}$]	Δv [km s $^{-1}$]	T_{mb} [K]
L 1457-A	159.22	-34.51	-5.36 ± 0.03	0.57 ± 0.12	0.69 ± 0.01
L 1457-B	159.24	-34.49	-4.47 ± 0.08	0.65 ± 0.16	0.46 ± 0.02
L 1457-C	159.26	-34.47	-2.64 ± 0.06	0.80 ± 0.13	0.57 ± 0.02

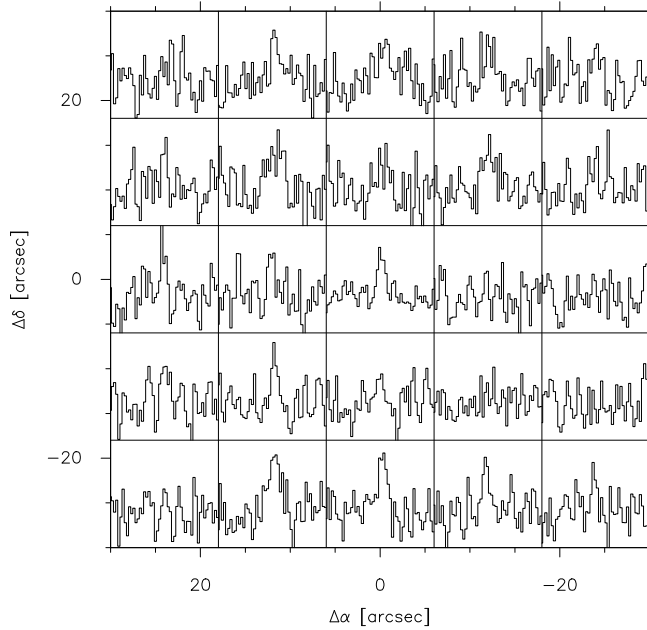


Figure 4.16: Maps of the CS ($2 \rightarrow 1$) emission line spectra towards the core in Draco obtained with the IRAM 30-m telescope. Positions are offsets in arcsec relative to (RA,DEC)(2000) = (16:49:12, 59:55:50). The temperature scale is $-0.13 \leq T_{\text{mb}} \leq 0.25$ K and the velocity scale is $-30 \leq v_{\text{LSR}} \leq -18$ km s $^{-1}$.

In Figure 4.16 the obtained spectra map towards the core in Draco is shown. The offsets are in arcsec relative to the core centre position. The line is clearly detected, however, not in all of the spectra. The centre position was integrated for 32 min, whereas all the other positions only got 8 min of integration time. The appearance of the line in the different spectra shows a patchy structure, again indicating a clumpy distribution.

From the analyses of the obtained spectra towards the cirrus cloud cores we gained the line parameters of the CS ($2 \rightarrow 1$) transition listed in Table 4.4. We used the IRAM 30-m data, because of the much better angular resolution. The line widths extracted from the FCRAO maps are generally larger. We already explained above the method we used for the sub-clumps in L1457. For the other cores we averaged the spectra within the core region, if possible, and fitted the line with a Gaussian. For MBM32 we could only use the central spectrum, hence the extracted line width could be slightly too narrow. For MCLD 123.5 we used the map presented by Heithausen (1999) and fitted on Gaussian to the full line, although the spectrum exhibits the double peaked signature of inward motion (Heithausen 1999). The extracted line width may thus be too wide, since the core centre itself is self-absorbed. However, we will discuss this topic later in much more detail (see Chapter 5.3).

Table 4.4: The CS ($2 \rightarrow 1$) line parameters towards the dust continuum cores or clumps. The values are derived from Gaussian fits to the spectra. The quoted errors represent the formal errors derived from the fits and do not include other uncertainties.

Core	l [deg]	b [deg]	v_{LSR} [km s ⁻¹]	Δv [km s ⁻¹]	T_{mb} [K]
MCLD 123.5	123.68	24.89	-4.34 ± 0.03	0.77 ± 0.05	2.16 ± 0.2
MCLD 126.6	126.62	24.55	-3.82 ± 0.01	0.40 ± 0.02	0.75 ± 0.1
L 1457 A	159.22	-34.51	-5.36 ± 0.03	0.57 ± 0.12	0.69 ± 0.1
L 1457 B	159.24	-34.49	-4.47 ± 0.08	0.65 ± 0.16	0.46 ± 0.2
L 1457 C	159.26	-34.47	-2.64 ± 0.06	0.80 ± 0.13	0.57 ± 0.2
MBM 32	146.84	40.67	3.81 ± 0.09	0.43 ± 0.26	0.21 ± 0.1
Draco	89.51	38.40	-23.87 ± 0.06	0.90 ± 0.12	0.19 ± 0.1

CS ($5 \rightarrow 4$)

To make full use of the telescope abilities we observed the CS ($5 \rightarrow 4$) line simultaneously. However, due to the not ideal weather conditions we could not detect the line. The achieved rms noise level of the averaged spectra is of the order of ≈ 0.1 K, hence not necessarily sufficient for a reliable detection.

HC₃N ($10 \rightarrow 9$)

We did not detect the HC₃N line in any of the cores except from MCLD 123.5+24.9. This was not the expected result, since NH₃ was already detected in MCLD 126.6+24.5 (Boden & Heithausen 1993) and MBM 32 (Mebold et al. 1987). We did not reach the rms level we would have liked, however, 3-sigma detections should have been possible, if abundances similar to MCLD 123.5+24.9 are assumed. Furthermore, we could not carry out maps, but only do some pointed observations. Therefore, it is possible that we have simply missed the HC₃N clumps. The results are upper limits of the line temperatures. In a combined spectrum of all observations towards L 1457 the rms reaches 0.02 K. For MBM 32 the rms is 0.06 K and for Draco it reaches 0.02 K. These values will help to estimate the abundances within the cores.

4.4 Interferometric Observations of MCLD 123.5+24.9

The cirrus cloud core in MCLD 123.5+24.9 has, to some extent, already seen a number of spectral line studies. Based on maps obtained with the IRAM 30-m telescope (Heithausen 1999; Heithausen et al. 2002) we obtained interferometric pointings in HC₃N (10-9) and CS (2 → 1) with the IRAM Plateau de Bure (PdB) interferometer and the Owens Valley Radio Observatory (OVRO) millimeter array, respectively.

4.4.1 Observations and Data Reduction

The observations of the HC₃N (10 → 9) transition at 90.98 GHz were conducted between May and November 2002 with the Institut de Radio Astronomie Millimétrique (IRAM) Plateau de Bure (PdB) interferometer. It is located near Grenoble in the South of the French Alps in the Département of Hautes Alpes at an altitude of 2552 m and consists currently of six 15-m antennas. During four runs five antennas in the configuration 5D were used, one run was carried out with 6 antennas in configuration 6Dp. Because of poor weather conditions only the 3 mm data were usable and the standard CLIC reduction procedure was applied. The phase and amplitude were calibrated with frequent observations of the quasars 1928+738 and 0716+714 and the amplitude scale was derived from measurements of MWC349 and CRL618.

We observed MCLD 123.5+24.9 in the CS (2 → 1) line using the Owens Valley Radio Observatory (OVRO) millimeter array from January to April 2001. It is located on the east side of the Sierra Nevada near Bishop, California, approximately 250 miles north of Los Angeles and operated by the California Institute of Technology (Caltech). The array consists of six 10.4 meter telescopes with rms surface precision of 35 microns. The aperture efficiencies are 0.70 and 0.45 at 2.7 mm and 1.3 mm, respectively. The pointing accuracy is about 4", except for brief excursions at sunrise and sunset. The halfpower beam-width of one antenna is 65" at 100 GHz. In total, 5 tracks were spent on source (2 pointings each) in the 'C' and 'L' configurations, resulting in a beam size of ~ 5". The final rms in the data is about 100 mJy/beam in 0.1 km/s channels. The nearby source J1803+784 (1.5 Jy) was used for phase calibration. The data for each array were edited and calibrated separately with the MMA and the MIRIAD packages. The uv-data were inspected and bad data points due to either interference or shadowing between telescopes were removed, after which the data were calibrated. The observations with OVRO and the data reduction were conducted by Fabian Walter.

We then corrected the data for zero spacing (see Weiß2000) with our dataset from the IRAM 30-m telescope. In the CS (2 → 1) a larger fraction of diffuse emission was missing, whereas in the HC₃N (10 → 9) line only a small correction of the flux was achieved.

The effective synthesized beam FWHM of $\approx 6'' \times 8''$ is similar in both observations (but with different position angles of PA = -72° and PA = -13.5°, respectively) equivalent to 900 AU × 1200 AU at the distance of 150 pc.

4.4.2 Results

Figure 4.17 shows the obtained integrated intensity distributions with the achieved spatial resolution of about $7''$. The clump is resolved and shows substructures down to the scale of the beam in both molecules. The self-absorption feature is still visible in the CS line. In Figure 4.18 a channel-map is shown and one easily recognises the infall signature, a blue- and a red-shifted part of the clump and the absorption dip.

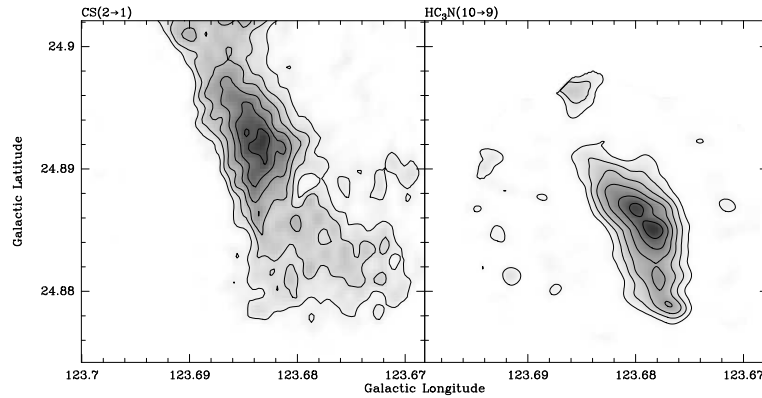


Figure 4.17: Integrated intensity distributions of the CS ($2 \rightarrow 1$) and the HC₃N ($10 \rightarrow 9$) interferometer observations made with PdB and OVRO. They are short-spacing corrected with the IRAM 30-m maps shown before. Contours are every 0.3 K km s^{-1} starting at 0.9 K km s^{-1} for the CS and every 0.1 K km s^{-1} starting at 0.2 K km s^{-1} for the HC₃N map.

The spatial displacement of the two peaks is still present. From the CS channel map in Figure 4.18 it becomes clear that the lower part of the clump is different from the upper one regarding the velocity. The upper part starts at a velocity of almost -5 km s^{-1} and is seen as a roundish clump showing the self-absorption feature interpreted as infall motion. The absorption dip is visible at a velocity of -4.3 km s^{-1} what is the systemic velocity of the whole clump seen for instance in the C¹⁸O line. The lower, and more diffuse emission, starts at a velocity of -4.6 km s^{-1} and reaches out to -3.8 km s^{-1} at a low level. The line in this part seems to be heavily self-absorbed without a clear infall signature and the integrated intensity is much lower. The HC₃N emission, on the other hand, arises solely from the lower part of the clump and corresponds almost perfect, spatially and in velocity, with the more diffuse CS emission (see Figure 4.19). A plausible interpretation of the integrated intensity peak shift appears to be possible with the help of time dependent chemistry models. We will discuss this topic later in more detail.

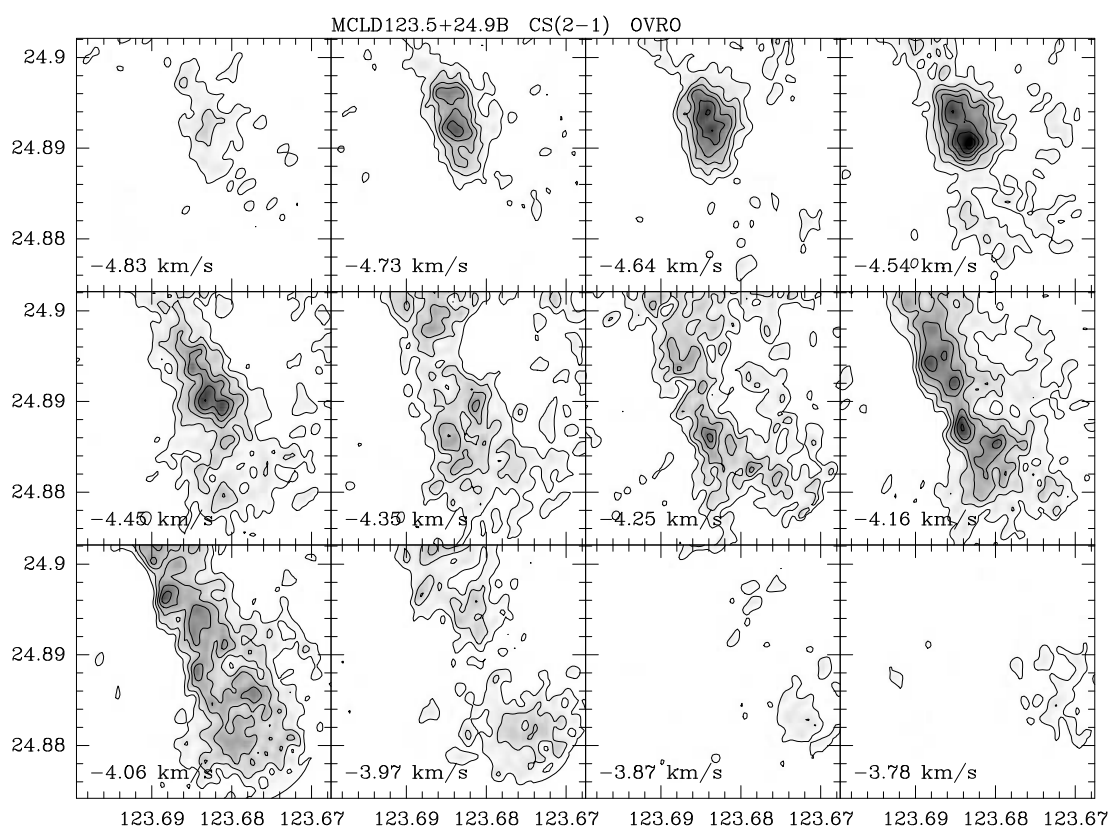


Figure 4.18: Velocity channel maps of the short-spacing corrected CS ($2 \rightarrow 1$) data cube. Contour lines are every 0.6 K starting at 0.8 K. The central velocity (v_{LSR}) of each map is given in the lower right corner.

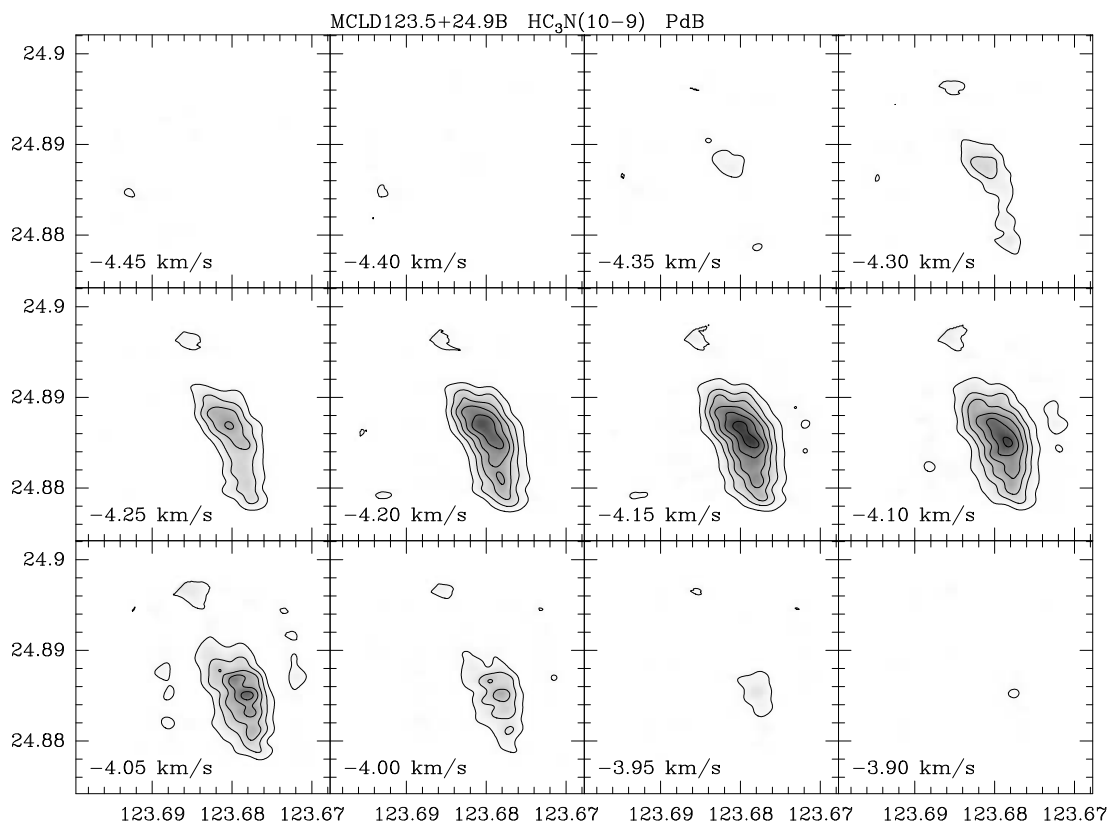


Figure 4.19: Velocity channel maps of the short-spacing corrected HC₃N(10 → 9) data cube. Contour lines are every 0.4 K starting at 0.4 K. The central velocity (v_{LSR}) of each map is given in the lower right corner. Note that the velocity starts at -4.45 km s^{-1} , i.e. at row two of the CS channel maps and the velocity resolution is twice as high.

5

Physical Core Properties and Scaling Relations

In this chapter we will compute basic core properties with our data. We start our analysis by deriving the column densities and masses of the cores. A basic simplification in our calculation is that we fit the cores with a 2 dimensional Gaussian. Later we assume the cores as ellipsoids with the third, line-of-sight axis equal to the minor axis of the fitted ellipse. This is a simple guess, and does make the calculations even a bit more uncertain, however, because we lack of any information on this axis it seems justifiable.

Another assumption or simplification, only partly based on observations, is the acceptance of a constant dust temperature of about 10 K throughout the cores. It is justified by, first, the observations of Bernard et al. (1999) who derived a temperature of 11.5 ± 1.4 K for the core region in MCLD 123.5+24.9 and 13.4 ± 0.8 K for the whole cloud, and second, by the work of, e.g., Evans et al. (2001) indicating that the dust temperature in a dense core decreases towards the centre because of extinction in the warming interstellar radiation field. However, their cores are much denser than the cirrus cloud cores and they model temperatures as low as 7 K in the centre of these cores. Therefore, in assuming a constant dust temperature of 10 K we introduce only a small error but simplify the calculations a lot.

An exact determination of the dust temperature within the cores would increase the accuracy of our analysis. However, to do this we would need at least a set of similar maps, especially with a comparable resolution at a second wavelength. We then could obtain colour temperatures, i.e., fit a grey body to the marginally determined spectral energy distribution. Unfortunately, we were not able to obtain a second dataset at a different wavelength for all the cores, mainly because of the very limited number of instruments available and the large amount of time such observations need.

Having accomplished the basic determinations on the dust continuum data, we will take

the CS ($2 \rightarrow 1$) line data into account and calculate typical scaling relations to derive information on the core stability and star-forming capability. This will also reveal if our cirrus cloud cores are typical or very different compared to cores in dark clouds. After this, with all the additional molecular line data at our disposal, we shall also determine molecular abundances, which will help to clarify the picture of the cores in more detail.

5.1 Column Densities and Core Masses

5.1.1 Two Dimensional Gaussian Fits

We start our analysis by deriving column and volume densities of the cores or the resolved clumps. We do this by fitting a two dimensional Gaussian to our 1.2 mm dust emission data. It can be done with the GILDAS task "gauss_2d". This procedure is, however, only able to fit one core at a time.

We also tried to fit smaller clumps, since the resolution of the maps would allow this. However, beside of L1457, for which the clumps are relatively well defined, it did not work. The problem was that the task is only semi-automatic and one has to define the starting values, especially the area to fit. The most simple approach was to fit one core in each map. This worked very well for MCLD 123.5+24.9, MCLD 126.9+24.5, MBM 32, and Draco. Only for L1457 we were able to definitely distinguish between three well defined sub-clumps and to fit them separately. For the other cores any further breakdown would have been highly arguable.

The obtained parameters are listed in Table 5.1 and the original and residual map of each core are displayed in the Figures 5.1 to 5.5.

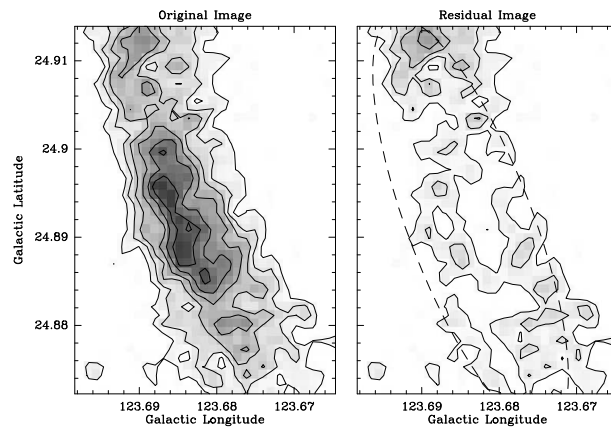


Figure 5.1: Map of the 1.2 mm dust continuum emission of the core in MCLD 123.5+24.9 and residual map after fitting a 2-dimensional Gaussian.

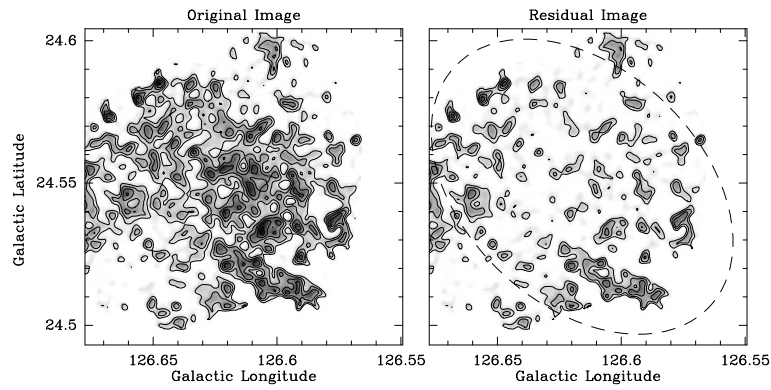


Figure 5.2: Map of the 1.2 mm dust continuum emission of the core in MCLD 126.9+24.5 and residual map after fitting a 2-dimensional Gaussian.

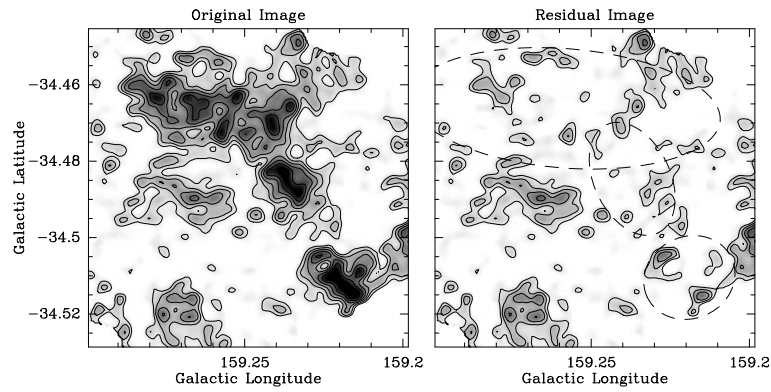


Figure 5.3: Map of the 1.2 mm dust continuum emission of the core in L 1457 and residual map after fitting a 2-dimensional Gaussian.

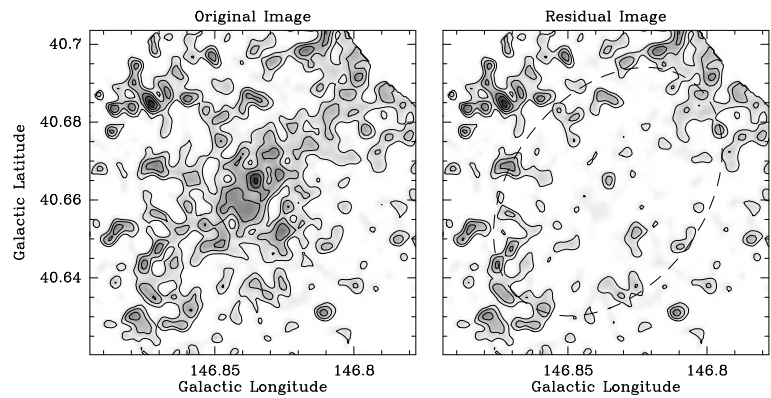


Figure 5.4: Map of the 1.2 mm dust continuum emission of the core in MBM 32 and residual map after fitting a 2-dimensional Gaussian.

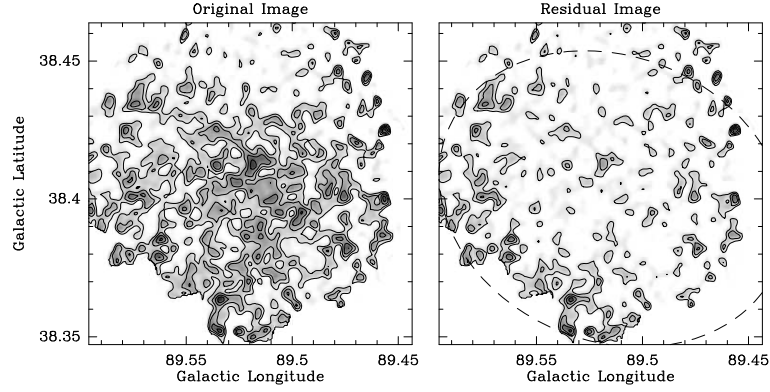


Figure 5.5: Map of the 1.2 mm dust continuum emission of the core in Draco and residual map after fitting a 2-dimensional Gaussian.

Table 5.1: The core or clump parameters derived from the 2-dimensional Gaussian fits to the dust continuum data.

Core	l [deg]	b [deg]	Peak flux [mJy/beam]	Major axis [arcmin]	Minor axis [arcmin]	P.A. [deg]
MCLD 123.5	123.684	24.892	11.0 ± 0.2	1.50 ± 0.01	0.44 ± 0.06	-21.7 ± 0.7
MCLD 126.6	126.616	24.549	7.7 ± 0.1	3.78 ± 0.03	2.54 ± 0.06	-50.3 ± 1.5
L 1457 A	159.219	-34.511	19.7 ± 0.4	0.73 ± 0.02	0.64 ± 0.01	65.0 ± 0.3
L 1457 B	159.237	-34.485	17.1 ± 0.2	0.97 ± 0.01	0.59 ± 0.03	-31.5 ± 2.1
L 1457 C	159.258	-34.466	14.6 ± 0.1	2.43 ± 0.01	0.94 ± 0.03	-85.4 ± 0.4
MBM 32	146.836	40.667	5.5 ± 0.1	2.19 ± 0.02	1.54 ± 0.02	43.0 ± 1.7
Draco	89.514	38.400	6.1 ± 0.1	3.94 ± 0.03	3.11 ± 0.06	-69.2 ± 1.9

5.1.2 Determination of the Column Density

As mentioned before, the thermal dust emission flux density is directly linked to the H₂ column density. We will shortly derive the formula to convert the two values. The starting point is the **Equation of Radiative Transfer** which gives in local thermal equilibrium (LTE) the intensity emitted by a medium of temperature T and optical depth τ_ν

$$I_\nu = B_\nu(T_d)(1 - e^{-\tau_\nu}) \quad (5.1)$$

where B_ν is the Planck function. The definition of the optical depth we will use here reads

$$\tau_\nu = \int \kappa_\nu \rho ds, \quad (5.2)$$

where κ_ν is the so called specific absorption coefficient. One speaks of a specific absorption coefficient when the coefficient has to be weighted by density ρ to find the optical depth. This optical depth can be related to the column density via

$$N(\text{H}_2) = \frac{\tau_\nu}{\mu m_p \kappa_\nu}, \quad (5.3)$$

where $\mu = 2.33$ is the mean molecular weight per hydrogen molecule and m_p is the proton mass. With the simplification of optically thin emission (means $\tau_\nu \ll 1$) this reads

$$I \approx B_\nu(T_d)\tau_\nu. \quad (5.4)$$

Unfortunately, telescopes do not measure intensities but fluxes. The received flux is related to the intensity by

$$S_\nu = \int I_\nu P d\Omega, \quad (5.5)$$

where P is the normalized power pattern of the telescope (i.e. $\max(P)=1$). Defining the beam solid angle as

$$\Omega_A = \int P d\Omega, \quad (5.6)$$

one can derive a beam-averaged intensity

$$\langle I_\nu \rangle = \frac{S_\nu}{\Omega_A}. \quad (5.7)$$

Next we need the **Planck function**, which reads

$$B_\nu(T_d) = \frac{2h\nu^3}{c^2} \frac{1}{e^{h\nu/(kT)} - 1}, \quad (5.8)$$

where k is the Boltzmann's constant and h the Planck's constant. The Rayleigh-Jeans approximation is not applicable to observations at 1.2 mm wavelength. We can now directly write down the conversion formula to

$$N(\text{H}_2) = \frac{S_\nu}{\Omega \mu_{\text{m}_p} \kappa_\nu B_\nu(T_d)}. \quad (5.9)$$

It is much more useful in the following form

$$\left(\frac{N(\text{H}_2)}{\text{cm}^{-2}} \right) = 1.1 \cdot 10^{21} \left(\frac{S_\nu}{\text{mJy}} \right), \quad (5.10)$$

where we used the values:

$\kappa_{250\text{GHz}} = 0.005 \text{cm}^2 \text{g}^{-1}$, $T_d = 13 \text{K}$, $\nu = 250 \text{GHz}$, and the telescope beam $\Theta_{\text{FWHM}} = 11''$. The derived values for the peak column densities of the cores are listed in Table 5.2.

5.1.3 Determination of the Mass

From our 2-dimensional Gaussian fit we derive an area of the core of

$$A = 2 \cdot \pi \cdot \sigma_x \cdot \sigma_y \quad (5.11)$$

with $\sigma = 0.4247 \cdot \text{FWHM}$ and therefore

$$A = 1.13309 \cdot \text{FWHM}_x \cdot \text{FWHM}_y. \quad (5.12)$$

Together with the values for the distance ($1 \text{pc} = 3.086 \cdot 10^{18} \text{cm}$), and assuming the cores are ellipsoids (as explained, the smaller FWHM is assumed for the third axis, too) we derive the core masses listed in Table 5.2. Since the distance is not a measurement but a fixed value the stated errors of the core masses are solely due to the peak flux errors deduced from the Gaussian fits and not very meaningful. Considering the uncertainties in the distance estimates (see Chapter 2 for details) and the possible errors in the calibration of the dust emission (see Chapter 3 for details) a factor of 2 or even more is easily conceivable. However, this holds true for all the cores and would most likely be a systematical effect. Since it is not possible at all to give any estimation of some of these sources of

Table 5.2: The properties of the cores derived from the Gaussian fits to the dust continuum maps.

Core	$N(\text{H}_2)_{\text{peak}}$ $\times 10^{21} [\text{cm}^{-2}]$	$n(\text{H}_2)$ $\times 10^5 [\text{cm}^{-3}]$	distance [pc]	mass [M_{\odot}]
MCLD 123.5	12.1 ± 0.2	2.3 ± 0.04	150	0.31 ± 0.005
MCLD 126.6	8.5 ± 0.1	0.5 ± 0.01	150	3.27 ± 0.038
L 1457 A	21.7 ± 0.4	13.1 ± 0.24	65	0.08 ± 0.002
L 1457 B	18.8 ± 0.2	12.3 ± 0.13	65	0.08 ± 0.001
L 1457 C	16.1 ± 0.1	6.2 ± 0.04	65	0.28 ± 0.002
MBM 32	6.1 ± 0.1	1.1 ± 0.02	100	0.37 ± 0.006
Draco	6.7 ± 0.1	0.1 ± 0.002	500	36.5 ± 0.545

error, we will not consider them any more in the further analysis.

The values for MCLD 126.6 and Draco are a bit more uncertain or questionable, because of the not ideal Gaussian fits for the cores. The fitted areas do seem somewhat too large, what would also make the derived masses too large. This can happen due to the location of the cores near to one edge of the observed dust map and the higher noise at the borders. For the core in Draco an additional effect plays a significant role. This is the much larger distance of this cloud compared to the other cores of our sample, what does not allow the same spatial resolution. Nevertheless, all the values are reasonable, and we may continue our analysis of the cores by a check for the scaling correlations. To do so we need the molecular data, especially the line widths, to get an access to the kinetic energies within the cores.

5.2 Core Structure within the CS-maps

At this point we directly encounter a problem. The cores visible and defined in the dust continuum emission are not seen one-to-one in the CS maps. To elude this problem there are two possibilities. The first one is to average the spectra within the area of the core defined in the dust continuum map and to determine the line width of the resulting spectrum. For this purpose we use the higher-resolution IRAM 30-m CS observations. For MCLD 123.5, MCLD 126.6 and Draco this works very well, for L1457 it is very difficult to assign one line to one clump, because they strongly overlap and may even interact with each other. For MBM 32 we can only use the central position, since we do not have more data of this core. The resulting line widths are listed in Table 4.2 in Chapter 4.3.

The second possibility is to define the cores anew within the CS maps and to compare those with the dust continuum cores. For this purpose we use the CS ($2 \rightarrow 1$) maps obtained with the FCRAO 14-m telescope. However, to fit a two dimensional Gaussian onto the integrated intensity map would ignore the additional information on the velocity. Hence, this analysis is accomplished directly on the data cubes using the *GAUSSCLUMP* algorithm developed by Stutzki & Guesten (1990). The results of that analysis are presented in the Tables 5.3 to 5.4. Listed are the number of the sub-clump in column 1, the position in galactic coordinates (column 2 and 3), the centre velocity in column 4, the velocity full width at half maximum of the clump (column 5), deconvolved from the instrumental velocity resolution, the size of the clump in column 6, and in column 7 the intrinsic peak temperature (corrected for beam dilution). The size is defined by the mean of the major and minor axis of the fitted Gaussian, deconvolved from the intrinsic beam width ($54''$) of the telescope.

The result is very different from the Gaussian fitting of the dust continuum data. The derived CS clumps are much smaller than the dust cores, distributed and located elsewhere, and they contain only a fraction of the total flux. Clumps that were fitted with sizes smaller than, or equal to, the beam-size or a velocity FWHM smaller than two times the velocity resolution had to be excluded from the further analysis, because they are not reliable. It is very likely that observations with higher angular resolution, like the 30-m observations, will reveal even more and smaller clumps. The errors of the analysis are hard to estimate. For the fitting procedure itself and the derived parameters the formal error is less than 1% (citep:stutz90), however, the results depend on the map quality (e.g. signal-to-noise, noise level) and strongly on the angular and the velocity resolution. Hence, the errors of the individual parameters for some of the clumps may be large, and we therefore abstain from stating the formal errors.

Table 5.3: The parameters of the CS clumps in MCLD 126.6 derived from the *GAUSSCLUMP* analysis.

#	l	b	v	Δv	Size	peak temperature
	[deg]	[deg]	[km s ⁻¹]	[km s ⁻¹]	[pc]	[K]
1	126.621	24.539	-3.74	0.11	0.072	0.48
2	126.621	24.560	-3.52	0.21	0.106	0.38
3	126.573	24.496	-3.52	0.26	0.043	0.42
4	126.562	24.528	-3.66	0.24	0.067	0.33

We will analyse in the next section if the CS clumps or the dust-cores fit to the scaling relations, which are well known for cores in dark clouds. However, we can already point out some of the differences in the core properties, either observed in the dust continuum or in the CS line.

Table 5.4: The parameters of the CS clumps in MBM 32 derived from the GAUSSCLUMP analysis.

#	l [deg]	b [deg]	v [km s ⁻¹]	Δv [km s ⁻¹]	Size [arcsec]	peak temperature [K]
1	146.769	40.645	3.66	0.24	0.016	0.35
2	146.869	40.696	3.74	0.17	0.054	0.20
3	146.862	40.711	3.36	0.11	0.037	0.24

Generally, the CS clumps are much smaller than the dust continuum cores, despite the fact that the resolution of both observations is different. One reason for this is possibly found in the third axis information of the CS line emission, where one can easily separate different clumps due to the slightly varying velocities they exhibit. However, this information is not unique and can sometimes also be caused by self-absorption effects. The dust continuum emission, on the other hand, only reveals properties that are integrated over the line of sight. The small CS clumps also represent only a fraction of the total emission. A large fraction of the CS is distributed within the diffuse component. However, as already indicated several times this may apply to the dust continuum emission too, but cannot be observed with the present technique.

Another fact to note is the lower line width of the CS clumps compared to the line width of the averaged spectra and the varying central velocities of the individual clumps. This strongly indicates that the turbulence within the cores is distributed on a scale larger than the CS clump size. Hence, smaller structures are more gravitationally bound than larger structures and turbulence dissipates on the smallest scales. We will investigate this conclusion more closely in the following section by the help of scaling relations also known as Larson's Laws.

Table 5.5: The parameters of the CS clumps in L 1457 derived from the GAUSSCLUMP analysis.

#	l [deg]	b [deg]	v [km s ⁻¹]	Δv [km s ⁻¹]	Size [pc]	peak temperature [K]
1	159.270	-34.519	-5.14	0.32	0.021	0.47
2	159.207	-34.505	-5.07	0.35	0.043	0.30
3	159.275	-34.524	-4.84	0.12	0.032	0.39
4	159.325	-34.461	-4.32	0.14	0.018	0.44
5	159.256	-34.483	-4.32	0.17	0.043	0.32
6	159.275	-34.499	-4.62	0.11	0.048	0.29
7	159.281	-34.478	-2.60	0.16	0.031	0.33
8	159.274	-34.451	-5.14	0.22	0.013	0.37
9	159.306	-34.467	-4.10	0.17	0.012	0.39
10	159.274	-34.394	-4.39	0.11	0.018	0.35
11	159.363	-34.483	-4.54	0.12	0.021	0.36
12	159.224	-34.499	-4.69	0.17	0.013	0.35
13	159.243	-34.456	-4.77	0.19	0.019	0.25
14	159.205	-34.509	-5.52	0.16	0.037	0.23
15	159.287	-34.457	-5.74	0.13	0.022	0.32
16	159.243	-34.436	-5.14	0.16	0.024	0.30
17	159.211	-34.519	-5.74	0.11	0.028	0.27
18	159.288	-34.509	-5.22	0.23	0.017	0.27

5.3 Scaling Relations

Larson (1981) discovered empirical correlations among line width, cloud mass, volume density, and cloud size by extracting a value for each quantity from a spectral line map of a cloud or core and then plotting line width as a function of size, line width as a function of mass, and density as a function of size. Larson's compilation included data from spectral line maps of about 50 different regions. The maps were made using many different molecular lines which trace gas in the density range from 10 to 10^5 cm^{-3} over size scales from 0.1 pc to 100 pc. Larson fitted power laws by eye to the size – line width and mass – line width relations and showed that the clouds in his study were close to virial equilibrium.

Larson also pointed out that a power law index of 0.38 for the size - line width relation he found is very close to the value 0.33 that is predicted for a turbulent flow in incompressible gas (Kolmogorov 1941). But he also noted that good agreement of these two exponents is not necessarily expected, since molecular clouds are compressible and self-gravitating. In fact, the ISM is also magnetized, and a theoretical value for a magnetized, compressible gas is not readily derived, since it depends on field geometry and the gas equation of state. The correlations that Larson discovered have come to be known as Larson's Laws, and they have become the subject of intense study (e.g., Myers 1983, Fleck 1988, or Goodman et al. 1998).

Physically, no complete explanation of Larson's Laws has yet been established. Turbulence (e.g. Falgarone et al. 1994) and/or an array of magnetohydrodynamic waves (e.g. Gammie & Ostriker 1996) remain the leading hypotheses, but the ultimate origin and exact nature of the "suprathermal" kinetic energy is still unclear. However, it was noted several times (e.g. Myers 1983 or Goodman et al. 1998) that turbulence must dissipate on smaller scales in order to permit star formation.

5.3.1 The Size – Line Width Relation

To study if our cores are "normal" compared to cores in dark clouds we now scrutinise our data for these well known scaling relations. The first one is the size – line width relation. Observations of large molecular clouds (e.g., Larson 1981) and dense cores in dark clouds (e.g. Myers 1983) show the following correlation between the parameters

$$\Delta v \propto r^\beta \tag{5.13}$$

with β in the range of 0.3 to 0.6 for different clouds (Fleck 1988). This is most likely a consequence of the turbulence within the cores (Heithausen 1996). Although, it was long thought that it might be due to the virial equilibrium in the cloud (see, e.g., Myers 1983 or Fleck 1988). This was, because most of the studies have been made for gravitationally bound clouds.

However, Heithausen (1996) showed that this correlation also holds true for high-latitude clouds and these clouds are totally dominated by turbulent motions and not at all at virial equilibrium. This analysis was based on the CO survey conducted with the CfA 1.2 m telescope and revealed the relation for structures on the scale of clouds like shown in the IRAS maps in Chapter 2. Together with data for more massive clouds from Dame et al. (1986) and Falgarone & Perault (1987) he found the best fit was given by

$$\log(\Delta v) = (0.46 \pm 0.03)\log(r) + (0.16 \pm 0.03) \quad (5.14)$$

over 3 magnitudes in size and 2 magnitudes in line width. In this relation Δv is expressed in km s^{-1} and r in pc.

We now want to analyse if this relation is still applicable at the even smaller scale of our cores. Therefore, we define the radius of the cores and clumps by calculating the mean of the major and minor axis derived by the Gaussian fits. For the line width we use the CS ($2 \rightarrow 1$) line measured with the IRAM 30-m telescope and the Gaussian fits to the spectra. Were it was possible, i.e. for MCLD 123.5+24.9, MCLD 126.6+24.5, and Draco, we averaged the spectra over the core area and derived the line width from the combined spectrum. For MBM 32 we only have the spectrum at the central position, therefore we had to use this. For L 1457 we had to assign one line component to each clump. This is described in detail in Chapter 4.3.

The resulting values are listed in Table 5.6 and the data are shown in Figure 5.6 as red rectangles together with the CS clumps (green triangles) of MCLD 126.6+24.5, L 1457, and MBM 32 found in the previous section, the SO clumps (black crosses) of MCLD 126.6+24.5 found by Heithausen et al. (1998), and the data and fit of Heithausen (1996). The line is given by equation 5.14.

Table 5.6: Core radius, CS line width, density, and core mass

Core	radius [pc]	Δv [km s^{-1}]	$n(\text{H}_2)$ $\times 10^5 [\text{cm}^{-3}]$	mass [M_\odot]
MCLD 123.5	0.042	0.77	2.3	0.31
MCLD 126.6	0.138	0.40	0.5	3.27
L 1457 A	0.013	0.57	13.1	0.08
L 1457 B	0.015	0.65	12.3	0.08
L 1457 C	0.032	0.80	6.2	0.28
MBM 32	0.055	0.43	1.1	0.37
Draco	0.513	0.90	0.1	36.5

The radius is the mean of major and minor axis and the indicated density is the peak density derived from the Gaussian fits to the dust continuum data. The line widths, Δv , are derived from the IRAM 30-m CS ($2 \rightarrow 1$) line measurements.

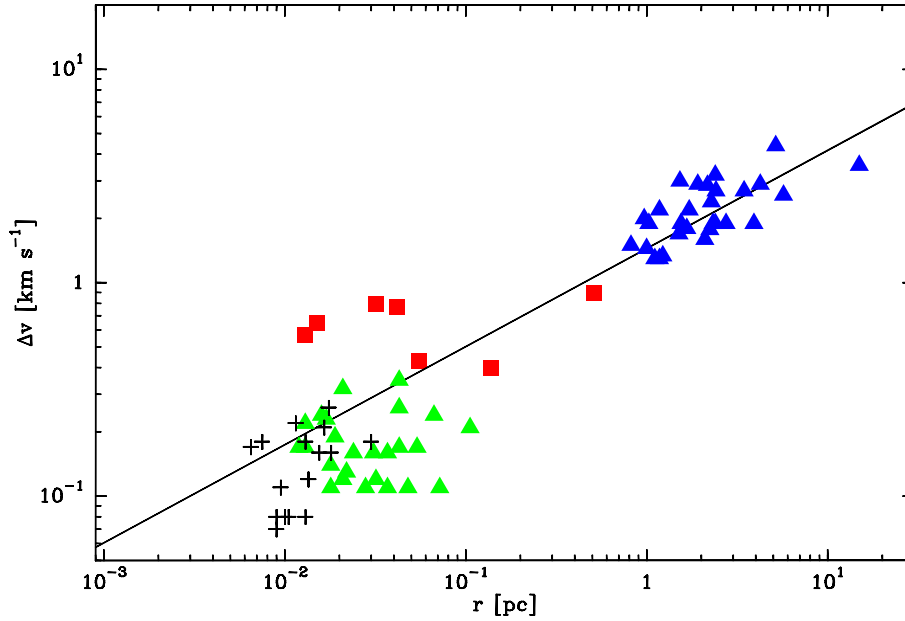


Figure 5.6: Size – line width relation for cores and clumps in cirrus clouds. The red squares represent the dust continuum cores and clumps, the green triangles show the clumps found in the CS maps of MCLD 126.6+24.5, L 1457, and MBM 32, the black crosses display the clumps found in the SO map of MCLD 126.6+24.5 by Heithausen et al. (1998). The line is no fit to the data, but the correlation found by Heithausen (1996) for high-latitude molecular clouds, which are indicated by the blue triangles.

The dust continuum cores and clumps, indicated by the red squares in Figure 5.6, fit nicely to the relation, located 1 to 2 orders of magnitudes lower in radius than the clouds investigated by Heithausen (1996) (blue triangles). It is apparent that most of our cirrus cores and clumps are distributed above the correlation line, demonstrating somewhat larger line widths than expected.

This is easily comprehensible as the CS spectra obviously trace larger and less dense volumes than the dust emission peaks. We already noted this above. Additionally, as mentioned before, we had some problems to assign the CS lines and sub-clumps to each other in L 1457. They constitute the smallest clumps in the diagram. The core in MCLD 123.5+24.9 also shows a slightly larger CS line width than expected from the correlation, caused most likely by the self-absorption feature due to the infall motion. Nevertheless, we can disclose that the cirrus cloud cores follow the size – line width relation.

The CS clumps, which were defined in the previous section and are indicated by the green triangles in Figure 5.6, fall slightly short of the relation. This is, in principle, a similar result as the one found by the study of Heithausen et al. (1998) for the SO clumps in MCLD 126.6+24.5. In Figure 5.6 they are shown as black crosses. The small difference between both samples can easily be explained by the different resolutions, spatial and in velocity, of the observations. This result strongly indicates the dissipation of the turbu-

lence on the smallest observed scales. Hence, the cirrus cloud cores show the very same behaviour as cores in star forming regions.

5.3.2 The Size – Density Relation

The next well known correlation is the size – density relation, that relates the size and the average volume density of the cores. It can be described by the equation

$$n \propto r^\alpha. \quad (5.15)$$

It was investigated by, e.g., Larson (1981), Myers (1983), and Heithausen (1996). Larson (1981) derived a slope of $\alpha = -1.1$ for molecular clouds. The study of Myers (1983), for instance, found a slope of $\alpha = -1.3$ for dense cores in dark clouds, whilst Heithausen (1996) found a significantly lower slope of $\alpha = -0.8$ for high-latitude clouds. He suggested that the difference was created by a lower volume filling factor of the cirrus clouds and an observational effect caused by a different cloud size definition as well as a higher sensitivity of the data.

Since our cores are observed with a substantially higher angular resolution the volume filling factor should be higher and this effect is expected to be irrelevant. The values were already calculated in a previous section and are listed again in Table 5.6. Figure 5.7 shows the relation and the solid line represents the fit to the data.

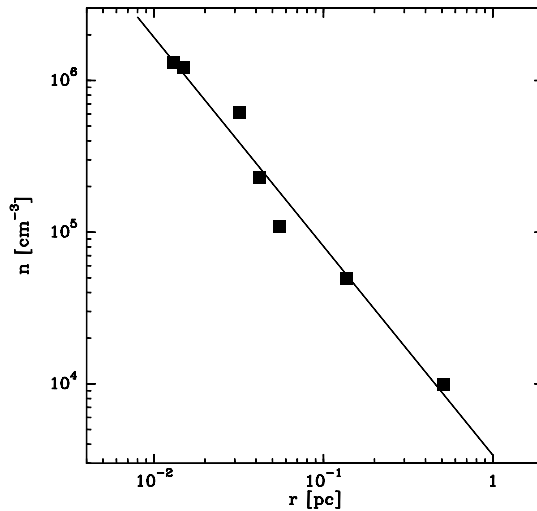


Figure 5.7: Size – density relation for the cirrus cloud cores and clumps. Both values are exclusively calculated from the dust emission observations. The solid line represents the fit to the data with a slope of -1.38.

The fit do the data gives

$$\log(n) = -(1.3764 \pm 0.047)\log(r) + (3.5323 \pm 0.073) \quad (5.16)$$

with the linear regression correlation coefficient $r = 0.97$. In this equation n is expressed in cm^{-3} and r again in pc.

The cores and clumps follow the size-density relation perfectly. The slope of $\alpha = -1.38$ agrees very well with the one determined for cores in dark clouds. This is a surprising result and was not expected. It also shows that our selection based on the thermal dust emission in fact reveals the most dense cores and the volume filling factor is irrelevant. Both of the values are exclusively calculated from the dust emission observations, what may contribute to the strong correlation.

We did not calculate densities and masses of the CS clumps, because to determine these values one has to assume excitation conditions, an opacity, and the abundance of the molecule. Heithausen et al. (1998) calculated the values for the SO clumps in MCLD 126.6 and found a large offset compared to the relation found for high-latitude clouds on larger scales (Heithausen 1996). Hence, we think it is not worth the effort, since the values which shall be assumed are not based on reliable, physical facts.

Instead we want to compare our cirrus cloud cores to the starless cores investigated by Tafalla et al. (2002). They studied five round starless cores in the Taurus-Auriga complex (L 1498, L 1495, L 1517B, and L 1544, and L 1400K), which are all well known and fairly well studied e.g. by Benson & Myers (1989), Ward-Thompson et al. (1999), or Caselli et al. (2002). Tafalla et al. (2002) derived a density distribution for each core by modeling the 1.2 mm dust continuum emission. They averaged the data in circles or ellipses and fitted density profiles of the form:

$$n(r) = \frac{n_0}{1 + (r/r_0)^\alpha}, \quad (5.17)$$

where n_0 is the central density, r_0 the radius of the "flat" region ($2r_0$ is the FWHM) and α is the asymptotic power index, which ranges from 2 to 4 in the derived fits.

We can adopt their values ($2r_0$ and n_0) and compare them with the values of the cirrus cores. The values are indicated in Table 5.7. In Figure 5.8 we show again the size - density relation, together with the cores of Tafalla et al. (2002) represented by the red triangles, and the SO clumps of Heithausen et al. (1998), displayed by the blue triangles.

The starless cores investigated by Tafalla et al. (2002) fit perfectly to the derived relation. Size and density of these cores are very similar to the cirrus cloud cores, indicative of our speculation that cirrus clouds may be able to form stars. The SO clumps defined by Heithausen et al. (1998) do not fit to the relation. There is a large offset in size and/or density, however, the slope appears to be similar. This may be due to wrong assumptions

Table 5.7: The properties of the cores investigated by Tafalla et al. (2002).

Core	radius [pc]	$n(\text{H}_2)$ $\times 10^5 [\text{cm}^{-3}]$
L 1498	0.10	1.0
L 1495	0.06	1.1
L 1400K	0.05	1.2
L 1517	0.05	2.2
L 1544	0.03	14.0

The radius is the $\text{FWHM} = 2r_0$ of the fitted density profile and the cited density is the central density n_0 . The values are adapted from Table 2 of Tafalla et al. (2002).

for the excitation conditions or the molecular abundance and therefore, a wrong density. However, it may also solely due to the fact that molecular observations trace different volumes and may be less sensitive to density structures than to chemical properties. We will investigate the issue of abundances in more detail in the next chapter.

The result is a strong additional hint, that cores in cirrus clouds are very similar to starless cores in dark clouds and star forming regions, and that they may be able to form stars or brown dwarfs.

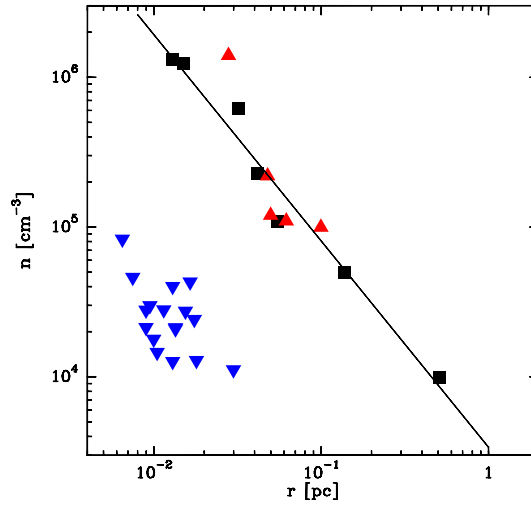


Figure 5.8: Size – density relation for the cores and clumps, respectively. The black squares and the solid line are the same as in figure 5.7. Additionally, the SO clumps of MCDL 126.6 found by Heithausen (1998) are shown as blue triangles, and the starless cores investigated by Tafalla et al. (2002) are displayed by red triangles.

5.3.3 The Mass – Line Width Relation

Larson (1981) in his study of molecular clouds noted, that the cloud mass and the velocity dispersion or line width should strongly correlate if the clouds are close to virial equilibrium. He found the following correlation

$$\Delta v \propto M^{0.20}. \quad (5.18)$$

The idea behind is that more massive cores are more turbulent, since they are more bound by their own gravity. However, theoretically this only applies to fully stabilised cores or clouds. Nevertheless, since the size – line width relation and the size – density relation are valid, it is clear that the mass calculated from size and density should also correlate with the line width.

We show the relation in Figure 5.9. The cirrus cloud cores and clumps, represented by the black triangles, fit in principle to the solid line, which represents the correlation found by Larson (1981) with a slope of 0.2. The blue triangles show the clouds investigated by Larson (1981).

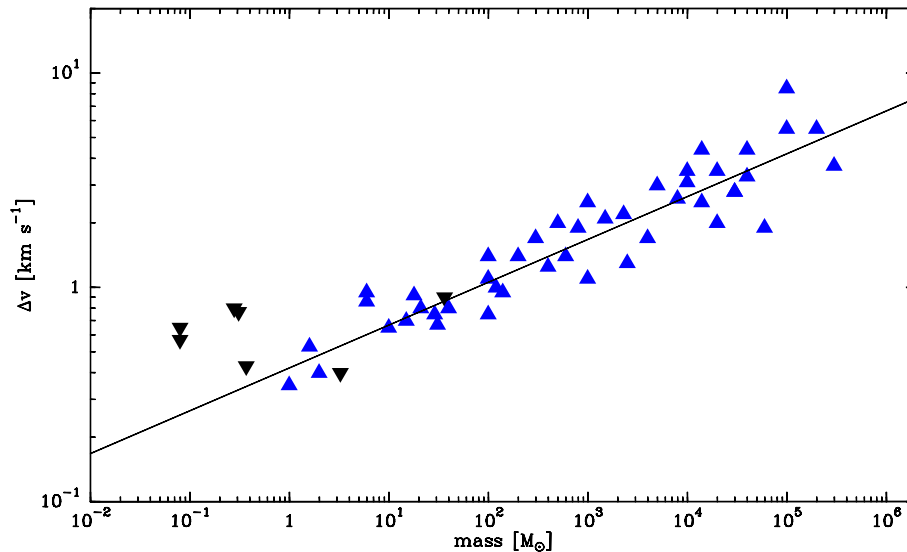


Figure 5.9: Core mass vs. line width for molecular clouds and cirrus cloud cores. The cirrus cloud cores and clumps are represented by black triangles. The blue triangles display the molecular clouds investigated by Larson (1981) and the solid line represents the correlation he found.

However, the cirrus cloud cores and clumps do not follow the correlation as closely as expected from the work of Larson (1981). This is, most likely, due to the different volumina traced by the dust continuum and the CS molecule, respectively. Nevertheless, it may also indicate that not all of the cores are in virial equilibrium.

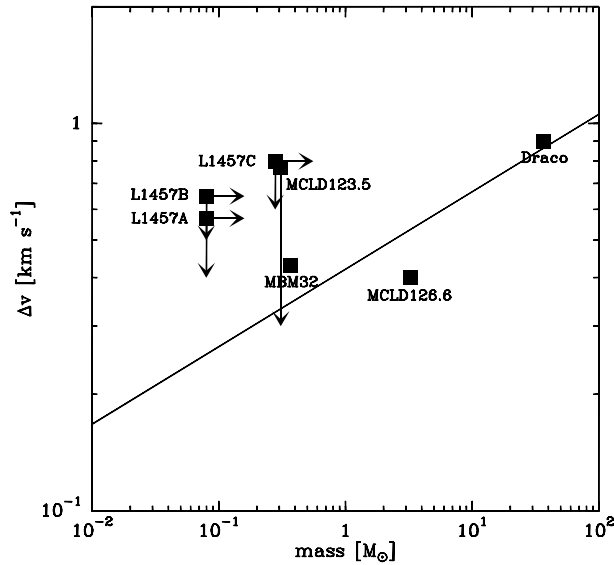


Figure 5.10: Core mass vs. line width for the cirrus cloud cores and clumps. The solid line shows again the correlation found by Larson (1981). The cores are labelled and the arrows indicate possible corrections discussed in the text.

In order to discuss this topic in a bit more detail we labelled the individual cores in Figure 5.10. One recognises immediately that the clumps in L 1457 and MCLD 123.5 lie above the correlation. We already discussed several times the possible causes for the large line widths in these cores. Thus, a lower line width of them is very likely.

For MCLD 123.5 the CS ($2 \rightarrow 1$) line is probably self-absorbed and traces the envelope of the core itself. The line width of the CS ($5 \rightarrow 4$) transition amounts to only $\Delta v = 0.29 \text{ km s}^{-1}$, thus the core would lie directly at the line. In Figure 5.10 this is indicated by the arrow.

For the clumps in L 1457 there are actually two possibilities for corrections. The first one is the line width. The lines emanating from the individual clumps may be much more narrow but superposed and broadened by the diffuse component between the clumps. The second possible correction is the mass of each clump. Caused by the large uncertainty of the exact distance towards this cloud we assumed the former value of 65 pc, however, it is possible that the cloud is much farther, up to 200 pc (see Chapter 2.3 for details). This would make the clumps larger and more massive. In addition, there are strong indications that we missed a significant fraction of the dust continuum emission, especially in this core, because it is more diffuse and distributed between the clumps. This would also account for higher masses. We indicated the possibilities in Figure 5.10 by arrows. The cirrus cloud cores and clumps would thus follow the correlation more closely.

We will investigate this topic further in the next paragraph by calculating the virial masses of the cores. However, the errors or corrections discussed here will remain unchanged.

5.3.4 Virial Masses of the Cores

In a previous section we calculated a mass for each of the cores by using the dust continuum emission. This mass only depends on the core size and the peak flux derived from the dust continuum maps by Gaussian fits. In the following we will refer to this molecular mass as the total mass of the cores. However, one can also calculate a virial mass of the core by applying the virial theorem to the measured gas velocity dispersion. If a core is gravitationally bound the total mass should be of the same order or larger than the virial mass. However, this does, for instance not take into account the pressure of the ambient medium, which may significantly contribute to the core stability.

For a core with the radius r (in our case, this is the mean of the minor and major axis) applies

$$M_{\text{vir}} = 5\sigma^2 r / G. \quad (5.19)$$

(Bertoldi & McKee (1992)), where $\sigma = \Delta v / 2.355$ is the one-dimensional gas velocity dispersion and G is the gravitational constant.

We will use again the line widths derived from the CS ($2 \rightarrow 1$) IRAM 30-m measurements, although we already know that this may not lead to a reliable result. The values are listed in Table 5.8 together with some previously calculated values for ease of comparison. Additionally, we plotted the total and virial masses in Figure 5.11.

Table 5.8: Comparison of the total masses and the virial masses of the cores

Core	radius [pc]	Δv [km s ⁻¹]	total mass [M _⊙]	virial mass [M _⊙]
MCLD 123.5	0.042	0.77	0.31	5.23
MCLD 126.6	0.138	0.40	3.27	4.64
L 1457 A	0.013	0.57	0.08	0.89
L 1457 B	0.015	0.65	0.08	1.33
L 1457 C	0.032	0.80	0.28	4.30
MBM 32	0.055	0.43	0.37	2.14
Draco	0.513	0.90	36.5	87.3

The line widths and, out of it, the virial masses are derived from the IRAM 30-m CS ($2 \rightarrow 1$) line measurements, whereas the total masses are the H₂ masses derived from the dust continuum maps.

As one sees immediately the virial masses estimated from the CS line widths are nearly all larger by an order of magnitude than the total masses of the cores. This result was almost expected by us, as it can also be seen in the relations calculated above. The most likely explanation for this is not that the cores are totally dominated by turbulence and are just

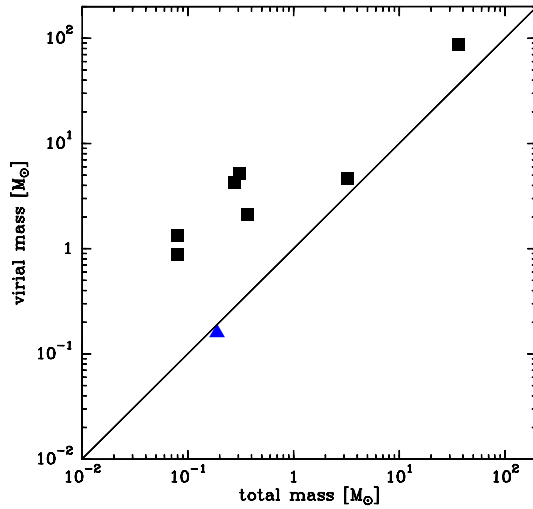


Figure 5.11: The total mass vs. the virial mass for the cores and clumps, respectively. The solid line represents the line of parity. All cores (black squares) lie above the line, implying that they are not gravitationally bound. The blue triangle represents the HC_3N core in MCLD 123.5 defined by Heithausen et al. (2002), which appears to be gravitationally bound.

transient objects, but that the CS does not trace the same volume as the dust emission. The line width of the optically thick CS ($2 \rightarrow 1$) line seems to be strongly influenced by the less dense gas around the core, which has a much larger velocity dispersion than the core itself.

For this reason we have to find another tracer of the dense core that also provides the velocity information but is less abundant in the surrounding gas. Heithausen et al. (2002) used the HC_3N ($10 \rightarrow 9$) transition to assess the stability of the core in MCLD 123.5+24.9. They measured a line width of only $\Delta v = 0.19 \text{ km s}^{-1}$ resulting in a virial mass of $M_{\text{vir}} = 0.16 M_{\odot}$ for the HC_3N clump. The clump is displayed in Figure 5.11 by the blue triangle. We have to note that the clump defined by the HC_3N emission is a lot smaller than the clump we defined from the dust emission map. We show in Section 4.4 that the HC_3N does not at all trace the same volume as the dust continuum. In Section 6.1 we try to give a possible explanation for this behaviour.

Unfortunately, we did not detect the HC_3N line in the other cores, as described in Chapter 4, to check for similar patterns. Furthermore, due to the complications discussed in the next section and in Section 6.1 the molecule also seems not qualified for the targeted aim. Tafalla et al. (2002) and other authors (e.g., Zhou et al. 1989) already noted a systematic NH_3 -CS line width discrepancy. The NH_3 line always appears more narrow than the CS line width.

This has been traditionally interpreted as resulting from the increase of gas turbulence with radius and the CS is generally tracing a larger volume than the NH_3 . However, Tafalla et al. (2002) concluded from their models, that it can arise from a combination of

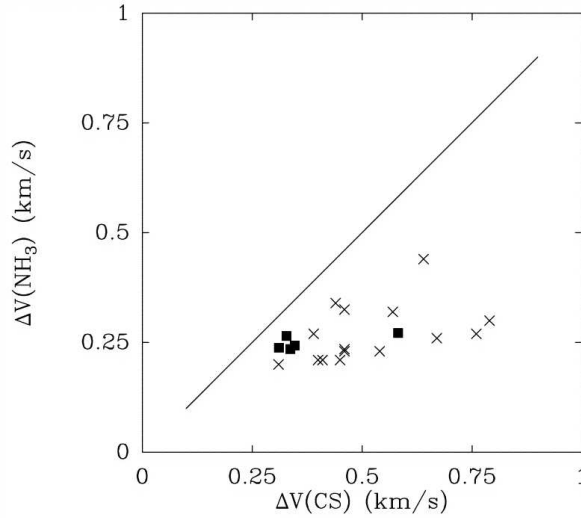


Figure 5.12: Comparison of CS and NH_3 line widths from dense cores. The Figure is adapted from Tafalla et al. (2002). Although this line width discrepancy has been traditionally interpreted as resulting from the systematic increase of turbulence with core radius, they claim that optical depth broadening and self-absorption are the two causes of the broader CS lines.

optical depth and self-absorption in the CS line as well. We tend to subscribe to this view from what our data show.

In Table 5.9 we have compiled the line widths of three molecules in the cores. They are all thought to trace about similar regions, but show significant differences. The C^{18}O ($2 \rightarrow 1$) line, for instance, is always a bit more narrow than the CS ($2 \rightarrow 1$) line. The same holds true for the SO ($1_0 \rightarrow 0_1$) transition, however, for this molecule it is known to exhibit a different behaviour, caused by the completely different formation scenario.

This suggests, that the turbulent fraction of the line widths is mostly caused by the clumpy structure of the ISM and the relative velocities of the small clumps to each other. In cirrus clouds the high dependency on abundance variations on smallest scales, due to the low density regime, enhances the differences between various molecules. Virial masses estimated from the C^{18}O line width are smaller compared to the ones estimated from the CS ($2 \rightarrow 1$) line width. For more complicated or late type molecules, respectively, this discrepancy becomes even larger. Hence, it seems questionable to use the line widths of just one molecular species to derive virial masses of the cores.

From the estimates made above and the result of the comparisons we can, nevertheless, conclude that the virial masses of the cores are generally larger than the total masses derived from the dust continuum or the gas density. However, this does not imply that the cores are not influenced by self-gravity or gravitationally bound. But the dominant force seems to be turbulence.

Table 5.9: Comparison of line widths of several molecules in the investigated cores.

Core	$\Delta v_{\text{CS}(2 \rightarrow 1)}$ [km s ⁻¹]	$\Delta v_{\text{C}^{18}\text{O}(2 \rightarrow 1)}$ [km s ⁻¹]	$\Delta v_{\text{SO}(1_0 \rightarrow 0_1)}$ [km s ⁻¹]
MCLD 123.5	0.77±0.05	0.52±0.02	0.51±0.03 ^a
MCLD 126.6	0.40±0.02	0.34±0.03	0.26±0.03 ^b
L 1457 A	0.57±0.12	0.39±0.04	-
L 1457 B	0.65±0.16	0.39±0.05	-
L 1457 C	0.80±0.13	0.75±0.13	-
MBM 32	0.43±0.26	-	0.41±0.16 ^b
Draco	0.90±0.12	-	0.46±0.11 ^b

^a Heithausen et al. (1995)

^b Heithausen et al. (1998)

- no detection or no data available

For the smallest sub-clumps, traced by complex or late type molecules, and which are not distributed throughout the whole core, virial and total mass become equal as the example of the HC₃N clump in MCLD 123.5+24.9 shows (Heithausen et al. 2002). The clumpy structure does not allow a more secure predication of the gravitational stability of the cores. Nevertheless, since the core properties are very similar compared to starless cores in the Taurus-Auriga complex, it seems likely that they also have a similar evolution.

6

Chemical Core Properties and Star Formation Capability

We detected all selected cores in the dust continuum emission as well as in the CS ($2 \rightarrow 1$) line. This provides a first hint, that dense cores in cirrus cloud indeed are common. Although they are difficult to detect and have a small volume filling factor, due to the large volume cirrus clouds are distributed in. Nevertheless, they seem to exist in nearly every cirrus cloud. The detection appears to be mostly a matter of observational sensitivity. It is evident that large surveys with small telescopes often miss these cores, due to the low resolution or the lack of integration time. With large telescopes like the IRAM 30-m dish the cores are detectable but one has to know exactly where to look.

We can already conclude here that cores in cirrus clouds are very similar to (starless) cores in dark clouds and star-forming regions. However, mostly due to the low density environment in cirrus clouds there also exist significant differences. This may find its natural explanation by the help of new and more detailed models of turbulent motions (see, e.g., Klessen et al. 2000). Because these models show that turbulence on different scales is able to account for the origin of a high number of such cores. In dark clouds, in contrast, it is thought that gravity plays a significant role in the core formation process. However, it is possible that both methods lead to a very similar result and the major differences are solely due to the somewhat lower densities in cirrus cloud cores.

The overall appearance of the cirrus cloud cores is in principle comparable in several tracers, e.g. the dust continuum emission and various molecules like $C^{18}O$ or CS. Although, the CS emission generally shows a broader extent and seems to trace much better the more diffuse component around the condensation, but not the dense core itself. Admittedly, the angular resolution of the observations we have carried out is highly different ($11''$ for the dust continuum versus $54''$ for the FCRAO CS ($2 \rightarrow 1$) maps) and we definitely missed a noticeable fraction of the more diffuse dust emission due to the observational technique

(see Chapter 3 for details on this topic). As it can be seen in the interferometric CS map of MCLD 123.5+24.9 a higher angular resolution always reveals new substructures.

We now shall investigate the different appearance of the cores in different molecules in more detail. The most likely explanation are strong abundance variations of the molecules on relatively small scales. The chemical differentiation has additional implications for the studies of low-mass star formation. CS, for example, is one of the molecules of choice for density determinations in the literature (see, e.g. Evans 1999). We already showed that it may not be the best choice to study low-mass cores. Other molecules, like HC₃N or NH₃, are affected by the timescales of low-density gas chemistry. Although it may be argued that dust continuum observations may suffice to derive core densities and masses, a confirmation of these estimates with molecular observations seems necessary, given the uncertainties in the dust emission properties. Additionally, kinematical information are solely provided by molecular observations.

Hence, in the next section we want to analyse the abundance variations within the cirrus cloud cores provided by the molecular observations. Subsequently we are able to briefly discuss some aspects of the chemistry in cirrus clouds.

6.1 Abundance Variations

It was already noted by various investigators, e.g., Großmann & Heithausen (1992), Gerin et al. (1997), Heithausen et al. (1998), or Bensch et al. (2003), that strong abundance variations on relatively small scales become very important in the interpretation of molecular line observations. In studies conducted in star-forming regions the effects of time dependent chemistry often do play only a minor role. For cirrus cloud cores, in contrast, this seems to be the major admission for molecular species, as the heating is done mainly by the rather smooth ISRF, than by nearby stars. Therefore, the physical conditions should not vary much within small scales, but densities and chemical ages of small sub-clumps become the important factors.

Based on the H₂ column densities estimated from the dust continuum and our additional molecular line observations we analysed the column densities and abundances of the observed molecules. This was done by a LVG (*Large Velocity Gradient*) model analysis, where we tried to match the observed line intensities. The code was written and provided by P. Schilke. We also made additional calculations with RADEX, a non-LTE (*Local Thermal Equilibrium*) molecular radiative transfer model in an isothermal medium written by J. H. Black and F. van der Tak (Schoeier et al. 2004). Both results were always in very good agreement. We used a dust temperature of 10 K and the H₂ densities derived from the dust continuum observations. The resulting column densities of the molecules are listed in Table 6.1 together with the H₂ column density. Some of the values are just upper limits, since we did not detect the appendant lines. In Table 6.2 we compile the resulting fractional molecular abundances relative to H₂, together with values of star-forming cores from the literature, for comparison. We do not state errors for the calculated values, since

this is just a qualitative analysis at individual positions. For more reliable and precise results a detailed model is needed that treats the physical and chemical properties of the cores simultaneously.

Table 6.1: The peak column densities of various molecules in the cores derived from LVG and RADEX calculations.

Core	$N(\text{H}_2)$ $\times 10^{21} [\text{cm}^{-2}]$	$N(\text{C}^{18}\text{O})$ $\times 10^{14} [\text{cm}^{-2}]$	$N(\text{CS})$ $\times 10^{12} [\text{cm}^{-2}]$	$N(\text{HC}_3\text{N})$ $\times 10^{12} [\text{cm}^{-2}]$
MCLD 123.5 ¹	12.1	25	21	1.9
MCLD 123.5 ²	11.6	18	14	3.3
MCLD 126.6	8.5	6	5	-
L 1457 A	21.7	5	2	0.1*
L 1457 B	18.8	4	1	0.1*
L 1457 C	16.1	4	2	0.1*
MBM 32	6.1	1*	1	0.4*
Draco	6.7	1*	6	1*

¹ at the position of the CS peak

² at the position of the HC₃N peak

* upper limit

- no data available

Our results are qualitatively in very good agreement with the investigation of Gerin et al. (1997) for Polaris and Taurus. One of their conclusions was, that the core MCLD 123.5+24.9 is similar to a dark cloud. However, one sees immediately that this core features the highest molecular abundances compared with the other cores in this study. Does this make MCLD 123.5+24.9 a special case and unusual for cirrus cloud cores?

The comparison of the molecular column densities shows strong variations not solely due to the different H₂ densities. Therefore, they must be caused by abundance variations. It can be assumed that the excitation conditions are not as different in the various cores. Hence, a very important factor may be the age of the condensations. Most molecules need an initial density to build up measurable high abundances. This process is closely connected to the dust grains which are mostly serve as catalysts for the reactions. On the other hand, they also strongly effect the abundances. Molecules freeze out onto the dust grains, get locked or released by the particles, depending on densities and excitation conditions. The chemical reactions feature characteristic timescales. It is obvious, that complicated molecules do need more time to build up higher abundances than more simple molecules.

Taylor et al. (1998) proposed that the mismatch between CS and NH₃ maps arises from the clumpy nature of the clouds. Most of the sub-clumps may be dissipated before NH₃ abun-

Table 6.2: The peak abundances of several molecular species relative to H_2 . The second part shows literature values from cores in dark clouds or star-forming regions for comparison.

Core	$X(\text{C}^{18}\text{O})$ $\times 10^{-8}$	$X(\text{CS})$ $\times 10^{-10}$	$X(\text{HC}_3\text{N})$ $\times 10^{-11}$
MCLD 123.5 ¹	20.7	17.4	15.7
MCLD 123.5 ²	15.5	12.1	28.4
MCLD 126.6	7.1	5.9	-
L 1457 A	2.3	0.9	< 0.5
L 1457 B	2.1	0.5	< 0.5
L 1457 C	2.5	1.2	< 0.6
MBM 32	< 1.6	1.7	< 6.6
Draco	< 1.5	9.0	< 14.9
Taurus ³	5.1	1.7	-
L134N ⁴	17*	16.5	8.7
TMC 1 ⁵	17*	15	225
L 1251 ⁶	17*	34	-

- no data available

¹ at the position of the CS peak

² at the position of the HC_3N peak

³ Gerin et al. (1997), at the position (RA,DEC)(1950) = (04:34:07, +24:10:00)

⁴ Dickens et al. (2000)

⁵ Pratap et al. (1997), at the Cyanopolyne peak position

⁶ Nikolić et al. (2003)

* The value is taken from Frerking et al. (1982) and in the cited studies used as a standard conversion factor to determine the H_2 column density.

dances could be build up to a significant level, but they already contained substantial CS. A few clumps, maybe slightly denser or more massive, are sufficiently longer lived to allow NH_3 to increase in abundance. These may be the ones that are continue to form pre-stellar cores. A very similar situation applies for the HC_3N molecule, which we tried to observe here. The highest abundance of this molecule in a pre-stellar core can be found in the Cyanopolyne (CP) peak of TMC 1 (Pratap et al. 1997). However, at most other positions within this core it is significantly less abundant, averaged over the whole core its relative abundance is about a factor of 3 lower. Though the density in TMC 1 is generally one order of magnitude higher than in the cirrus cloud cores and the lines are optically thick. The results for L134N are very similar to the ones derive for the core in MCLD 123.5+24.9.

Time dependent chemical models do strongly depend on the reaction set used and the physical conditions assumed. In the literature only a few models can be found that ap-

ply to this low-density regime. Markwick et al. (2000) constructed a model for TMC 1, the core in the Taurus molecular cloud, that should be applicable to cirrus cloud cores as well. Taurus is a well known low-mass star-forming region, but the core TMC 1 does not show any signs of a proto-stellar object. The initial conditions in this model are a temperature of 10 K, a hydrogen number density $n(\text{H}_2) = 2 \times 10^4 \text{ cm}^{-3}$, a cosmic ray ionization rate of $1 \times 10^{-17} \text{ s}^{-1}$, and the UMIST Database for Astrochemistry 1995 reaction set (Millar et al. 1997). It predicts a time delay of $(3 - 10 \times 10^5)$ years between HC_3N and CS in reaching measurable high abundances after the core was formed (see Figure 6.1).

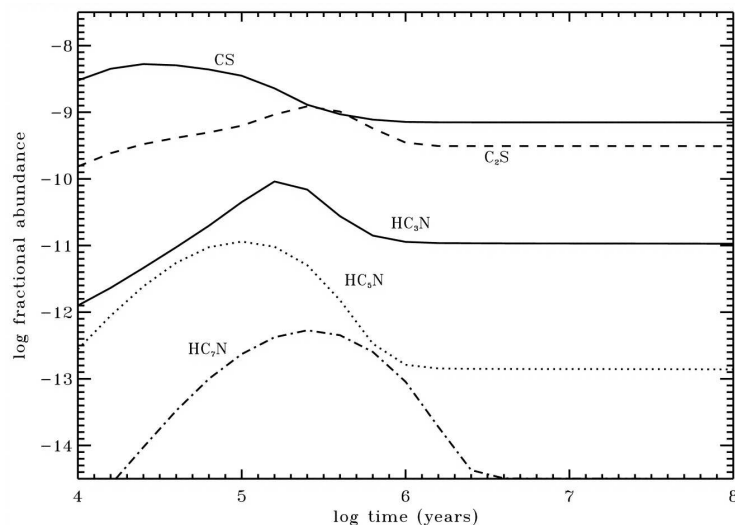


Figure 6.1: Variation of the fractional abundances of CS, C_2S , and the cyanopolyynes HC_nN ($n = 3, 5, 7, 9$) The model was run for 10^8 yr using the physical parameters and initial conditions detailed in the text to reach a typical steady state composition. The Figure was adapted from Markwick et al. (2000). We want to emphasise here the time HC_3N needs to reach its highest abundance.

We tend to explain the observed small scale abundance variations with a very clumpy nature of the clouds. Within the core region several small, dense clumps have been formed. The cores are most likely not gravitationally bound, however, most of them seem long-living and, hence, somehow stabilised against a disbandment. This seems possible due to the pressure from the surrounding medium. The dust continuum observations show a integrated intensity view, only. It is a bit surprising that most of the cores exhibit a centrally condensed structure anyway. The CS ($2 \rightarrow 1$) line arises from, more or less, all of the sub-clumps and is often absorbed by foreground clumps or even self-absorbed. Thus it is hard to interpret, but is a very good tracer for young cores. Maps with a sufficient resolution, both spacial and in velocity, can reveal the clumpy substructure effectively. HC_3N is only partly suited as a density tracer in this kind of cores, as the majority of the core is not dense enough to build up a high abundance of this molecule.

In the following we will discuss the properties of the cores in a bit more detail. We will start with the values calculated in the previous section. Abundance variations are hard to interpret and often do complicate the analysis. Detailed chemical models can help a lot but have to be adapted to the specific situation of each core.

6.2 Gas Chemistry in Cirrus Cloud Cores

After having calculated some of the basic core properties we now compare the individual molecular observations with each other in more detail. We shall concentrate the analysis on the best studied cores, but the results are generally valid for the other cores of our sample as well.

It is known for some time that molecular cores look different if observed in different tracers. This also holds true for cirrus cloud cores. As all molecules are affected by abundance variations and excitation conditions, dust is thought to represent the best tracer for the total molecular material within the core. Limitations are mostly caused by the observational procedure. However, this provides merely a line-of-sight integrated pattern. To obtain a more precise picture of the studied core we clearly need kinematical informations as well. Molecular line observations do contain these data, but the interpretation is often difficult.

The choice of the molecule to observe is crucial for a success. To get a as much as possible strong signal one has to choose an abundant and excited molecule. The transition should also be in a frequency band observable with available instruments. The most abundant, easiest to excite and to observe molecule is carbon monoxide (CO). However, it was shown that CO is not a good tracer for dense gas, especially cold and dense cores. First, it becomes optically thick already for medium densities and the emission from the core region is absorbed by the surrounding material. Second, the molecule starts to freeze out onto dust grains rather fast. Another often used tracer molecule, carbon monosulfide (CS), is much more suitable for this purpose, but it gets similar problems for really high densities.

Originally, we thought that CS is the ideal tracer for the cores in cirrus clouds, since the densities are not as high as in star-forming regions. However, we found a very clumpy substructure and the lower densities to be partly caused by beam filling effects. The determined values for the innermost core regions and sub-clumps are comparable to dark cloud densities. Therefore CS proved to be not the ideal choice, since the superposition of lines originating in different sub-clumps changes the line profile significantly.

We also searched for other molecules that are known to be good density tracers. In a number of studies ammonia (NH_3) (e.g., Tafalla et al. 2002) or carbon-chain molecules, such as cyanoacetylene (HC_3N) (e.g., Ladd & Covey 2000), were considered as good probes for the innermost dense core region, however, as shown by, e.g., Heithausen et al. (2002) they

rarely trace the same volumes as other high density tracers. This is most likely caused by the different formation time scales of these relatively complicated molecules. Compared to the much easier build CS, for instance, they need at least 3×10^5 years more to reach measurable high abundances. This, of course, depends strongly on the chemical model (e.g., the time dependent chemical model for TMC 1 by Markwick et al. 2000).

We compare again various data of some of the cores in detail. To get a visual overview we first display the dust continuum and integrated intensity maps next to each other. Figure 6.2 shows MCLD 123.5+24.9 and Figure 6.3 MCLD 126.6+24.5.

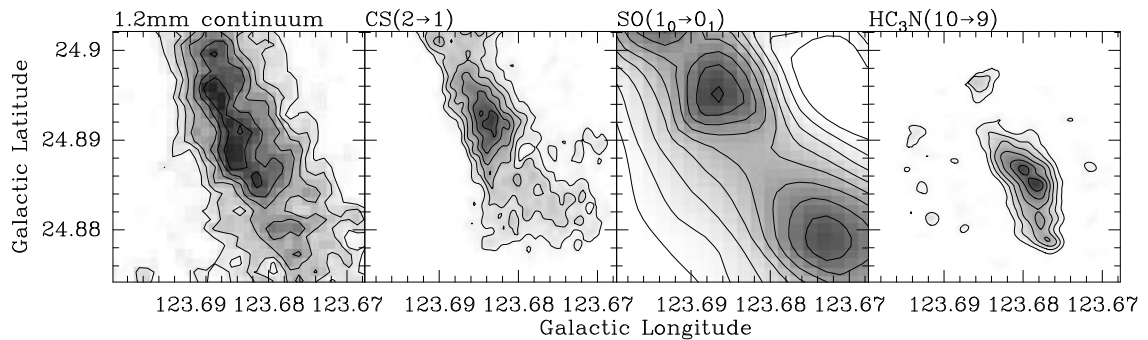


Figure 6.2: Maps of the 1.2 mm dust continuum, the integrated CS (2 → 1), SO (1₀ → 0₁), and HC₃N (10 → 9) emission of the core in MCLD 123.5+24.9. Note that the beam sizes of the observations are different.

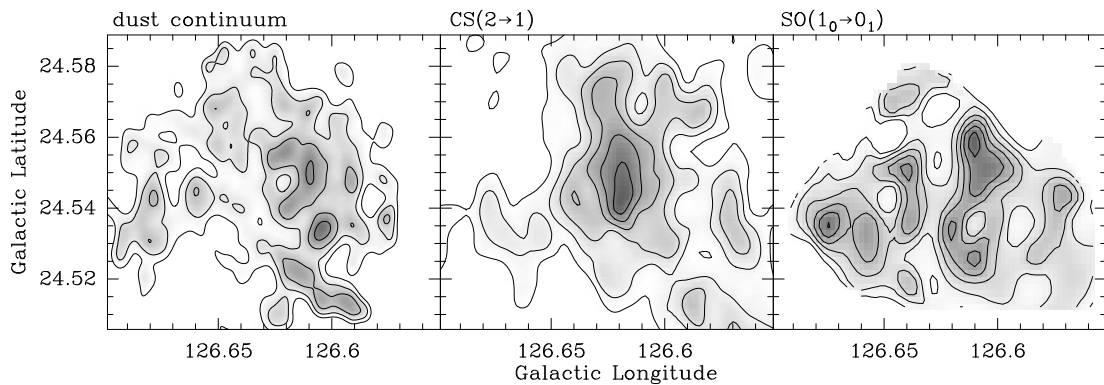


Figure 6.3: Maps of the 1.2 mm dust continuum, the integrated CS (2 → 1), and SO (1₀ → 0₁) emission of MCLD 126.6+24.5. Note that the beam sizes of the observations are different.

One recognises immediately the differences in the core appearance when observed in different molecular tracers. A core that shows up with a simple and symmetric structure in one tracer reappears as completely chaotic when observed in another one. The two cores displayed are located relatively near to each other, roughly 3° apart, in the same cloud complex, the Polaris Flare, and do have a very similar systemic velocity. The conclusion of

comparable conditions in both cores may be admissible. However, the differences between both cores are significant and strongly suggest a pure turbulent origin.

MCLD 123.5+24.9 appears as a filamentary structure as a whole, with several sub-clumps showing up in different molecular tracers. They are distributed along the major axis. MCLD 126.6+24.5 shows no clear density condensation in the dust continuum emission map. However, in the CS line emission it appears almost centrally condensed. However, this was observed with a relatively low resolution. SO, on the other hand, shows a high number of sub-clumps distributed in a completely different way. Heithausen et al. (1998) showed that both molecules trace different volumes inside a cloud and no correlation between the column densities of both molecules can be found. One is induced to say that CS and SO always occur in different sub-clumps. This behaviour may be explainable by chemical reactions, but how this works in detail is still somewhat unclear.

6.3 Core Stability and Star Formation Capability

To assess the core stability we have calculated the virial masses from the CS line width in the previous chapter (see Table 5.8). However, as already noted the CS most likely does not trace the same, or even a comparable, volume than estimated from the dust continuum observations. The reasons are the missing of the more diffuse component in the continuum data and the very clumpy structure of the material. In the CS-channel map of MCLD 123.5+24.9 (Figure 4.18) this can very clearly be seen. The CS emission arises from various clumps with slightly different velocities and the resulting CS line width is rather broad. This becomes even more clear if one examines the HC₃N line (Figure 4.19). This molecule is observed in only one sub-clump possessing a very narrow line width of only 0.19 km s⁻¹.

Hence, a comparison of virial and total mass is strongly affected by the molecular line of choice. In the case of MCLD 123.5+24.9 the line width of CS is 4 times the total width of the HC₃N line. This strongly suggests that both molecules do not trace the same parts of the core. Heithausen et al. (2002) used the HC₃N transition to calculate the virial mass and obtained a value below the total mass calculated from the dust emission. They concluded that the clump is gravitationally bound.

In our analysis we used the CS line width and obtained a virial mass of 17 times the total mass (see Table 5.8, hence, the conclusion would be that it is not gravitationally bound but totally dominated by turbulence. As shown before, one of the best correlations between the dust continuum and molecular line emission was found for the C¹⁸O. The line width of the (1 → 0) transition is about 0.61 km s⁻¹ and we derive a virial mass of 3.28 M_⊙. This is much less than calculated for the CS (2 → 1) transition. We even get a lower virial mass of 0.74 M_⊙ for the CS (5 → 4) transition, where the line width is about 0.29 km s⁻¹, tracing again a different volume as the lower transition of the same molecule. Hence, the virial mass would be only twice the total mass and thus of the same order. One may argue that

such a core seems to be gravitationally bound. However, a confident conclusion is difficult.

Our observational results indicate a limited star formation capability. We could not detect any direct signs of ongoing star formation. Nonetheless, we can also not exclude that the observed cores are able to form stars. The dust continuum maps and scaling relations show that they are not different from cores in star-forming clouds. The cores seem to be chemically young. This suggests that the density is not high enough to build up a high abundance of late-type molecules. Although, there are a number of sub-clumps, which are possibly slightly denser or longer-living, that can be detected in, for instance, Ammonia or Cyanoacetylene. Abundances of early-type molecules are generally higher and very similar to those in dark clouds. Therefore we have strong indications that the cirrus cloud cores are similar compared to cores in dark clouds, however, representing the low-density and low-mass regime.

The star-forming efficiency of cirrus cloud cores is certainly lower than for dark cloud cores. On the other hand, the number of small cores seems to be very high. We detected all chosen cores in the dust continuum and the CS ($2 \rightarrow 1$) transition. They are located within local IRAS $100 \mu\text{m}$ emission peaks, but do not stand out in CO ($1 \rightarrow 0$) maps. Most of the available large molecular surveys are not sensitive enough or do not have the required spacial resolution to detect the cores. One also needs a very high velocity resolution, because the lines are very narrow. We therefore expect a large number of small, dense cores within the filaments of the Galactic Cirrus, in perfect agreement with recent hydrodynamic simulations (e.g., Klessen et al. 2000). They noted that local collapse occurs even when the turbulent velocity field carries enough energy to counterbalance gravitational contraction on global scales. However, the simulations are mostly run for denser clouds and the resolution is not as good as one would need to identify such small cores like the ones investigated here.

Nevertheless, a large dust continuum survey with good angular resolution and very good sensitivity is needed to reveal the number and properties of cirrus cloud cores. However, here the problem of the extended, diffuse emission plays a major role, and may not easily be solved.

7

Conclusions and Future Prospects

7.1 The Results of this Study

We have imaged the dust emission and CS line emission in a small sample of 5 cirrus cloud cores. All cores were detected with column densities of the order of 10^{21} cm^{-2} . The basic properties of the cores, calculated from these observations, are typical ones compared to cores in known low-mass star-forming regions. It is strongly suggested that the cirrus cloud cores are very similar to dark cloud cores, representing the low-density and low-mass regime.

We calculated several scaling relations which are well known to be followed by star-forming cores and found that they are generally applicable to cirrus cloud cores as well. Especially, the cores and clumps follow the size – density relation perfectly, indicating a negligible volume filling factor of the dust at this high spatial resolution. Particularly notable is the very good agreement of the size – density relation of the cirrus cloud cores and starless cores in Taurus investigated by Tafalla et al. (2002). It indicates that both are very similar. However, for the mass – line width relation we found deviances. The correlation is not as strong as expected. This result is most likely caused by the discrepancy between the volume traced via CS and the dust-traced core.

Due to this effect, we were not able to decide reliably about the gravitational stability of the cores. The virial masses estimated from the CS ($2 \rightarrow 1$) transition line widths are much larger by about an order of magnitude than the total molecular masses derived from the dust continuum measurements. This would clearly disapprove gravitationally bound cores. However, there exists a significant systematic discrepancy between the CS ($2 \rightarrow 1$) line width and line widths of other density tracers, such as C^{18}O , HC_3N , or NH_3 . Unfortunately, we were not able to get good data of these molecules for all the cores with the required quality in time. Hence, this is a still ongoing project with very promising prospects.

A possible explanation for the discrepancy between the different line widths can be found in the very clumpy substructure of the cores. These were revealed by our high resolution interferometric observations. The cores harbour various sub-clumps, which exhibit different molecular abundances. We therefore see strong abundance variations on smallest scales and different line widths of the miscellaneous molecules.

The relatively broad CS ($2 \rightarrow 1$) line can be explained by the superposition of the emission of various sub-clumps, combined with self-absorption effects. More complicated and late-time molecules like HC₃N or NH₃, on the other hand, can only be found in longer-living, slightly denser sub-clumps and thus show a very narrow line width. These sub-clumps appear to be gravitationally bound, however, caused by the strong abundance variations their total molecular mass remains to be accurately determined.

Hence, such complex molecules may also not ideally suited to determine the kinetic energy of cirrus cloud cores. A possible solution may be a detailed but plain model of the chemical evolution in this low-density limit regime. A quantum leap could be a merger between the hydrodynamic turbulence simulations and the chemical evolution models. This could lead to directly observable predictions. The observations carried out here and the estimated properties can help to develop the basics for such simulations.

7.2 Future Prospects

New investigations always come up with new questions. Our knowledge about the star-forming capability of cirrus cloud cores is still very limited. Clearly, further studies are imperatively needed. They could bring forward our understanding of the low mass star formation process greatly.

Some of the results of this thesis are preliminary. We have shown that dense cores in cirrus clouds are definitely worth to be studied in more detail. Large dust continuum emission maps with the new bolometer arrays soon available are probably the best starting point. The proposed SCUBA-2 array at the *James Clerk Maxwell Telescope* (JCMT) or the *Large Bolometer Camera* (LABOCA) at the *Atacama Pathfinder Experiment* (APEX) telescope will make such observations feasible. We demonstrated in this thesis that they reveal the most dense parts of the cores and allow for a good estimate of the densities, despite the limiting observational difficulties. Space telescopes like the *Spitzer Space Telescope* (SST) or *Herschel* will even afford more accurate observations and can assess the cores in unchallenged details. However, the lifetimes of these instruments are highly limited and they have to concentrate on the best studied and most promising objects. Therefore, initial and preparatory investigations, like the one presented here, are essential for the success of such projects.

Though to distinguish between a condensed core and some cumulated clumps, molecular line observations are essential. Existing and newly build large single dish telescopes, like

the IRAM 30-m or the *Large Millimeter Telescope* (LMT) in Mexico provide the unique possibility to carry out sensitive observations with high spatial resolution. However, to understand the results we also need to know more about abundance variations and chemical evolution effects. Theoretical models, together with the nowadays available database technology, should be developed further on in both hydrodynamic turbulence simulations and chemical evolution. A merger between both could probably provide direct observable results.

New observational opportunities will be available soon with, for instance, SOFIA, an airborne telescope, or ALMA, the large millimeter array at the Atacama desert in Chile. Especially the latter will allow highest spatial resolution observations. The combination of these observations with maps taken by smaller telescopes may highly increase our understanding of the clumpy structure of cirrus cloud cores. But also small telescopes can contribute significantly with large surveys or very deep pointed observations. Altogether, the combination and comparison of as many as possible miscellaneous observations should help to reveal the true nature of these intriguing objects.

8

Summary

In this thesis a small sample of five cirrus cloud cores has been studied in detail to investigate the general capability of these clouds to form stars or brown dwarfs. It is not known up to now, if such diffuse clouds do have this ability. Nevertheless, it is essential for our understanding of the star formation process in general, because the starting conditions of low-mass star-formation are still rather poorly conceived. The formation and evolution of a molecular core is the crucial basic point within this process. In regions with known star formation the investigation of pre-stellar cores is often hampered by the influences of adjacent young stars. Finding cores, that are able to form low-mass stars, in a relatively quiescent environment could help to determine the starting conditions more accurately.

The thermal dust continuum emission at 1.2 mm has been observed using the MAMBO arrays at the IRAM 30-m telescope. The detection of all 5 cores can be reported and basic properties of the cores were derived. We conclude that cirrus cloud cores are basically similar to cores in dark clouds or star-forming regions, but they are residing at the low-mass and low-density end. This matches perfectly our expectations. However, the cores do not show a simple spheroidal geometry, but they are elongated and divide into many sub-clumps. Our results strongly indicate a pure turbulent origin of the cores out of their parental clouds and we are not able to decide if they are influenced by self-gravity.

The CS ($2 \rightarrow 1$) line emission has been observed using the FCRAO 14-m and the IRAM 30-m telescope, respectively. All cores were detected, confirming the relatively high densities, already derived from the dust continuum observations. Although the beam sizes of the dust continuum and the molecular line observations are different, significant distinction can be found between the distributions of both tracers. This is not necessarily surprising, as the dust continuum emission provides only an integrated picture, however, the CS-line emission does not show a lot of substructure in velocity, but seems just differently spatial distributed.

We also looked for other dense gas tracers. The cores were observed in the HC_3N ($10 \rightarrow 9$) line and the CS ($5 \rightarrow 4$) transition using the IRAM 30-m telescope. Unfortunately, we did not detect these lines in any other than the previously observed core in MCLD 123.5+24.9. This was partly caused by not ideal weather conditions during the observations. Nevertheless, the non-detections already provide upper limits for the abundances of the molecules. We performed LVG and RADEX analyses to determine the molecular abundances in the cores. A comparison with a time dependent chemical model, originally constructed for a core in Taurus, TMC 1, and other cores in dark clouds and known star forming regions shows that the cores are chemically young, except for MCLD 123.5+24.9. We can partly explain this behaviour by a very clumpy nature of the cirrus cloud cores, caused by their turbulent origin.

The dense cirrus cloud cores fragment into many sub-clumps embedded in a less dense intra-clump medium. Only the longer-living, probably slightly larger and denser, sub-clumps are able to develop higher abundances of molecules such as HC_3N or NH_3 . The CS molecule, on the other hand, is formed very fast if the critical density is reached and is abundant also in the intra-clump medium. It may even start to deplete in some of the sub-clumps, hence pretending a different spatial distribution than the dust continuum. One important result is the discovery of the systematically broader line width of the CS ($2 \rightarrow 1$) transition compared to other molecules, like C^{18}O or SO . This is most likely caused by the superposition and blending of the lines arising from different sub-clumps and blurred by the intra-clump CS emission. Altogether, also due to self-absorption effects of the CS ($2 \rightarrow 1$) line, the CS molecule is less suited to determine the kinetic energy content of the cores.

Due to the difficulties caused by the very clumpy structure and the strong abundance variations we could not decide if the observed cores are able to form stars or brown dwarfs. Our interpretation of the data suggests a pure turbulent origin of the cores. Hence, they could be transient objects. However, the further evolution is still unclear, since it seems possible that some of the sub-clumps merge and become gravitationally bound. This scenario is strongly favoured by us for the core in MCLD 123.5+24.9, our best studied prime example. For this cirrus cloud core we strongly tend to infer from our data a pre-stellar core formation setting. It is also possible for the cores in L 1457 and MBM 32. To clarify the situation, more observations, with the highest spatial resolution available, and detailed specific models including the chemical evolution, are needed. This will be a very time consuming work, however, the result could help to understand not only the basics of low-mass star formation, but maybe even the appearance of the galaxy.

Zusammenfassung

In dieser Arbeit wurde eine kleine Auswahl von 5 dichten Kernen in galaktischen Zirkuswolken genauer untersucht, um das generelle Potential dieser Wolken, Sterne oder braune Zwerge bilden zu können, zu erforschen. Bisher ist es vollkommen unbekannt, inwieweit solche diffusen Wolken überhaupt diese Fähigkeit besitzen. Allerdings ist es unverzichtbar für unser Verständnis des Prozesses der Sternbildung im allgemeinen, da die Anfangsbedingungen bei der Entstehung Sterne niedriger Massen noch immer nur wenig begriffen sind. Die Bildung und Entwicklung eines molekularen Kernes ist dabei ein kritischer Hauptpunkt des ganzen Prozesses. In Regionen mit bekannter Sternentstehungsaktivität werden Untersuchungen von prä-stellaren Kernen oft durch die Aktivitäten nahegelegener junger Sterne behindert. Findet man Kerne, die Sterne niedriger Masse bilden können, in einem relativ ruhigen Umfeld, könnte das sehr helfen die Anfangsbedingungen der Sternentstehung genauer zu bestimmen.

Es wurde die thermische Kontinuumsstrahlung des Staubes bei 1,2 mm mit den MAMBO Arrays am IRAM 30 m Teleskop beobachtet. Der Nachweis aller 5 Kerne kann hier berichtet werden, und es wurden die fundamentalen Eigenschaften der Kerne daraus abgeleitet. Wir folgern, daß Kerne in Zirkuswolken grundsätzlich ähnlich zu Kernen in Sternentstehungsgebieten oder Dunkelwolken sind, allerdings im unteren Massen und Dichten Bereich angesiedelt sind. Dieses Ergebnis bestätigt auf perfekte Weise unsere Erwartungen. Aber, die Kerne zeigen keineswegs eine einfache, sphärische Geometrie, sondern sind größtenteils gestreckt und unterteilen sich in eine Vielzahl von Unterklumpen. Unsere Ergebnisse deuten daher auf die Entstehung dieser Kerne durch turbulente Prozesse hin. Wir können mit diesen Daten leider noch nicht eindeutig entscheiden, inwieweit sie durch Selbst-Gravitation beeinflusst sind.

Desweiteren wurde die CS (2 \rightarrow 1) Linienstrahlung mit dem FCRAO 14-m und dem IRAM 30-m Teleskop beobachtet. Auch hier konnten alle Kerne nachgewiesen werden, was die relativ hohen Dichten, abgeleitet aus den Staub-Kontinuum Beobachtungen, bestätigt. Obwohl die räumliche Auflösung bei den Staub und Moleküllinien Beobachtungen unterschiedlich ist, lassen sich doch erhebliche Unterschiede in der räumlichen Verteilung der beiden Indikatoren feststellen. Das ist nicht unbedingt überraschend, da die Staub Kontinuumsstrahlung lediglich ein integriertes Bild liefert. Allerdings zeigt die CS-Linienstrahlung nicht allzuviel Unterstruktur in der Geschwindigkeit, sondern erscheint vielmehr tatsächlich unterschiedlich räumlich verteilt zu sein.

Wir haben außerdem nach weiteren Indikatoren für dichtes Gas Ausschau gehalten. So wurden die Kerne ebenfalls in der HC₃N (10 \rightarrow 9) Linie und dem CS (5 \rightarrow 4) Übergang mit dem IRAM 30-,m Teleskop beobachtet. Bedauerlicherweise konnten wir diese Linien in keinem weiteren Kern detektieren, außer in dem bereits zuvor untersuchten Kern in MCLD 123.5+24.9. Zum Teil wurde dies durch nicht ideale Wetterbedingungen während der Beobachtungen verursacht. Aber auch ein Nicht-Nachweis liefert bereits obere Grenzen für die Häufigkeit des Moleküls. Wir führten daher LVG und RADEX Analysen durch,

um die Molekülhäufigkeiten in den Kernen zu bestimmen. Ein Vergleich mit einem die Zeitabhängigkeit berücksichtigendem chemischen Modell, ursprünglich entworfen für einen dichten Kern in Taurus, TMC 1, und mit anderen Kernen in Sternentstehungsgebieten und Dunkelwolken zeigt, daß die Kerne chemisch jung sind. MCLD 123.5+24.9 bildet dabei möglicherweise eine Ausnahme. Wir denken, daß wir diesen Befund mit einer sehr klumpigen Struktur der Zirkus-Kerne erklären können, verursacht durch ihre Entstehung durch turbulente Prozesse.

Die dichten Kerne in den galaktischen Zirkuswolken fragmentieren in eine große Anzahl kleiner Klumpen, die in einem etwas weniger dichten Zwischenklumpen-Medium eingebettet sind. Allerdings können wohl nur die langlebigeren, etwas größeren und dichteren Klumpen höhere Häufigkeiten von Molekülen wie HC_3N oder NH_3 ausbilden. Das CS-Molekül, andererseits, wird sehr schnell gebildet, sofern die kritische Dichte erreicht ist und ist auch in dem Zwischenklumpen-Medium recht häufig. Es ist sogar möglich, daß CS in einigen der Klumpen bereits abgereichert wird. Dies geschieht ebenfalls ab einer bestimmten Dichte, z.B., durch Ausfrieren der Moleküle auf Staubkörnern. Ein wichtiges Ergebnis ist die Entdeckung der systematisch größeren Linienbreiten des CS ($2 \rightarrow 1$) Übergangs, verglichen mit anderen Molekülen wie C^{18}O oder SO. Dies wird, sehr wahrscheinlich, durch die Überlagerung und Vermischung der Linien verschiedener Unterklumpen, zusätzlich verwischt durch die Strahlung des Zwischenklumpen-Mediums, verursacht. Insgesamt betrachtet müssen wir feststellen, daß sich das CS Molekül nicht sehr gut eignet, um die kinetische Energie dieser Kerne zu bestimmen. Das wird noch zusätzlich durch Effekte der Selbstabsorption des CS ($2 \rightarrow 1$) Überganges erschwert.

Infolge der Schwierigkeiten, bedingt durch die sehr klumpige Struktur der Kerne und die starken Häufigkeitsänderungen, konnten wir noch nicht entscheiden, inwieweit die Kerne in der Lage sind Sterne oder braune Zwerge zu bilden. Unsere Interpretation der Daten deutet auf eine Entstehung der Kerne aus rein turbulenten Prozessen hin. Daher ist es möglich, daß es sich um vorübergehende Erscheinungen handelt, das heißt die Kerne lösen sich nach einiger Zeit wieder auf. Aber die weitere Entwicklung ist noch sehr unbestimmt, da es durchaus auch möglich ist, daß sich mehrere der kleinen Klumpen vereinigen und so gravitativ gebunden werden. Dieses Szenario wird von uns zumindest für den Kern in MCLD 123.5+24.9, den am besten untersuchten, stark favorisiert. Hier tendieren wir dazu, die Bildung eines prä-stellaren Kernes zu folgern. Allerdings sind zusätzliche Beobachtungen mit der höchsten verfügbaren räumlichen Auflösung und ein spezielles, detailliertes Modell nötig um die Situation eindeutig zu klären. Diese Arbeit wird sehr zeitaufwändig sein, allerdings kann das Resultat wesentlich dazu beitragen die Grundlagen der Sternentstehung von Sternen niedriger Masse besser zu verstehen und so möglicherweise sogar zu einem besseren Verständnis des Erscheinungsbildes unserer Galaxie beitragen.

Bibliography

- Andersson, B.-G., Idzi, R., Uomoto, A., Wannier, P. G., Chen, B., & Jorgensen, A. M. 2002, *AJ*, 124, 2164
- Bensch, F., Leuenhagen, U., Stutzki, J., & Schieder, R. 2003, *ApJ*, 591, 1013
- Benson, P. J., & Myers, P. C. 1989, *ApJS*, 71, 89
- Bernard, J. P., et al. 1999, *A&A*, 347, 640
- Bertoldi, F. & McKee, C. F. 1992, *ApJ*, 395, 140
- Blitz, L., Magnani, L., & Mundy, L., 1984, *ApJ*, 282, L9
- Boden, K.-P. & Heithausen, A. 1993, *A&A*, 268, 255
- Caselli, P., Benson, P. J., Myers, P. C., & Tafalla, M. 2002, *ApJ*, 572, 238
- Chabrier, G. 2003, *PASP*, 115, 763
- Clemens, D. P., Sanders, D. B., & Scoville, N. Z. 1988, *ApJ*, 327, 139
- Dame, T. M., Elmegreen, B. G., Cohen, R. S., & Thaddeus, P. 1986, *ApJ*, 305, 892
- de Vries, H. W., Thaddeus, P., & Heithausen, A. 1987, *ApJ*, 319, 723
- Dickens, J. E., Irvine, W. M., Snell, R. L., Bergin, E. A., Schloerb, F. P., Pratap, P., & Miralles, M. P. 2000, *ApJ*, 542, 870
- Draine, B. T. 2003, *ARA&A*, 41, 241
- Draine, B. T. & McKee, C. F. 1993, *ARA&A*, 31, 373
- Emerson, D. T., Klein, U., & Haslam, C. G. T. 1979, *A&A*, 76, 92
- Evans, N. J. 1999, *ARA&A*, 37, 311
- Evans, N. J., Rawlings, J. M. C., Shirley, Y. L., & Mundy, L. G. 2001, *ApJ*, 557, 193
- Falgarone, E. & Perault, M. 1987, *Protostars and Molecular Clouds*, 15

Falgarone, E., Lis, D. C., Phillips, T. G., Pouquet, A., Porter, D. H., & Woodward, P. R. 1994, *ApJ*, 436, 728

Falgarone, E., Panis, J.-F., Heithausen, A., Perault, M., Stutzki, J., Puget, J.-L., & Bensch, F. 1998, *A&A*, 331, 669

Fleck, R. C. 1988, *ApJ*, 328, 299

Frerking, M. A., Langer, W. D., & Wilson, R. W. 1982, *ApJ*, 262, 590

Gammie, C. F., & Ostriker, E. C. 1996, *ApJ*, 466, 814

Gerin, M., Falgarone, E., Joulain, K., Kopp, M., Le Bourlot, J., Pineau des Forets, G., Roueff, E., & Schilke, P. 1997, *A&A*, 318, 579

Gladders, M. D., et al. 1998, *ApJ*, 507, L161

Goodman, A. A., Barranco, J. A., Wilner, D. J., & Heyer, M. H. 1998, *ApJ*, 504, 223

Großmann, V. & Heithausen, A. 1992, *A&A*, 264, 195

Großmann, V., Meyerdierks, H., Mebold, U., & Heithausen, A. 1990, *A&A*, 240, 400

Hearty, T., Magnani, L., Caillault, J.-P., Neuhäuser, R., Schmitt, J. H. M. M., & Stauffer, J. 1999, *A&A*, 341, 163

Hearty, T., Fernández, M., Alcalá, J. M., Covino, E., & Neuhäuser, R. 2000, *A&A*, 357, 681

Heithausen, A., Mebold, U., & de Vries, H. W. 1987, *A&A*, 179, 263

Heithausen, A. & Thaddeus, P. 1990, *ApJ*, 353, L49

Heithausen, A., Stacy, J. G., de Vries, H. W., Mebold, U., & Thaddeus, P. 1993, *A&A*, 268, 265

Heithausen, A., Corneliussen, U., & Großmann, V. 1995, *A&A*, 301, 941

Heithausen, A. 1996, *A&A*, 314, 251

Heithausen, A., Corneliussen, U., & Grossmann, V. 1998, *A&A*, 330, 311

Heithausen, A. 1999, *A&A*, 349, L53

Heithausen, A., Bertoldi, F., & Bensch, F. 2002, *A&A*, 383, 591

Heithausen, A. 2004, *ApJ*, 606, L13

Herbig G.H., Bell K.R., 1988, *Lick Observatory Bulletin* 1111, 1

- Heyer, M. H., Narayanan, G., Brewer, M., 2001, "On the Fly Mapping at the FCRAO 14m telescope" Online Manual at <http://donald.astro.umass.edu/fcrao/library/manuals/otfmanual.html>
- Hobbs, L. M., Blitz, L., & Magnani, L. 1986, ApJ, 306, L109
- Hogerheijde, M. 1998, *The molecular environment of low-mass protostars*, Ph.D. Thesis, Leiden University
- Hogerheijde, M. R., Johnstone, D., Matsuyama, I., Jayawardhana, R., & Muzerolle, J. 2003, ApJ, 593, L101
- Jayawardhana, R., Wolk, S. J., Barrado y Navascués, D., Telesco, C. M., & Hearty, T. J. 2001, ApJ, 550, L197
- Jeans, J. H. 1928, *Astronomy and Cosmogony*, p. 340, Cambridge, U.K.: Cambridge Univ. Press
- Johnstone, D., Fich, M., Mitchell, G. F., & Moriarty-Schieven, G. 2001, ApJ, 559, 307
- Kerp, J. 1994, A&A, 289, 597
- Klessen, R. S., Heitsch, F., & Mac Low, M. 2000, ApJ, 535, 887
- Kolmogorov, A. N. 1941, *Comptes Rendus de l'Academie des Sciences de l'URSS*, 30, 301; reprinted in Friedlander, S. K. and Topper, L., eds. 1961. *Turbulence: Classic Papers on Statistical Theory* (New York: Interscience)
- Kreysa, E. 1990, *From Ground-Based to Space-Borne Sub-mm Astronomy*, 265
- Kroupa, P. 2001, MNRAS, 322, 231
- Ladd, E. F. & Covey, K. R. 2000, ApJ, 536, 380
- Larson, R. B. 1981, MNRAS, 194, 809
- Low, F. J., Young, E., Beintema, D. A., et al., 1984, ApJ, 278, L19
- Luhman, M. L. & Jaffe, D. T. 1996, ApJ, 463, 191
- Luhman, K. L. 2001, ApJ, 560, 287
- Luhman, K. L. 2004, ApJ, 614, 398
- Lynds, B. T. 1962, ApJS, 7, 1
- Lynds, B. T. 1965, ApJS, 12, 163
- Mac Low, M. & Klessen, R. S. 2004, *Reviews of Modern Physics*, 76, 125
- Magnani, L., Blitz, L., & Mundy, L., 1985, ApJ, 295, 402

- Magnani, L. & de Vries, C. P. 1986, *A&A*, 168, 271
- Magnani, L., Caillault, J., Hearty, T., Stauffer, J., Schmitt, J. H. M. M., Neuhaeuser, R., Verter, F., & Dwek, E. 1996, *ApJ*, 465, 825
- Markwick, A. J., Millar, T. J., & Charnley, S. B. 2000, *ApJ*, 535, 256
- Mebold, U., Cernicharo, J., Velden, L., Reif, K., Crezelius, C., & Goerigk, W. 1985, *A&A*, 151, 427
- Mebold, U., Heithausen, A., & Reif, K. 1987, *A&A*, 180, 213
- Millar, T. J., Farquhar, P. R. A., & Willacy, K. 1997, *A&AS*, 121, 139
- Miller, G. E., & Scalo, J. M. 1979, *ApJS*, 41, 513
- Motte, F., Andre, P., & Neri, R. 1998, *A&A*, 336, 150
- Motte, F., & André, P. 2001, *A&A*, 365, 440
- Motte, F., André, P., Ward-Thompson, D., & Bontemps, S. 2001, *A&A*, 372, L41
- Myers, P. C. 1983, *ApJ*, 270, 105
- Myers, P. C. 1998, *ApJ*, 496, L109
- Neuhäuser, R. 1999, *Reviews of Modern Astronomy*, 12, 27
- Nikolić, S., Johansson, L. E. B., & Harju, J. 2003, *A&A*, 409, 941
- Noh, H. & Scalo, J. 1990, *ApJ*, 352, 605
- Nordlund, ., & Padoan, P. 2002, in *Simulations of Magnetohydrodynamic Turbulence in Astrophysics: Recent Achievements and Perspectives*, ed. E. Falgarone & T. Passot (Berlin: Springer)
- Onishi, T., Mizuno, A., Kawamura, A., Tachihara, K., & Fukui, Y. 2002, *ApJ*, 575, 950
- Penprase, B. E., Rhodes, J. D., & Harris, E. L. 2000, *A&A*, 364, 712
- Pfenniger, D. & Combes, F. 1994, *A&A*, 285, 94
- Pound, M. W., Wilson, R. W., & Bania, T. M. 1990, *ApJ*, 351, 165
- Pratap, P., Dickens, J. E., Snell, R. L., Miralles, M. P., Bergin, E. A., Irvine, W. M., & Schloerb, F. P. 1997, *ApJ*, 486, 862
- Reach, W. T., Pound, M. W., Wilner, D. J., & Lee, Y. 1995, *ApJ*, 441, 244
- Richter, P., 1999, *FUV Spectroscopy of Interstellar Molecular Hydrogen towards the Magellanic Clouds*, PhD thesis, University of Bonn

- Salpeter, E. E. 1955, ApJ, 121, 161
- Schoeier, F. L., van der Tak, F. F. S., van Dishoeck, E. F., Black, J. H., astro-ph/0411110, accepted for publication in A&A
- Schreiber, W., Wouterloot, J. G. A., Heithausen, A., & Winnewisser, G. 1993, A&A, 276, L5
- Shu, F. H. 1977, ApJ, 214, 488
- Snowden, S. L., Egger, R., Finkbeiner, D. P., Freyberg, M. J., & Plucinsky, P. P. 1998, ApJ, 493, 715
- Spitzer, L. Jr. 1978, Physical Processes in the Interstellar Medium, p. 282, New York: Wiley
- Steinacker, J., Henning, T., Bacmann, A., & Semenov, D. 2003, A&A, 401, 405
- Straižys, V., Černis, K., Kazlauskas, A., & Laugalys, V. 2002, Baltic Astronomy, 11, 231
- Stutzki, J., & Guesten, R. 1990, ApJ, 356, 513
- Tafalla, M., Myers, P. C., Caselli, P., Walmsley, C. M., & Comito, C. 2002, ApJ, 569, 815
- Taylor, S. D., Morata, O., & Williams, D. A. 1998, A&A, 336, 309
- Testi, L. & Sargent, A. I. 1998, ApJ, 508, L91
- Thum, C., Kreysa, E., Gemünd, H. P., et al., 1992, IRAM Working Report No. 212, IRAM, Grenoble
- Ungerechts, H. & Thaddeus, P. 1987, ApJS, 63, 645
- van Dishoeck, E. F. & Black, J. H. 1988, ApJ, 334, 771
- Ward-Thompson, D., Motte, F., & Andre, P. 1999, MNRAS, 305, 143
- Wakker, B. P. 2004, Ap&SS, 289, 381
- Weiland, J. L., Blitz, L., Dwek, E., Hauser, M. G., Magnani, L., & Rickard, L. J., 1986, ApJ, 306, L101
- Weiß, A., 2000, *The Effect of Violent Star Formation on the Molecular Gas in M82*, PhD thesis, University of Bonn
- Westmeier, T., 2003, *HI-Beobachtungen zur Struktur und Verteilung Kompakter Hochgeschwindigkeitswolken*, Diploma Thesis, University of Bonn
- Whitworth, A. P. & Zinnecker, H. 2004, A&A, 427, 299

Wouterloot, J. G. A., Heithausen, A., Schreiber, W., & Winnewisser, G. 2000, A&AS, 144, 123

Zagury, F., Boulanger, F., & Banchet, V. 1999, A&A, 352, 645

Zhou, S., Wu, Y., Evans, N. J., Fuller, G. A., & Myers, P. C. 1989, ApJ, 346, 168

Zimmermann, T. & Ungerechts, H. 1990, A&A, 238, 337

Acknowledgments

Mein ganz besonderer Dank gilt meinem Betreuer, Herrn Priv. Doz. Dr. Andreas Heithausen, der diese Arbeit erst ermöglicht hat. Ohne seine Ratschläge, Ideen und Anregungen wäre ich nicht bis zu diesem Punkt gekommen. Weiterhin danke ich ihm auch für die Bereitstellung seiner Meßdaten, die diese Arbeit jedenfalls sehr aufgewertet haben.

Ich danke ganz herzlich Herrn Prof. Dr. Uli Klein für die freundliche Unterstützung und die Bereitschaft diese Arbeit zu begutachten. Er hat mir mit seiner ansteckenden Begeisterung den Weg zur Radioastronomie eröffnet, und mir oftmals hilfreiche Ratschläge gegeben.

Bei Herrn Dr. Frank Bensch und Herrn Dr. Frank Bertoldi möchte ich mich ebenso herzlich für die wissenschaftliche Betreuung und zahlreiche Hinweise bedanken. Herrn Prof. em. Dr. Ulrich Mebold danke ich für die Förderung meiner wissenschaftlichen Arbeit und die freundliche Aufnahme im Radioastronomischen Institut.

Mein ganz besonderer Dank gilt auch allen Mitarbeitern des Radioastronomischen Instituts der Universität Bonn, die die vergangenen Jahre zu einer wirklichen Bereicherung meines Lebens gemacht haben. Ich fand hier eine freundliche Aufnahme, Unterstützung und kollegiale Atmosphäre. Insbesondere moechte ich mich bei den neuen und alten Mitgliedern der Kaffeerrunde, Andreas Horneffer, Christian und Claudia Brüns, Ylva Schubert, Gernot Thuma, Yvonne Dzierma, Nadja Ben Bekhti und Benjamin Winkel bedanken, die mir oftmals neue Motivation gegeben haben. Nicht nur als Kollegen, sondern auch als gute Freunde. Auch meinen beiden Zimmergenossen Leonidas Dedes und Gianfranco Gentile moechte ich für die sehr angenehme Arbeitsatmosphäre danken. Sehr viel gelernt habe ich auch von und durch Gyula Jozsa "Josh", Franz Kenn, Stefanie Mühle, Meikel Kappes, Juan Pradas, Jorge Pineda, Tobias Westmeier, Stefan Stanko, Peter Kalberla, Jürgen Kerp und Anne Pagels. Vielen Dank dafür, und auch an alle, die hier nicht namentlich genannt wurden.

Diese Arbeit wurde ermöglicht durch den Sonderforschungsbereich **SFB 494: Die Entwicklung der Interstellaren Materie** und die **International Max Planck Research School (IMPRS) for Radio and Infrared Astronomy** des Max-Planck-Instituts für Radioastronomie.

Mein größter Dank gilt meinen Eltern und meiner Familie, die mir stets beigestanden und mein Studium überhaupt erst möglich gemacht haben. Sie haben mir auch immer die Freiheit gelassen, daß zu tun was mich am meisten interessiert hat. Mein letzter und herzlichster Dank gilt Astrid für ihre Liebe, Gedult und Unterstützung, ganz besonders in den letzten Wochen.

Lebenslauf

Angaben zur Person

Name	Christoph Böttner
Geburtsdatum	01.11.1974
Geburtsort	Lobenstein
Familienstand	ledig
Staatsangehörigkeit	deutsch
Wohnort	Rauschengesees 16 07368 Remptendorf
Kontakt	Tel.: 03664322373 e-mail: christoph-boettner@gmx.de

Schulbildung

1981 - 1990	Polytechnische Oberschule "Edwin-Hörnle" Ruppertsdorf
1990 - 1993	Staatliches Gymnasium "Christian Gottlieb Reichard" Lobenstein
26.06. 1993	Abitur

Beruflicher Werdegang

1994 - 2001	Studium der Physik und Astronomie an der Rheinischen Friedrich-Wilhelms-Universität Bonn
2000 - 2001	Diplomarbeit am Radioastronomischen Institut der Univ. Bonn
14. 11. 2001	Diplom
ab Dez. 2001	Doktorand am Radioastronomischen Institut der Univ. Bonn und der International Max-Planck Research School (IMPRS) des Max-Planck-Institut's für Radioastronomie in Bonn

Hiermit versichere ich, daß ich die vorliegende Arbeit selbständig und ohne andere als die angegebenen Hilfsmittel angefertigt habe. Weiterhin versichere ich, daß ich die Dissertation in dieser oder ähnlicher Form noch bei keiner anderen Fakultät der Rheinischen Friedrich-Wilhelms-Universität Bonn oder einer anderen Hochschule eingereicht habe.

Bonn, im März 2005

